

**OXIDATION-RESISTANT CATALYST SUPPORTS FOR PROTON EXCHANGE MEMBRANE
FUEL CELLS (PEMFCs)**

by

HARMEET CHHINA

B.Sc., University of Victoria, 2001

**A THESIS SUBMITTED IN PARTIAL FULFILLMENT OF
THE REQUIREMENTS FOR THE DEGREE OF
MASTER OF SCIENCE**

in

THE FACULTY OF GRADUATE STUDIES

(Materials Engineering)

THE UNIVERSITY OF BRITISH COLUMBIA

August 2006

© Harmeet Chhina, 2006

ABSTRACT

Proton exchange membrane fuel cells (PEMFCs) are electrochemical energy conversion devices that react hydrogen and oxygen to produce electricity. PEMFCs can be used for power generation in the portable, stationary and transportation sectors. Severe performance degradation during extended operation is hindering commercialization of PEMFCs. One of the mechanisms causing performance degradation includes catalyst support corrosion.

Tungsten carbide (WC) and indium tin oxide (ITO) were selected as supports of choice. Platinum was dispersed on commercial samples of WC and ITO. Both the thermal and electrochemical stability of the supported catalyst was determined. The stability of the supports was compared with both commercial catalyst (Hispec 4000) and in-house Pt catalyst. The in-house Pt catalyst was supported on commonly used high surface area carbon Vulcan XC-72R catalyst support. The electrochemical testing involved applying oxidation cycles between +0.6 V to +1.8 V and monitoring the loss in activity of the supported catalyst over 100 oxidation cycles.

Tungsten carbide was found to be extremely stable. However, direct comparison of its stability to Vulcan XC-72R is currently difficult. The electrochemical stability of 40 wt% Pt dispersed on WC was compared with that of 40 wt% Pt/C. Even though there are large differences in the densities of C and WC some comparisons are possible. An alternative method to more directly compare the stabilities of WC and C involved dispersing a similar amount of Pt on similar powder volumes of WC and C. The solid densities of both carbon and WC were also used to disperse similar volumes of Pt on both supports in order to more directly compare the electrochemical stability.

Indium tin oxide lost approximately 50% of its activity after 30 oxidation cycles, whereas Vulcan XC-72R lost almost 100% of its activity after 10 oxidation cycles. Both the electrochemical oxidation and thermal stability tests showed that ITO is extremely stable compared to Vulcan XC-72R.

TABLE OF CONTENTS

ABSTRACT	ii
TABLE OF CONTENTS	iii
LIST OF FIGURES	v
LIST OF SYMBOLS AND ABBREVIATIONS	viii
ACKNOWLEDGEMENTS	x
DEDICATION	xi
1 Literature Review	1
1.1 Catalyst support materials- Introduction	1
1.2 Studies of catalyst supports.....	6
1.2.1 Carbon	6
1.2.2 Summary	14
1.3 Carbides	14
1.3.1 Tungsten carbide and electrocatalysis.....	15
1.3.2 Summary	19
1.4 Oxides.....	19
1.4.1 Summary	22
1.5 Conclusions	22
2 Introduction to the three electrode electrochemical cell, voltammetry and rotating disc electrode (RDE)	23
2.1 Three electrode electrochemical cell.....	23
2.2 Voltammetry.....	23
2.2.1 Cyclic voltammetry (CV).....	23
2.3 Convection and rotating disc electrode (RDE)	25
3 Objectives	26
4 Experimental Procedure	26
4.1 Pt addition using chlorplatinic acid (method I)	26
4.2 Pt addition using Pt (II) pentan-2,4-dionate (method II)	27
4.3 Pt addition to equal powder volumes of support (for WC studies only)	27

4.4	<i>Pt addition to carbon and tungsten carbide by solid density method (for WC studies only)</i>	28
4.5	<i>Thermogravimetric analysis (TGA)</i>	28
4.6	<i>Rotating disc electrode (RDE) and electrochemical test set-up</i>	28
4.7	<i>X-Ray Diffraction (XRD)</i>	29
4.8	<i>Scanning electron microscopy (SEM)/Transmission electron microscopy (TEM) and Energy Dispersive X-Rays (EDX)</i>	30
5	Determining potential and time for electrochemical stability tests	30
6	Results and discussion for tungsten carbide studies	33
6.1	<i>Alfa Aesar WC with Pt deposition using chlorplatinic acid</i>	33
6.2	<i>Alfa Aesar WC with Pt deposition using Pt (II) pentan-2,4-dionate</i>	37
6.3	<i>Comparing activities of Pt deposited using Pt (II) pentan-2,4-dionate on similar volumes of both Alfa Aesar WC and Vulcan XC-72R</i>	49
6.4	<i>Pt addition in equal solid volume ratios to carbon and tungsten carbide</i>	53
7	Results and discussion for indium tin oxide (ITO) studies	57
7.1	<i>ITO with Pt deposition using chlorplatinic acid</i>	57
7.2	<i>ITO with Pt deposition using Pt (II) pentan-2,4-dionate</i>	68
8	Conclusions	70
8.1	<i>Tungsten carbide</i>	70
8.2	<i>Indium tin oxide</i>	71
9	Future Work	72
9.1	<i>Tungsten carbide</i>	72
9.2	<i>Indium tin oxide</i>	72
10	References	73

LIST OF FIGURES

Figure 1: Schematic showing the principle of operation of a proton exchange membrane fuel cell (PEMFC)	1
Figure 2: Schematic showing potentials in different regions along the fuel and oxidant sides of a PEMFC before startup (A) and during startup (B). Figure redrawn from work by Reiser et al ¹⁰	5
Figure 3: Structure of a) quinone; b) hydroquinone	7
Figure 4: Cyclic voltammogram of Pt GDE in 1.0 mol/dm ³ in H ₂ SO ₄ at 25°C, v = 30mV/s	25
Figure 5: Current vs. time plot obtained from oxidation cycles for Hispec 4000 cycled between +0.6 V (held for 60s) and +1.8V (held for 20s); 0.5 M H ₂ SO ₄ , 30°C, 100 mV/s, 2000 RPM. .	32
Figure 6: Normalized activity at different potentials and times as a result of repeated cycling for Hispec 4000. Average of three samples with limits of error for each condition are plotted...	33
Figure 7: XRD spectrum of Pt dispersed on Vulcan XC-72R.	34
Figure 8: XRD spectrum of Alfa Aesar WC sample	35
Figure 9: WC with flakes of unknown material.....	35
Figure 10: Cyclic voltammogram of Alfa Aesar WC supporting Pt, both before and after 10 oxidation cycles; 0.5 M H ₂ SO ₄ , 30°C, 100 mV/s, 2000 RPM.	36
Figure 11: Change in anodic activity at 1.8 V as a result of repeated cycling for 40 wt% Pt/AAWC and 40 wt% Pt/Vulcan XC-72R.	36
Figure 12: XRD pattern for Alfa Aesar WC with Pt deposition by Pt (II) reduction to Pt.....	37
Figure 13: XRD pattern for 40wt % Pt on Vulcan XC-72R with Pt deposition by Pt (II) reduction to Pt.....	38
Figure 14: TGA data for Alfa Aesar WC, 40 wt% Pt on Alfa Aesar WC, and 40 wt% Pt on Vulcan XC-72R under air at 40ml/min, temperature ramped from 50°C to 1000°C at 2°C/ min.	39
Figure 15: Change in anodic activity at 1.8 V as a result of repeated cycling for Alfa Aesar WC, 40 wt% Pt on Vulcan XC-72R and 40 wt% Pt on Alfa Aesar WC. Average of three samples with limits of error for each material are plotted.	41
Figure 16: Cyclic voltammograms for Alfa Aesar WC both before and after 100 oxidation cycles; 0.5 M H ₂ SO ₄ , 30°C, 100 mV/s, 2000 RPM.	42
Figure 17: Cyclic voltammograms for 40 wt% Pt on WC both before and after 100 oxidation cycles; 0.5 M H ₂ SO ₄ , 30°C, 100 mV/s, 2000 RPM.	42
Figure 18: Cyclic voltammograms for 40 wt% Pt on Vulcan XC-72R, both before and after 100 oxidation cycles; 0.5 M H ₂ SO ₄ , 30°C, 100 mV/s, 2000 RPM.	43
Figure 19: SEM images of Alfa Aesar WC.....	44

Figure 20: SEM images of 40 wt% Pt on Alfa Aesar WC, (A), (B) secondary electron mode; (C), (D) mixed secondary and backscattered electron mode.	44
Figure 21: SEM images of 40 wt% Pt on Vulcan XC-72R deposited using chlorplatinic acid; images taken using mixed secondary and backscattered electron mode.	45
Figure 22: SEM images of 40 wt% Pt on Vulcan XC-72R deposited using Pt (II) pentan-2,4-dionate; (A-C) mixed secondary and backscattered electron mode, (D) secondary electron mode.	46
Figure 23: TEM images and EDX of Pt dispersed on Alfa Aesar WC using Pt (II) pentan-2,4-dionate. Elemental spectrum and weight concentration for spots 1 and 2 on the TEM image of Pt dispersed on Alfa Aesar WC.	48
Figure 24: TEM image and Pt map for Pt dispersed on Vulcan XC-72R using Pt (II) pentan-2,4-dionate.	49
Figure 25: Cyclic voltammograms for Pt dispersed on Vulcan XC-72R; 0.5 M H ₂ SO ₄ , 30°C, 100 mV/s, 2000 RPM.	50
Figure 26: XRD pattern for Vulcan XC-72R with Pt deposition by Pt (II) reduction to Pt.	51
Figure 27: Cyclic voltammograms for Pt dispersed on Alfa Aesar WC, initially and after 100 oxidation cycles; 0.5 M H ₂ SO ₄ , 30°C, 100 mV/s, 2000 RPM.	52
Figure 28: XRD pattern for Alfa Aesar WC with Pt deposition from Pt (II) reduction to Pt.	53
Figure 29: Cyclic voltammograms for Pt dispersed on Alfa Aesar WC, initially and after 100 oxidation cycles; 0.5 M H ₂ SO ₄ , 30°C, 100 mV/s, 2000 RPM.	55
Figure 30: XRD pattern for Alfa Aesar WC with Pt deposition from Pt (II) reduction to Pt.	56
Figure 31: TGA data for Hispec 4000 and Vulcan XC-72R; under air at 40ml/min, temperature ramped from 50°C to 1000°C at 2°C/min.	58
Figure 32: TGA data for Hispec 4000, Vulcan XC-72R, Pt on Vulcan XC-72R, Pt on ITO, and ITO; under air at 40ml/min, temperature ramped from 50°C to 1000°C at 2°C/min.	59
Figure 33: XRD pattern for 40 wt% Pt on ITO deposited using method I.	59
Figure 34: Normalized activity at different potentials as a result of repeated cycling for different 40 wt% Pt catalysts. Average of three samples with limits of error for each material are plotted.	61
Figure 35: Cyclic voltammograms for ITO both before and after oxidation cycles at 1.8V. 100 oxidation cycles were run; 0.5 M H ₂ SO ₄ , 30°C, 100 mV/s, 2000 RPM.	61
Figure 36: Cyclic voltammograms for 40 wt% Pt on ITO both before and after oxidation cycles at 1.8V. 100 oxidation cycles were run. Electrochemical stability with no change in the CV curves is observed from cycle 30 onwards; 0.5 M H ₂ SO ₄ , 30°C, 100 mV/s, 2000 RPM.	62

Figure 37: Cyclic voltammograms for Hispec 4000, both before and after 100 oxidation cycles; 0.5 M H ₂ SO ₄ , 30°C, 100 mV/s, 2000 RPM.	63
Figure 38: Cyclic voltammograms for 40 wt% Pt on VulcanXC-72R, both before and after 50 oxidation cycles; 0.5 M H ₂ SO ₄ , 30°C, 100 mV/s, 2000 RPM.	64
Figure 39: SEM images of ITO	65
Figure 40: SEM images of 40 wt% Pt on ITO	66
Figure 41: TEM/EDX of 40 wt% Pt on ITO.....	67
Figure 42: XRD pattern for Pt deposited on ITO by reduction of Pt (II) pentan-2,4-dionate.....	68
Figure 43: Cyclic voltammograms of Pt deposited on ITO by reduction of Pt (II) pentan-2,4-dionate after oxidation cycles 2 and 4. The inset shows the CV at initial point.	69
Figure 44: Normalized activity at different potentials as a result of repeated cycling for Pt deposited using chlorplatinic acid (method I) and Pt (II) pentan-2,4-dionate (method II) on ITO. Average of 3 separate samples with limits of error for each material are plotted.	70

LIST OF SYMBOLS AND ABBREVIATIONS

PEMFC	Proton exchange membrane fuel cell
Pt	Platinum
W	Tungsten
ITO	Indium tin oxide
C	Carbon
WC	Tungsten carbide
AAWC	Alfa Aesar tungsten carbide
Vulcan XC-72R	Commercial carbon support widely used in PEMFCs (Cabot, Inc.)
PAFC	Phosphoric acid fuel cell
Oxidation	Removal of electrons
Electrochemical Oxidation	Removal of electrons occurs at electrode of interest. Electrons pass through external circuit to cathode where they carry out reduction.
Corrosion	Unlike electrochemical oxidation, in corrosion both the anode and cathode are on the same surface and no external power supply is required for corrosion to occur. Both oxidation and reduction occur on the same surface, where a potential difference arising from a locally varying chemical environment drives the reaction.
RDE	Rotating disc electrode
CV	Cyclic Voltammetry

MEA

Membrane electrode assembly

ACKNOWLEDGEMENTS

I would like to express my sincere gratitude to my supervisors Dr. Olivera Kesler and Dr. Stephen Campbell for their support and guidance throughout my project. They both provided good laughs and a very safe and stimulating atmosphere.

I would also like to thank Dr. Stephen Campbell, Dr. Paul Beattie and Dr. Silvia Wessel (Ballard Power System Inc.) for their guidance and allowing me to find a way to do my graduate work while continuing to work on other projects at Ballard Power Systems, Inc.

I would also like to thank Mary Mager, for helping me with the Transmission Electron Microscope and High-Resolution Scanning Electron Microscope, and Anita Lam for helping me with X-Ray Diffraction.

Finally, I would like to acknowledge Natural Science and Engineering Research Council of Canada (NSERC) for Industrial Postgraduate Scholarship, Ballard Power Systems Inc., and research funding from the Advanced Systems Institute of British Columbia.

DEDICATION

For my husband and family who were always there for me.

1 Literature Review

1.1 Catalyst support materials- Introduction

Proton exchange membrane fuel cells (PEMFCs) are electrochemical energy conversion devices that react hydrogen and oxygen to produce electricity. They can be used for power generation in portable, stationary, and transportation applications. Loss of performance during extended operation is a major problem hindering commercialization of PEMFCs. Proposed mechanisms that contribute to performance degradation include catalyst particle sintering, catalyst dissolution, membrane degradation, and catalyst support corrosion¹.

The main component of the PEMFC is the membrane electrode assembly (MEA). The MEA consists of two porous electrodes; each catalyzed on one side and bonded with a thin membrane. On the anode side, the hydrogen oxidizes to produce protons and electrons. The protons pass through the electrolyte to the cathode and the electrons are forced through an external circuit, which leads to the cathode side. The electrons travel to the cathode, where they combine with oxygen to produce water. When the electrons are forced through the external circuit, direct electrochemical energy conversion is achieved (Figure 1), resulting in lower pollution and higher efficiency compared to combustion-based energy conversion.

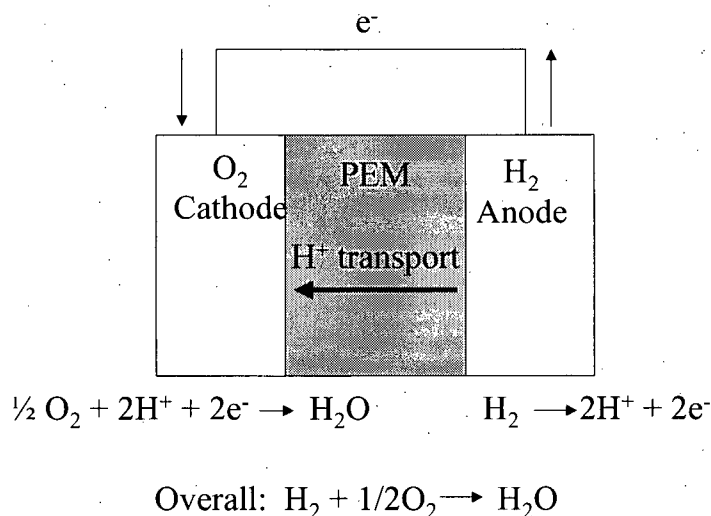


Figure 1: Schematic showing the principle of operation of a proton exchange membrane fuel cell (PEMFC)

The cathode or oxygen reduction electrode is held at relatively oxidative potentials at elevated temperatures, where during the oxygen reduction process atoms generated by the Pt particles may react with carbon atoms to generate gaseous products such as CO and CO₂, resulting in a loss of carbon. This degradation mechanism is very difficult to study because it occurs very slowly compared with the intended catalytic reaction of oxygen with protons and electrons to form water.

In the literature, carbon catalyst support corrosion has been predominantly reported in Phosphoric Acid Fuel Cells (PAFCs). Although the operating temperature range of PEMFCs is lower than that of PAFCs, degradation in performance due to catalyst support corrosion has been observed in PEMFCs during duty cycling. The thermodynamics show that although the rate of oxidation is lower in the case of PEMFCs, it cannot be avoided^{2,3}.

Development of MEAs with longer lifetimes and higher power efficiencies and made from the lowest cost components is ongoing. The electrocatalyst on either electrode (anode and cathode) is usually impregnated into the porous structure of a carbon support material. These support materials can be chemically or physically activated carbons, carbon blacks, and graphitized carbons. Their roles are:

- To provide high surface area over which small metallic particles can be dispersed and stabilized
- To allow facile mass transport of reactants and products to and from the active sites
- To provide electronic and thermal conductivity

Also critical are properties such as porosity, pore size distribution, crush strength, surface chemistry, and microstructural and morphological stability that need to be considered before selecting a suitable support. Catalyst support oxidation has been observed as a serious problem that leads to extensive MEA degradation⁴, limiting MEA lifetimes. Electrochemical oxidation produces microstructural degradation and surface chemical changes, which lead to lost catalytic activity or even catastrophic electrode failure. It is known that carbon oxidizes in aqueous solution, by the following reaction⁵:



Equation 1

The standard electrode potential for this reaction at 25°C is 0.207 V vs. SHE. Carbon is therefore thermodynamically unstable above this potential. Since fuel cell cathodes operate at higher potentials than 0.2V, the carbon catalyst support will oxidize during use.

The carbon support in a PEMFC is susceptible to corrosive conditions such as high water content, low pH, high oxygen concentration, temperature ranging from 50-90°C, and high potential (0.6-1.2 V)⁶. The Pt catalyst also plays a role in accelerating the carbon corrosion. Results from Differential Electrochemical Mass Spectroscopy (DEMS) studied by Roen et al⁶ showed that CO₂ emission was directly proportional to the Pt surface area for carbon in 0.5 M sulphuric acid. At temperatures 30, 50, and 70°C it was found that Pt catalyzed support was easily oxidized compared to the non-catalyzed supports.

PEMFCs in automotive applications are expected to experience up to 30,000 startup/shutdown cycles in their operating lifetime. After shutdown, the hydrogen is removed from the stack. When hydrogen is re-introduced during start-up, electrode potentials in excess of 1.5V may be experienced for short periods of time. This leads to a significant degradation in the fuel cell performance due to oxidation of the carbon catalyst support. The catalyst support must be able to survive the accumulated time at these high potentials, up to 100 hours, in order to provide the necessary durability. According to Mathias et al² the carbon supports currently used in automotive applications (Vulcan XC-72R and Ketjen) do not meet automotive requirements. It is critical, therefore, to have a catalyst support that is more stable than carbon in PEMFCs. Severe catalyst support oxidation has also been observed when a PEMFC is driven into a voltage reversal, which can occur if a cell receives an inadequate supply of fuel. In order to pass current, reactions other than fuel oxidation can take place at the anode, including water electrolysis and oxidation of anode components. The carbon black support at the anode can severely oxidize when the cell goes into reversal. There have been various techniques employed in order to make the cells more tolerant to cell reversal. These include adding a higher catalyst loading or coverage on a corrosion-resistant support⁷. Another approach to make a reversal tolerant anode catalyst involves adding electrocatalyst such as Ru along with Pt⁸. Even though extensive research has been done in making reversal tolerant anodes, similar mitigation strategies cannot be used for cathode support corrosion. The potentials experienced by the anode during reversal are extremely high (in excess of 2 V) when compared to the cathode, and the Ru addition to the anode only aids at these higher potentials. Ruthenium addition to the cathode would not make the cathode oxidation-resistant, since the potentials experienced by the cathode are lower (1.5V to 1.8V) compared to the anode⁹. Therefore, alternative methods need to be sought in order to minimize the cathode support oxidation in PEMFCs.

Reiser et al¹⁰ explain the mechanism of potential excursion (Figure 2). Before startup, both anode and cathode potentials (E_a and E_c) are at the equilibrium potential of oxygen (Figure 2A)

leading to a zero cell potential (V_{cell}). When hydrogen is introduced into the fuel electrode, the anode potential (V_a) reaches the equilibrium potential of hydrogen ($E_{\text{H}_2} = 0\text{V}$), increasing V_{cell}^1 to $\sim 1.2\text{ V}$ (in region 1, Figure 2B). The anode and cathode potentials remain at 1.2V in region 2, where oxygen is still present. Therefore, the cell potential in region 2 is still $V_{\text{cell}}^2 \sim 0\text{V}$. Due to the conductive plates on either side of the MEA, the cell potential of 1.2 V in region 1 then drives the reactions in region 2 in order to have equal cell potential across regions 1 and 2. Due to high electronic conductivity between regions 1 and 2, the cathode cell potential in region 2, which was already at 1.2V, then reaches a maximum theoretical potential of 2.4V. Due to several potential losses the actual potential excursion on the cathode in region B is usually $\sim 1.5\text{V}$. The maximum theoretical potential of $\sim 2.4\text{V}$ is not observed by the cathode in region 2 due to several kinetic losses (high overpotentials for the reactions). The high potential of 1.5V on the cathode leads to oxygen evolution and carbon corrosion at the cathode. The mechanism of this potential excursion is shown in Figure 2¹⁰.

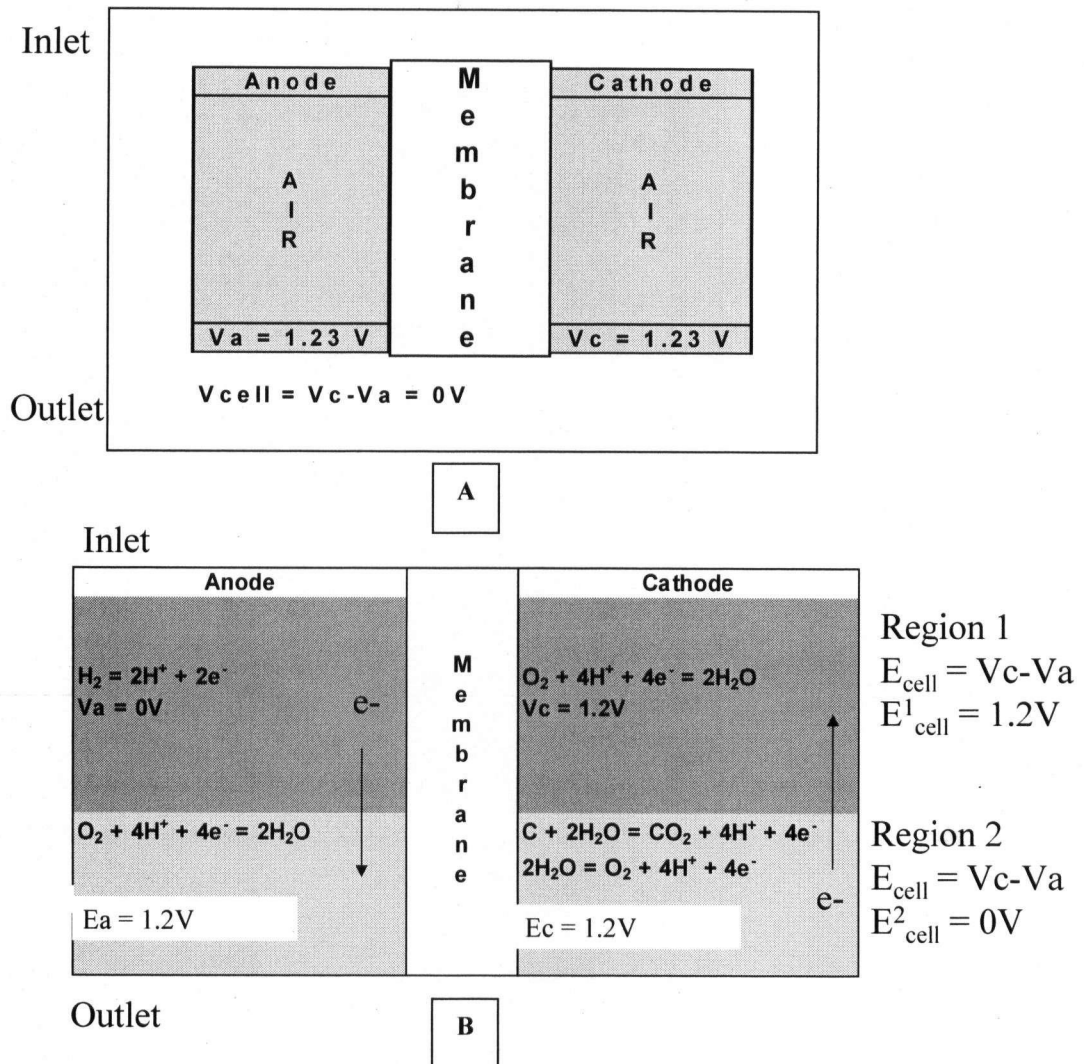


Figure 2: Schematic showing potentials in different regions along the fuel and oxidant sides of a PEMFC before startup (A) and during startup (B). Figure redrawn from work by Reiser et al¹⁰.

Mitigation strategies reviewed by Reiser et al¹⁰ include maintaining a reducing fuel in the anode, e.g., H_2 , CH_4 , etc. Another approach includes reduction of cell voltage by intentionally drawing an electrical load during startup/shutdown¹⁰. Using an inert or somewhat inert gas for purging, such as N_2 , before introducing fuel is another approach suggested by Reiser et al¹⁰. Using inert gas is not an issue for stationary applications, since a cylinder of an inert gas can be attached to the module. However, for the automotive sector, the extra components to be added would add cost in terms of space and weight.

Carbon oxidation in the cathode is not only an issue during startup/shutdown, but also when the car is under operation. During operation, air crosses over and reacts with hydrogen on the anode, causing local fuel starvation. Many approaches have been tried to stop carbon oxidation, but simply finding an alternative support would result in a simpler system. A variety of materials can be used as catalyst supports. A detailed review explaining the problems with carbon supports and the mitigation strategies explained by various researchers is presented here.

1.2 Studies of catalyst supports

1.2.1 Carbon

There are a variety of carbons that are available as catalyst supports, and many characteristics (physical, electrochemical, etc.) must be studied before down-selecting a support for a particular application. The following section reviews the carbon oxidation problems encountered in PAFCs, the proposed microstructures of carbon that accelerate oxidation, and the modifications made to carbon to increase its stability. The carbon oxidation problem in PEMFCs and the role of Pt are also explained in the following section.

Studies using phosphoric acid as the electrolyte

Gruver¹¹ studied the corrosion of carbon black in phosphoric acid; he explains that carbon is thermodynamically unstable under phosphoric acid fuel cell cathode operating conditions. Gruver¹¹ dispersed Pt on Vulcan XC-72 (Cabot Corp.) and investigated the change in microstructure of the carbon by TEM both before and after operating for 1000 hrs at 0.835 V at 91°C. Micrographs showed that the outermost crystalline shell of the carbon particle remained intact, while the central portion, which is more disordered, oxidized away.

Kinoshita et al¹² studied the electrochemical oxidation of high surface area carbon black (Neo Spectra, Columbia Carbon) with surface area of 1000 m²/g in concentrated phosphoric acid at 135°C. They explain qualitatively that two processes occur initially: oxide formation on the surface and CO₂ evolution. As the surface oxide formation decreased, the CO₂ evolution became the major anodic process. The surface oxide growth did not inhibit CO₂ formation. Kinoshita and Bett¹³ later studied the effects of graphitization on the corrosion of carbon blacks. They used three brands of carbon black: Neo Spectra (1000 m²/g), Graphon (100 m²/g, graphitized spheres),

and Vulcan ($220 \text{ m}^2/\text{g}$). Significant CO_2 evolution was observed for non-graphitized carbon compared to graphitized carbon. They also explain that other researchers used potentiodynamic tests to indicate the presence of a quinone/hydroquinone surface species during electrochemical oxidation of carbon blacks. Quinone is a class of aromatic compounds, and the structures of quinone and hydroquinone are shown in Figure 3. Kinoshita and Bett¹³ explain that a wide range of surface oxides is possible during the electrochemical oxidation of carbon.

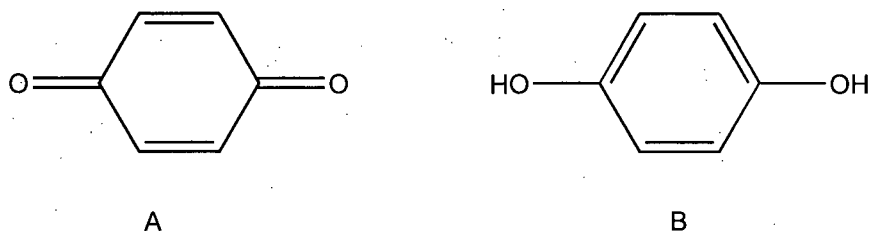


Figure 3: Structure of a) quinone; b) hydroquinone

Microstructural Studies

Heckman and Harling¹⁴ studied the microstructures of thermal blacks, which are a type of high surface area pyrolyzed carbon. The electron micrographs of non-graphitized thermal blacks show that there is some crystallinity on the outer side of these carbons, and the oxidative attack removes the carbon from the inside out, forming hollow capsules. They also claim that not all carbon particles oxidize. For a graphitized thermal black the oxidative attack is very slow compared to in non-graphitized carbons. Also, the oxidative attack on graphitized thermal black occurs from the outside in, and the outer planes generally flake off as they are consumed. Heckman and Harling¹⁴ explain that graphitization seems to produce a thick shell, which is "airtight" and strongly resists oxidative attack.

Smith and Polley¹⁵ studied the oxidation of graphitized carbon black. Graphitized carbon blacks were researched mainly in the 1950's because they have outstanding surface uniformity. Smith and Polley¹⁵ report that when a standard carbon black was treated with air or oxygen at temperatures from $300\text{--}650^\circ\text{C}$, a six-fold surface area increase without particle size change was observed. The increase in area without particle size change was recognized as an increase in porosity upon air oxidation. It was proposed that the increase in area might be caused by preferential attack of the oxygen at the high-energy edge sites of the quasi-graphitic parallel layers of the carbon particles. They further explain that the edge atoms are more susceptible to chemical attack than are the atoms in the center of the basal plane. Heat-treating carbon at

temperatures above 2700°C destroys the high-energy sites. Therefore, Smith and Polley¹⁵ studied whether the preferred sites for oxygen attack are also diminished when carbon is graphitized. They heat-treated carbon black from 1000-2700°C and found a decrease in surface area (determined by adsorption of N₂) with increasing temperature of heat treatment due to some particle sintering. By characterizing the samples under the electron microscope, they observed that as the degree of graphitization was increased, the particle shapes changed from spherical to regular polyhedra. Oxidation of the carbon blacks led to an increase in area of 63.5 m²/g for untreated carbon material, and an increase of 4 m²/g in area was observed for the graphitized carbon. The increase in area of non heat-treated carbon further supports the hypothesis that non heat-treated carbon has high-energy edge sites that are susceptible to oxygen attack.

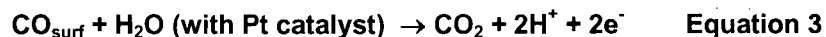
Effect on carbon oxidation after Pt addition

Willsau et al¹⁶ investigated the dependence on the potential of the anodic oxidation of NORIT BRX carbon electrodes using differential electrochemical mass spectroscopy (DEMS) in sulfuric acid. The half wave potentials for the ORR in sulfuric acid are 888 mV (RHE) at the Pt-activated electrode and 483 mV at the pure carbon electrode, respectively. They report that no H₂O₂ was detected in the case of the Pt-activated electrode, whereas peroxide was the main reaction product on pure carbon. Pure carbon undergoes significant oxidation at potentials higher than 0.9V, with CO₂ as the main product. The Pt-activated carbon electrode undergoes oxidation to CO₂ at much lower potentials. Two anodic peaks in cyclic voltammetry resulting from two different oxides are observed for Pt-catalyzed carbon:

- 1) The formation of a CO-surface layer at E > 0.3V (RHE)



- 2) Oxidation of CO_{surf} on Pt between 0.6 to 0.8V

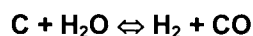


Pt catalyzes the oxidation of a CO-surface layer at potentials between 0.6V and 0.8V, and this potential range coincides with the reduction of the oxygen on these electrodes, causing surface destruction and loss of the active Pt sites.

Stevens et al¹⁷ studied how catalyst support degradation contributes to long-term PEMFC performance degradation. They used samples containing from 5 to 80 wt% platinum supported

on either BP2000 or Vulcan XC-72 carbons. The Pt-loaded carbons were held at elevated temperatures under either dry or humidified conditions for extended periods of time. In order to test samples under humidified conditions, a sealed humidity box was installed in the oven with a steam generator set at 95°C, which was fed with compressed air. At regular intervals, the steam flow was stopped and dry air was fed for two hours in order to dry the samples prior to weighing. If the amount of carbon lost was small after 1000h the catalyst support was considered stable. BET surface area was measured using a 30 vol% N₂/70 vol% He gas mixture. The stability of the catalyst and the support were assessed through a 1.2 V accelerated test protocol. The 1.2 V accelerated test involved testing a 50cm² MEA under H₂/N₂ at 80°C for 50 hours. The cell was held potentiostatically at 1.2 V for 5 hr per cycle and 50 cyclic voltammograms (CVs) were collected, one after each 5 hour interval. They also generated a polarization curve by stepping the cell potential from 0.9 to 0.3V, and then from 0.3 to 0.9 V in 0.05V increments. After monitoring the fuel cell performance the sample was switched back to 1.2 V test conditions.

It was found that carbons with no Pt addition had very low reactivity and were stable up to 150°C under both dry and humid air conditions. The samples containing 5 to 10 wt% Pt on BP2000 showed no weight loss even after 2500 h of exposure, implying slow carbon oxidation reaction kinetics. It was reported that the number of Pt particles per unit area of carbon increased as the Pt loading increased. It was found that Vulcan XC-72 has less carbon loss than BP2000. This difference is mainly because Vulcan XC-72 (BET = 220m²/g) is more graphitic than BP2000 (BET=1300 m²/g). The rate of oxidation was higher for both carbons under humidified conditions. Carbon can be consumed through the water-gas shift reaction:



Equation 4

This is a concern for PEMFCs, as humidification is essential for these types of fuel cells, and the ORR has water as its main product. The high-surface-area Ketjen black carbon supported catalyst was electrochemically more active than the graphitized carbon-black-based catalyst. However, the performance of Ketjen-black based catalyst deteriorated significantly with time, leading to almost complete loss of catalytic activity at 800 mV after only 30 h of accelerated testing. The performance of the Vulcan XC-72 based catalyst also deteriorated with hold time at 1.2 V. The stability of the graphitized carbon black makes the support a more attractive candidate for PEMFCs intended to operate for an extended period.

Kangasniemi et al³ also studied whether a common carbon black, Vulcan, oxidizes under simulated PEMFC conditions. They reported that a variety of carbon surface oxides have been identified by titration and infrared spectroscopy. These surface oxides may be phenols, carbonyls, carboxylic acids, ethers, quinones, and lactones³. They deposited Vulcan XC-72 and 10 wt% polytetrafluoroethylene binder onto Toray carbon paper. A three-electrode electrochemical cell with 1M H₂SO₄ was used for the surface oxidation experiments. A constant potential of 0.8, 1.0, or 1.2V was applied, and CVs were recorded after every 2h. After 16, 60, and 120h of oxidation treatment, samples were removed for surface oxide analysis. They found that Vulcan experienced surface oxidation at potentials $\geq 1V$ at room temperature and $\geq 0.8V$ at 65°C. Surface analysis with XPS found an increase in atomic oxygen over time after the 1.2 V potential holds. An increased current of the cathodic current peak at $\sim 0.55V$ was observed in the CV after a 1.2V hold for 16h at 65°C, indicating a significant surface oxidation of Vulcan.

Kinoshita and Bett¹⁸ determined the impact of Pt on carbon surface oxides for the Pt-catalyzed carbon. The charge due to the electro-active carbon species is difficult to separate from the charge associated with Faradaic reactions on Pt for the Pt catalyzed carbon electrodes. They used 5 wt% and 20 wt% Pt-catalyzed and uncatalyzed Vulcan XC-72 graphitized at 2700°C (BET surface area of 70 m²/g). They explain that halide ions in solution strongly adsorb on Pt, and the current associated with electrochemical reaction on Pt can be significantly reduced in the presence of halide ions. By halide addition to Pt, both Faradaic and non-Faradaic currents of Pt can be minimized. A potentiodynamic sweep allows the determination of the concentration of electro-active carbon oxide. They found that the electrochemical oxidation current on Pt-catalyzed and uncatalyzed graphitized carbons in 96% H₃PO₄ at 160°C and 1200 mV were similar, indicating no catalytic influence of Pt on oxidation of graphitized Vulcan XC-72. The study by Kinoshita and Bett¹⁸ showing that Pt does not catalyze carbon oxidation contradicts the findings by Willsau et al¹⁶, Kangasniemi et al³, and Stevens et al¹⁷. This difference may be the result of interference with the halide ions on the Pt surface. A test with Pt addition and with halide addition to Pt could be compared to resolve the discrepancy.

Doping and other treatments to carbon

Studies by Kangasniemi et al³ and Stevens et al¹⁷ showed that the most common carbon (Vulcan) used for PEMFCs oxidizes under PEMFC conditions. Many modifications as discussed below have been made to carbon in order to stop carbon oxidation. The studies explained below examine various available carbons, as well as the effects of doping with boron (B)⁴ and phosphorus (P)⁵, and of using glassy carbon (GC). McDonald and Stonehart¹⁹ explain that doping carbon with B provides "trap sites" for the Pt crystallites. B enhances the rate of

graphitization at lower heat treatment temperature. They found that Pt supported on boron carbide is more resistant to agglomeration than Pt black (unsupported Pt) or Pt on graphite at equal surface coverage in hot H_3PO_4 . Vulcan XC-72R (Cabot) is the most conductive furnace black commercially available, and has a high BET surface area ($250\text{m}^2/\text{g}$). The drawback is that it does not remain stable at cathode operating temperatures. Since it has been used extensively, it was chosen as the first candidate for doping with B. Since the B doping allows graphitic character (low d_0 lattice spacing) at lower temperature (1600°C), the surface area remains higher than the surface area resulting from heat-treating Vulcan at 3000°C , which is normally necessary for graphitization. Results showed that 1600°C is the T above which no significant additional benefit was obtained when heating B-doped C. Thus B doping allows more efficient utilization of the noble metal electrocatalyst on a more stable support.

It was found by Young et al²⁰ that the oxidation behaviour of samples doped with B and P is quite different from that of only B or only P-doped samples. The concentration of B used was very low and this therefore did not improve carbon crystallinity. Phosphorus results in a proportional increase in oxidation inhibition as its concentration increases; in contrast, B exhibits both a catalytic and inhibiting effect on carbon oxidation. Boron's inhibiting effect can be manifested in the following ways:

- 1) Substitutional boron enhances the graphitization of carbon.
- 2) As the surface carbon atoms are consumed, substitutional boron forms an oxide film (B_2O_3), which acts as an O_2 diffusion barrier and an active site blocker.

Young et al²⁰ report that B acts as a catalyst at low B loadings and as an inhibitor at higher B loadings. The mechanism for the B loading effect was not explained. The formation of a B_2O_3 layer may impact the conductivity of the catalyst support. No tests were done by Young et al²⁰ to examine the impact on conductivity from the boron oxide layer.

Samant et al²¹ synthesized a high surface area mesoporous carbon support for methanol oxidation catalyst using a sol-gel technique. High-density xerogel was synthesized by condensation of the 1,3-dihydroxybenzoic acid and formaldehyde in a molar ratio of 2:1. The carbonization of the gel was carried out in a nitrogen atmosphere at 800°C . A BET area of $724\text{m}^2/\text{g}$ was measured for the synthesized carbon. Pt was anchored using an incipient wetness method where the support is saturated with a Pt salt with a minimal amount of solvent, and the reduction of Pt was carried out by slow addition of 0.1M sodium formate at 60°C . The Pt supported on the high surface area carbon had a particle size of $\sim 2\text{nm}$. Samant²¹ et al found

higher electrocatalytic activity for methanol oxidation in an alkaline medium than in acid solutions. Since the carbon support synthesized by Samant²¹ et al has low activity in acidic conditions, this support cannot be used for PEMFCs, which are known to operate under extremely acidic conditions.

As it is well known that the structure of the carbon support influences the structure of the catalyst layer, carbon materials such as graphite nanofibers, carbon nanotubes, and carbon spheres are being researched for novel supports for direct methanol fuel cell (DMFC) applications. Yang et al²² prepared hard carbon spherules (HCS), using sugar as the precursor. SEM images revealed HCS particles with average diameter of $\sim 2 \mu\text{m}$, which is significantly larger than the supports currently being used for PEMFCs with particle sizes in the 20-100 nm range.

Serp et al²³ analysed literature from the early 1990s until 2003 and discussed the use of carbon nanotubes and nanofibers as catalysts and catalyst supports. Nanotubes are made exclusively of covalently bonded carbon atoms, and they may be the most oxidation resistant fibres²³. When nanotubes are used in catalysis, these conductive supports present clear differences with respect to activated carbon. Carbon Nanotubes (CNT) and Graphite Nanofibers (GNF) were used as metal supports for fuel cell electrodes for the oxygen reduction reaction (ORR). The drawback is that the nanotubes do not have a controlled range of surface area, and the surface areas are usually low ($8 \text{ m}^2/\text{g}$ to $109 \text{ m}^2/\text{g}$) compared to that of Vulcan, $250 \text{ m}^2/\text{g}$. The industrial production of these materials is also currently poor, and homogeneous geometries with controlled diameters are not available. However, the lab-scale data have been promising. The production processes are moving towards more controllable atmospheres, but the homogeneity in characteristics such as geometry, purity, etc. still needs extensive work.

Wang and Swan²⁴ investigated Pt/diamond composite electrodes. Pt particles were galvanostatically deposited onto a boron-doped polycrystalline diamond thin-film surface and entrapped within the dimensionally stable microstructure by a subsequent diamond deposition. Pt particle sizes in the range of 10-300 nm were observed. This particle size range is too wide; Pt particle sizes of less than 20 nm are preferred. These methods may prove to be promising, but the particle size needs to be controlled in a lower range, and the cost of diamond processes may limit the use of this technique in the near future.

The ideal catalyst support should be gas and water permeable, with ability to conduct both electrons and protons. If a material could achieve both ionic and electronic conductivity, then it could replace both carbon and ionomer in the catalyst layer. Conducting polymer/proton

exchange polymer composites have been shown to exhibit high electron and proton conductivities, e.g. polypyrrole and polystyrene sulphonate (PPY/PSS)²⁵. In this work, fuel cells using composite polymer GDE's exhibited an open circuit voltage of 0.63 V and a maximum steady state current density of 97 mA/cm². These values are low compared to values of ~ 1.0V and > 1A/cm² with carbon supported catalysts. The synthesis of PPY/PSS composite and Pt deposition require more studies to produce substantial increases in performance.

Marie²⁶ et al have been doing research into using aerogel-supported catalysts for PEMFCs. Carbon aerogels have high conductivity, high mesoporosity, a small degree of microporosity, and high surface area. They have been considered for the diffusion layer in PEMFCs. A Rotating Disc Electrode (RDE) assembly was used to electrochemically characterize these supports. When synthesizing the aerogel materials, the number of large particles increased with increasing sintering temperature. Pt dispersed on Vulcan exhibited higher active areas than Pt dispersed on aerogel supports. The authors claim that the Pt particles are well dispersed for the aerogels, but most of them are inactive. Also, the porosity of aerogels needs to be monitored, since the Pt might enter pores that are not accessible for the three-phase boundary of ionic and electronic conductor and gas phase.

Rajesh²⁷ et al have studied hybrid materials based on transition metal oxide and conducting material for catalyst supports. The hybrid consists of an organic (polyaniline) and inorganic (vanadium pentoxide) composite. A TEM image of Pt loaded (C₆H₄NH)_{0.41}V₂O₅·0.5H₂O showed nanoparticles with particle size of ~ 10 nm. They claim that when cycling the electrodes between -0.2 and +0.8 V, excellent electrochemical stability was achieved. They also studied the variation of methanol oxidation current densities on Pt loaded (C₆H₄NH)_{0.41}V₂O₅·0.5H₂O nanocomposites and Pt/Vulcan carbon based electrodes. For the nanocomposite-based electrode, as the Pt loading increases, there is a continuous increase in activity. The nanocomposite electrode exhibited two times higher activity compared to the Pt/Vulcan XC-72R carbon electrodes. They also found the decrease in methanol oxidation activity to be 29% for Pt/(C₆H₄NH)_{0.41}V₂O₅·0.5H₂O nanocomposite based electrodes at the end of 2 h, and to be 78% for Pt/Vulcan XC-72R. Both Pt-WO₃ and Pt-MoO₃ have also been used as electrode materials for methanol oxidation. The main issue with these oxides is the severe leaching of the metals such as W and Mo. The technique provides improved electrochemical performance and stability; however, leaching effects of metals need to be closely studied.

1.2.2 Summary

Because carbon may oxidize at potentials above 0.2 V at 25°C, and Pt catalyzes the electrochemical oxidation of carbon, treatments of carbon to make it more oxidation resistant have been sought. A variety of supports is being researched, but detailed electrochemical studies involving cyclic voltammetry, potentiodynamic tests, and thermal stability tests need to be conducted for selection of novel oxidation resistant support materials. A method for rapid evaluation of stability of supports is also in high demand.

Adding dopants to carbon only delays the electrochemical oxidation, but does not prevent it. Aerogel based materials have a high surface area; however, the porosity can be a disadvantage to Pt activity. Organic-inorganic hybrid supports may lead to leaching of metals under fuel cell conditions. The electrochemical stability of nanotubes needs to be determined, and the cost needs to be decreased before they can be used as fuel cell catalyst supports.

Overall, it is of great advantage to the proton exchange membrane fuel cell industry that novel supports are being sought worldwide in order to overcome the electrochemical oxidation of the currently most widely used support (carbon). Little research, however, has been performed to date on the use of non-carbon catalyst supports. Some preliminary studies by several groups have shown the stability of carbides and oxides for some fuel cell applications.

Carbides and oxides are interesting categories that need to be further explored for PEMFCs. However, many commercially available carbides have low surface area, and synthesizing carbides using various methods has mostly been performed for non-fuel cell industrial applications. Tungsten carbide has been used as an anode catalyst in PEMFCs; however, it has not been used as a catalyst support in PEMFC cathodes, where oxidative stability is a more significant challenge. Titanium carbide has also been used as a catalyst support. These studies are reviewed here.

1.3 Carbides

There have not been many studies on using carbides as catalyst supports in PEMFCs. TiC has been used as a catalyst support in PAFCs, and a patent by Jalan et al²⁸ claims the use of titanium carbide as catalyst supports for electrodes in fuel cells. The claims were intended to use this

catalyst support in electrodes for the reduction of oxygen in phosphoric acid fuel cells. The TiC support was compared with conventional carbon black catalyst supports, and it exhibited a lower corrosion current (thus, better corrosion resistance) than the carbon black materials. The stability of TiC as a catalyst support for PAFCs was pointed out to be remarkable; however, more data on longer lifetime degradation would have further supported this claim. The support may provide corrosion resistance, but the overall activity from catalysts using TiC and conventional supports was not compared.

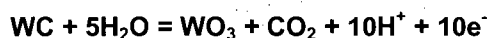
The catalytic behaviour of tungsten carbide for anodic reactions in fuel cells has been studied; however, tungsten carbide based catalyst supports have not been studied. Some studies conducted on the use of tungsten carbide in PAFCs, and its electrochemical and corrosion behavior are reviewed here. Group VI carbides have high thermal conductivity, especially WC, which has the highest thermal conductivity of any of the transition-metal carbides. Like the Group IV and V carbides, the Group VI carbides have low thermal expansion²⁹. WC has the lowest electrical resistivity (conductivity $\approx 10^5$ S/cm at 20°C) of any interstitial carbides and qualifies as the most metallic carbide. WC can be made by direct carburisation of the metal with carbon or graphite at 1400-2000°C in hydrogen or vacuum. The carbide formation process can also use tungsten oxide, tungstic acid, or ammonium tungstates as the starting materials²⁹.

1.3.1 Tungsten carbide and electrocatalysis

In order to reduce the cost by reducing the amount of Pt in a fuel cell, it is practical to search for a substitute base metal as a catalyst. Aside from being good electrical conductors and having good catalytic activity, electrocatalysts used in acidic electrolytes should also be acid resistant. The standard reversible potential for the oxygen reduction reaction (ORR) is 1.23V, but kinetic limitations for the ORR lead to cell overpotential loss of 0.3-0.4V. Meng et al³⁰ observed the synergistic effect of the addition of tungsten carbides (W_2C/C) to Pt catalysts on the ORR in alkaline media. They explain that pure W_2C with a particle size of <10 nm can be prepared by controlling the ratios of W to C to less than 20 wt%. They observed ten times larger current density for Pt- W_2C/C than for Pt/C. They did not explain the mechanism for the improvement of oxygen electroreduction. For direct methanol fuel cells (DMFCs) a major problem is the crossover of methanol from anode to cathode, which depolarises the cathode. They evaluated the catalytic effect of W_2C/C by measuring the kinetic parameters using Tafel plots with 1 M KOH solution, and studied the impact of addition of 0.1 M methanol on ORR at 25°C with a scan rate of 1 mV/s. The activity of ORR on the Pt/ W_2C/C electrode was hardly affected by methanol at concentrations up to 1 M at room temperature; however, the ORR on the Pt/C electrode was

seriously affected by methanol. The Pt/W₂C/C exhibited a more positive onset potential of 50mV compared to that of Pt/C (-48mV). Also, Pt/W₂C/C exhibited a higher exchange current density (*i*₀) of 0.180 x 10⁻⁴ mA/cm² than the Pt/C catalysts with *i*₀ 0.119 x 10⁻⁵ mA/cm². The W₂C modified Pt not only showed a synergistic effect to improve the activity for ORR, but also immunity to methanol.

Lee et al³¹ studied the stability and electrocatalytic activity of WC by addition of Ta catalyst. They report that studies have shown the instability of WC under acidic and oxidative conditions. The WC + Ta or the pure WC were deposited on glassy carbon using RF sputtering. The stability and the electrochemical activity for the ORR were investigated in a solid-state cell with Nafion 117 as the electrolyte. The cell was maintained under either oxygen or nitrogen atmospheres, which were humidified by passing through a bubbler. The XRD pattern had only two peaks at 35.8 and 41, corresponding to WC and Ta, respectively. The CV's of pure WC at 30°C and 60°C showed an anodic peak above 0.5 V at 30°C, and at 60°C larger anodic and cathodic currents were observed. The CV data showed that the Ta addition to WC showed no anodic peak up to 1V at both 30°C and 60°C. The oxidation of WC by anodic polarization may proceed as³¹:



Equation 5

Lee et al³¹ carried out slow scan voltammetry in N₂ and O₂ atmospheres. Under N₂ they observed an increase in the cathodic current for pure WC, which might have been due to partial reduction of W(VI) oxide to W(V) oxide. The increase in cathodic current was not observed for WC + Ta catalyst under the N₂ atmosphere. The onset potential for the ORR was observed at 0.8V (vs. SHE), which is 0.35V higher than that for pure WC catalyst. From these data they conclude that Ta addition to WC enhances its stability and electrocatalytic activity. They claim that the enhanced stability of WC with Ta catalyst might be due to the formation of W-Ta alloy in the WC + Ta catalyst. However, a key experiment using a pure Ta catalyst for ORR under these conditions was not conducted. Studying Ta catalyst alone would have allowed a determination of whether it is the Ta₂O₅ formation on the surface of WC causing the enhanced electrocatalytic activity or whether there is an interaction between Ta and WC. If Ta₂O₅ is active under the conditions used by Lee et al³¹ then it might be that WC is not required; therefore, the results should have been compared to Ta catalyst as the blank.

Ma et al³² studied the electro-oxidation behaviour of tungsten carbide electrodes in different electrolytes using a three-electrode electrochemical cell. They studied the anodic charge of tungsten carbide and Pt in 3.5 M HCl. The results showed that the charge consumed by hydrogen

adsorption and desorption on WC and Pt electrodes was 0.17 C/cm^2 and 0.48 C/cm^2 , respectively, proving that the tungsten carbide has lower electrocatalytic activity for hydrogen oxidation in HCl solution than Pt. When they tested a WC electrode in $2 \text{ M H}_2\text{SO}_4$ under H_2 , the potential increased significantly as a consequence of the oxidation of tungsten carbide. The color of the electrode also changed to blue (W_2O_5 and W_8O_{23}) and yellow (WO_3). Oxygen evolution and chlorine evolution were also observed when H_2SO_4 and HCl were used as the electrolytes, respectively. They also studied the electro-oxidation behaviour of tungsten carbide electrodes in 2.5 M KOH solution and found that the activity and stability of WC for hydrogen oxidation was extremely low, and that WC directly oxidized to WO_3 in basic media. The WC electrode exhibits high electrochemical stability for hydrogen ionization in acidic electrolytes when the potential is below 800 mV . Above 800 mV the authors claim that the overall electrochemical reaction of WC in acidic solutions follows equation 5.

Ma et al³³ also prepared and determined the electrocatalytic properties of tungsten carbide electrocatalyst. They report that WC displays "platinum-like" behaviour in several reactions. They also mention that a $\text{H}_2\text{-O}_2$ fuel cell stack with a continuous run lifetime of 5000 h at 150°C has been achieved using H_3PO_4 as the electrolyte, Pt as the cathode, and WC as the anode. They synthesized tungsten carbide electrocatalysts by reduction of H_2WO_4 under a flowing CO and CO_2 mixture with $\text{CO}:\text{CO}_2 \sim 1:10$. The samples were carburised at $750\text{-}800^\circ\text{C}$. After carburisation the WC electrodes with surface area of 3 cm^2 were prepared by cold pressing the mixtures of tungsten carbide particle and PTFE binder onto metal mesh substrates. When the material was heat-treated at 700°C , $\sim 71\%$ W_2C was present, and when the temperature was increased to 750°C , $\sim 69\%$ WC was synthesized. The $\text{W}_2\text{C}:\text{WC}$ ratios were calculated from XRD peak heights. The BET measurements showed that the samples with WC as the major phase had a higher surface area ($25\text{-}30 \text{ m}^2/\text{g}$) than the samples with W_2C as the major phase ($5\text{-}10 \text{ m}^2/\text{g}$). They report that the W_2C phase of tungsten carbide exhibits higher electrocatalytic properties than WC for the hydrogen anodic oxidation reaction in concentrated H_3PO_4 solution. However, the corrosion resistivity of W_2C derived from H_2WO_4 at elevated temperatures is poor. The anodic properties of W_2C and WC electrodes in 12% HCl solution were investigated. The overpotential of WC electrodes was found to be much lower than that of W_2C electrodes. The Tafel slope of the WC electrode was twice as large as that of the W_2C electrode, indicating the different mechanism of hydrogen anodic oxidation for the two electrodes³³. The surface area reported by Ma et al³³ is low compared to the available high surface area carbon supports ($\sim 300 \text{ m}^2/\text{g}$).

There are many patents filed regarding use of W or WC as anode electrocatalysts in fuel cells. Joel Christian et al³⁴ from Osram Sylvania have filed numerous patents on the use of W containing catalysts. The synthesis of catalyst is achieved by low temperature electrochemical activation of W containing precursor deposited on a C support. Ammonium meta tungstate (AMT) was dispersed on Carbon (Vulcan XC-72R), and this catalyst precursor was used as the anode of a PEMFC. The formation of a W-containing catalyst layer on a C support was confirmed by sputtered neutral mass spectroscopy (SNMS) and X-ray photoelectron spectroscopy (XPS). Na₂CO₃ (2M) solution was used as an electrolyte and 0.5-30 V DC was applied to activate the precursor to form W-containing catalyst. The loading of this catalyst precursor on to C can be increased by the use of a surfactant, cetylpyridinium chloride. They claim that power output can be increased by 20% relative to Pt containing catalysts. Similarly they claim that the MEA that they made (5 cm²; 0.5 mg catalyst/cm²) has similar performance to that of Pt catalyst with a similar loading. Joel et al³⁵ have also been looking at supporting WC on high surface area carbon in order to make WC containing catalysts. They synthesized WC material by reacting a mixture of a tungsten precursor and a high surface area support in flowing hydrocarbon with or without H₂ gas at 500°C-800°C in a tube furnace. They report that the composition they made might be WC_{1-x} (x = 0 to 0.5). Particulate sizes of 15 Å- 30 Å were achieved, with a surface area of 65 m²/g. Major claims were on the process of making WC. The application of WC catalyst in a PEM fuel cell was not demonstrated in this patent.

A main problem with using commercial carbides and nitrides is their low specific surface area. The search for methods of producing high surface area has been developing since 1985, when a patent was granted to Boudart et al³⁶ for high specific surface area carbides and nitrides. The desired carbides and nitrides were produced by reducing oxides of the desired element in a reducing environment at high temperatures with carbon and nitrogen present in this atmosphere. They showed that the BET surface area of molybdenum carbide made using this method (51 m²/g) was at least 4 times higher than that of the conventional catalyst (12.5 m²/g). This method results in increased surface area, but the surface area achieved by Boudart et al³⁶ is still lower than required for fuel cell electrode applications. Claridge et al³⁷ used the method tested by Boudart et al³⁶ to synthesize high surface area molybdenum and tungsten carbide based catalysts. They used temperature-programmed reduction (TPR) of the relevant oxides in flowing methane or methane/hydrogen mixtures. The formation of the carbide was monitored using XRD.

They claim that very broad peaks for the oxide were seen, indicating that a very small amount of oxide is present. However, usually broad peaks mean smaller crystallite size. The BET surface

areas of the samples were $30 \text{ m}^2/\text{g}$ for Mo_2C and $20 \text{ m}^2/\text{g}$ for WC; however, these surface areas are still small for fuel cell application.

Thompson et al³⁸ in their granted patent claimed use of noble metal catalysts supported on electrically conductive transition metal (Group IV to VI) based ceramics such as carbides, nitrides, borides, or silicides. They showed examples using WC, for which XRD data were acquired but no fuel cell data were shown. The desired surface area for the support was approximately $40 \text{ m}^2/\text{g}$, which is significantly lower than the surface area of the current carbon support ($\sim 300 \text{ m}^2/\text{g}$) being used extensively for PEMFCs.

1.3.2 Summary

Use of tungsten carbide (WC) as a fuel cell catalyst has been made in the past, but detailed study on its use has not been reported as a catalyst support in PEMFCs. Detailed tests involving oxidation cycles under simulated or actual fuel cell conditions need to be conducted in order to observe the oxidation stability of tungsten carbide. The possibility of tungsten carbide oxidizing to tungsten oxide and the conditions under which this happens need to be verified in order to use WC as a catalyst support in PEMFCs. High surface area carbides need to be synthesized before they can be used in PEMFCs. The impact on stability and performance from using WC or W_2C phases also needs to be determined.

Alternative supports such as conducting oxides are an emerging category of oxidation resistant catalyst supports, and are also of interest in this work. The use of conducting oxides in fuel cells by several groups is described in the following section.

1.4 Oxides

Metal oxides are one of the most important categories of solid catalysts or catalyst supports³⁹. Metal oxides such as TiO_2 , and In_2O_3 are n-type semiconductors. Tin doped In_2O_3 (ITO) is a widely used transparent conducting oxide (TCO). There are only a few studies conducted using Nb-doped titania as a catalyst support. The key findings of these studies are reviewed here. It is believed that since doping with aliovalent ions can enhance conductivity, both Nb-doped titania and ITO might be sufficiently electrically conductive to be used as catalyst supports.

Single cation stoichiometric oxides such as titanium dioxide (TiO_2) are resistive; however, titanium sub-oxide, including Ti_4O_7 and other phases, exhibit electronic conductivity. The drawback with titanium sub-oxide is that under fuel cell operation it becomes stoichiometric and forms a resistive layer of TiO_2 at the three-phase reaction interface⁴⁰. Chen et al⁴⁰ have studied Nb doped rutile, $\text{Ti}_{0.9}\text{Nb}_{0.1}\text{O}_2$. This material has many beneficial characteristics for use as a catalyst support in PEMFCs. They used Ebonex (Atraverda Ltd., U.K.), which is an electrically conductive ceramic consisting of several suboxides of titanium dioxide, mainly Ti_4O_7 and Ti_5O_9 . In spite of the presence of reduced titanium, Ebonex is electrochemically stable in both acidic and basic solutions. It also has a high conductivity ($\sim 10^3$ S/cm) and good corrosion resistance. It is well known that the electronic conductivity of titanium-based ceramics originates from the presence of Ti^{3+} ions. There are two ways to create the Ti^{3+} ions in the rutile structure: by creating oxygen vacancies by heating TiO_2 in a reducing atmosphere, or by introducing appropriate donor dopants, e.g., Nb. They synthesized two conductive titanium ceramics, Ti_4O_7 and $\text{Ti}_{0.9}\text{Nb}_{0.1}\text{O}_2$, made, respectively, by reducing and doping rutile titanium dioxide. Both ceramic samples were dark blue in color, and had an electrical conductivity in the range of 0.2-1.5 S/cm (two-point measurement technique). BET surface area was relatively low for all three supports, 2 and 1.4 m^2/g for the synthesized Ti_4O_7 and $\text{Ti}_{0.9}\text{Nb}_{0.1}\text{O}_2$, respectively, and 1 m^2/g for Ebonex. The CVs of the ceramics showed a wide potential window of stability ranging from -0.4 to 2 V vs. RHE, while Vulcan XC-72R carbon, a commonly used electrocatalyst support, experiences oxidation current at positive potentials as low as 1.0 V. These supports seem promising based on the electrochemical stability data; however, lifetime data are still needed to compare with conventional carbon supports to determine the benefits of the oxide supports.

The Ti_4O_7 -supported catalyst showed catalytic activity very similar to that of the Ebonex supported catalyst for ORR, while the catalyst supported on the $\text{Ti}_{0.9}\text{Nb}_{0.1}\text{O}_2$ exhibited higher currents at all applied voltages. The catalytic activity of Ebonex- and Ti_4O_7 -supported catalysts decreased with operation, and the authors explained that these non-stoichiometric oxides oxidized to resistive stoichiometric oxides, resulting in a greater internal iR drop. TGA data showed that both Ebonex and Ti_4O_7 are oxidized to TiO_2 , beginning at about 400°C and continuing to 600°C, whereas $\text{Ti}_{0.9}\text{Nb}_{0.1}\text{O}_2$ does not show a significant weight gain up to 1000°C. After heating in air for 20 h at 500°C, Ebonex and Ti_4O_7 turned white and their conductivity decreased by at least five orders of magnitude, consistent with complete oxidation to a Ti (IV) oxide. Under the same conditions, the conductivity of $\text{Ti}_{0.9}\text{Nb}_{0.1}\text{O}_2$ decreased by approximately 0.1% of its initial value and its color changed gradually from deep blue to blue-gray. Nb doped

titania is both thermally and electrochemically stable compared to reduced titania; however, the synthesis method used by Chen et al⁴⁰ does not provide a high surface area support. Sol-gel derived supports may provide a higher surface area.

An alternative doped oxide is ITO. Details on the studies conducted by other researchers on ITO are reviewed here. ITO is widely used as a transparent conducting oxide for smart windows. A conductivity of 10^4 S/cm is often quoted for an optimized ITO film. Study of this material as a catalyst support has not been extensive. Electronic characteristics studied by other research groups are reviewed here. However, because it is an n-type semiconductor, it may exhibit similar behavior to that of Nb doped titania. Liu et al⁴¹ prepared ITO films by sol-gel dip coating on glass substrates. Hall effect measurements showed an increase in electrical carrier concentration with increasing SnO₂ content. The effect of the SnO₂ content on the sheet resistance of 70 nm thick ITO monolayers showed that the sheet resistance was a minimum at ~11 mol% SnO₂.

Matveeva⁴² studied the electrochemical behavior of ITO in acid and base electrolytes and noted that it dissolves, especially at pH less than 1. Matveeva⁴² found that in 1 M NaOH during cathodic polarization, the electrode components are deeply reduced, so that ITO is gradually and irreversibly converted to a metallic mirror with a noticeable decrease of oxygen content. At a high anodic current density, the ITO electrode undergoes modifications and its conductivity decreases, also due to the change of oxygen content in the oxide lattice. Matveeva⁴² used electrochemical conditions that would allow the characterization of ITO for smart windows. The electrochemical stability of ITO as a catalyst support has not been studied.

Mason et al⁴³ found that up to 6-cation % Sn was soluble in In₂O₃, and the resulting materials were conductive with high electron populations. They hypothesized the existence of neutral reducible $(2\text{Sn}_{\text{In}}\text{O}''_{\text{i}})^{\times}$ associates, which form upon doping of In₂O₃.



Equation 6

The $(2\text{Sn}_{\text{In}}\text{O}''_{\text{i}})^{\times}$ cluster can be reduced at lower temperatures to remove the oxygen interstitials. It may be that $(2\text{Sn}_{\text{In}}\text{O}''_{\text{i}})^{\times}$ associates play a major role in the defect chemistry of ITO compared to the intrinsic defects (i.e. oxygen vacancies). These associates may be responsible for the high concentrations of Sn that can be incorporated into ITO. Once incorporated, the excess Sn tied up in neutral associates serves as a reservoir for the production of additional free Sn-donors upon removal of oxygen interstitials during reduction.

Within the oxide category, the use of zeolites as catalyst supports has also been reported. Scelel⁴⁴ filed a patent in which use of noble metal catalysts supported on conductive zeolite particulate material as catalyst support is claimed. This support material uses 65 wt% C and 35 wt% conductive zeolite. They claim that the zeolite preferably has a surface area of between about 100 to about 400 m²/g and C between 10 to about 50 m²/g. The zeolites have acidic protonic entities on the surface, making them hydrophilic relative to carbon. Zeolites consist of 1, 2, or 3 dimensional channels, and conductive polymers may fill these. This patent is based on a concept, and no proof of concept has been achieved. There are no data to prove if the desired surface area has been achieved, whether zeolites are sufficiently conductive, what is the impact of having 35% carbon in the support material, and finally whether this material can withstand the fuel cell conditions.

1.4.1 Summary

ITO is electrically conductive and is relatively stable in acid with pH greater than 1. As explained above, doping with pentavalent ions can enhance the electronic conductivity of tetravalent metal oxides. Oxygen deficient oxides may not be stable in PEMFCs, and therefore doping is one of the methods to stabilize the electronic conductivity. In the Nb doped titania system, lifetime durability testing still needs to be conducted and the surface area needs to be increased before it can replace carbon in widespread use. ITO prepared via sol-gel methods is a good candidate for non-carbon catalyst supports for PEMFCs; however, electrochemical stability and lifetime data are still not available for this material. There has been no published work showing the electrochemical stability of ITO as a catalyst support.

1.5 Conclusions

Carbon will oxidize at potentials above 0.2 V at 25°C, and adding dopants to carbon only delays the electrochemical oxidation but does not prevent it. Little research, however, has been performed to date on the use of non-carbon catalyst supports. Alternative catalyst supports such as tungsten carbide and Indium tin oxide can be used as catalyst support materials in PEMFCs. High surface area carbides and oxides are not yet commercially available. Detailed tests involving oxidation cycles under simulated or actual fuel cell conditions need to be conducted in order to observe the oxidation stability of tungsten carbide and ITO. There has been no published work showing the electrochemical stability of ITO and tungsten carbide as alternative catalyst supports for PEMFCs.

2 Introduction to the three electrode electrochemical cell, voltammetry and rotating disc electrode (RDE)

2.1 Three electrode electrochemical cell

A typical three-electrode electrochemical system consists of a working, reference and counter electrode immersed in an electrolyte solution. The electrochemical reaction occurs at the working electrode (WE), leading to an electron transfer. This electron transfer generates an electrical current termed Faradaic current. A potentiostat, which controls the potential, imposes a cyclic linear sweep on the working electrode, from which a current-potential curve is obtained. An auxiliary or counter electrode (AE) is driven by the potentiostat to balance the Faradaic process at the WE with an electron transfer of opposite direction. This causes oxidation to take place at the AE if reduction occurs at the WE. The reference electrode provides a fixed potential, which does not vary during the experiment (potential should be independent of the current density). Potential of the reference electrode is known and is kept constant. The potential between the WE and the

RE is controlled by a potentiostat and any change in applied potential to the cell appears directly across the WE-solution interface. The Faradaic current at the WE is transduced to a potential output at a particular sensitivity (A/V) and recorded in a digital or analog form.

2.2 Voltammetry

Voltammetry is an electroanalytical method allowing evaluation of an analyte by measuring current as a function of applied potential. Voltammetry is used for fundamental studies of oxidation and reduction processes in various media, adsorption on surfaces, and electron transfer mechanisms on electrode surfaces⁴⁵. In voltammetry, various excitation signal waveforms are possible. Linear-scan voltammetry, which is a potential vs. time waveform, is most commonly used.

2.2.1 Cyclic voltammetry (CV)

CV is a potential controlled electrochemical experiment, in which the direction of the potential is reversed at the end of the first scan. A cyclic potential is usually imposed on an electrode and the current response is measured. Reversibility is advantageous, since the product of the electron

transfer reaction that occurred in the forward scan can be probed again in the reverse scan. It is a powerful tool for determining formal redox potentials, detecting chemical reactions that precede or follow the electrochemical reaction, and evaluating electron transfer kinetics. A CV is usually plotted as current vs. potential. Figure 4 shows a typical CV of Pt in 1.0 mol/dm³ H₂SO₄ at 25°C. Four major regions are evident from the CV.

In forward sweep:

- 1) Oxidation of adsorbed H₂ at 0.0 to about +400 mV, with the twin peaks corresponding to weakly bound and strongly bound (at higher positive potentials) hydrogen atoms.
- 2) In the center of the voltammetric curve is a region where only low currents (positive anodic for the positive sweep and negative for the negative sweep) can be found. This is the double-layer region where only capacitive processes take place.
- 3) Oxide film formation occurs at about +750 mV and continues to potentials above +2000 mV.
- 4) Oxygen gas evolution starts at ~ +1500 mV.

In reverse sweep:

- 1) Oxide reduction is observed below +1000 mV.
- 2) Double layer region is followed by
- 3) Hydrogen adsorption at +400 mV and then
- 4) Hydrogen evolution at 0.0V

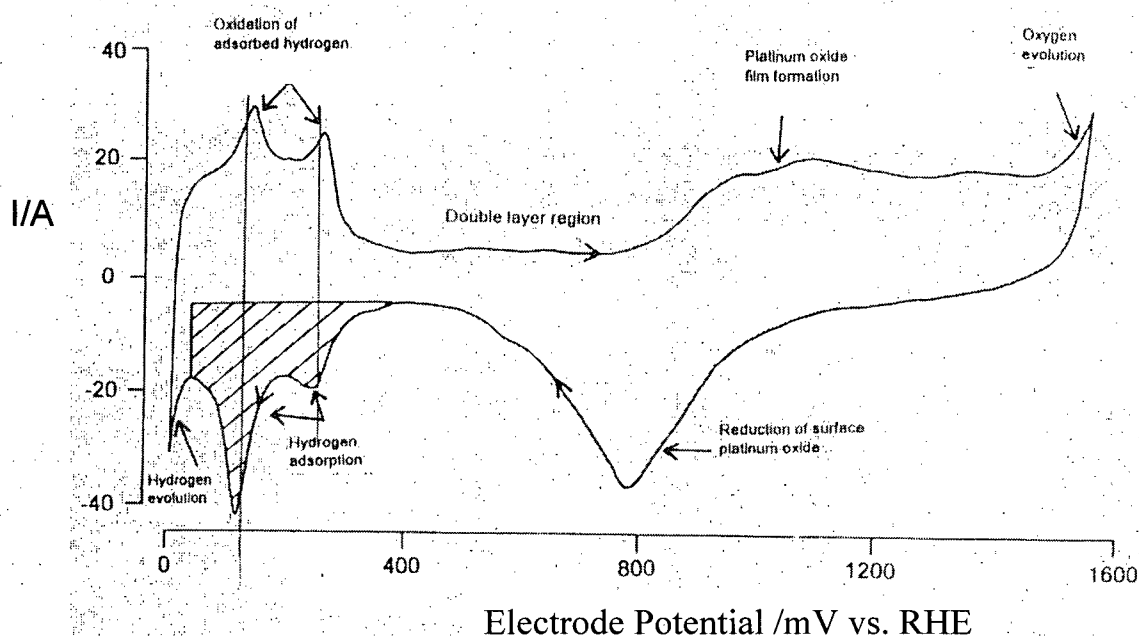


Figure 4: Cyclic voltammogram of Pt GDE in 1.0 mol/dm³ in H₂SO₄ at 25°C, $v = 30\text{mV/s}$

2.3 Convection and rotating disc electrode (RDE)

Convection allows transport of species due to external mechanical forces such as moving of the electrode or stirring of the solution. Convection is an important form of defined and reproducible mass transport; during which current densities 3-100 times greater than the steady state diffusion limited value are common⁴⁵. The rotating disc electrode is the most popular system for kinetic and mechanistic studies. An RDE consists of a working electrode material (usually glassy carbon or Pt) enclosed in a Teflon or ceramic sheath.

An RDE when rotated in a solution acts as a pump, pulling the solution vertically upwards towards the disc and then throwing it outwards. The key advantage with using an RDE is that the rate of mass transport to the electrode may be varied over a substantial range and in a controlled way, without rapid change in the electrode potential. Some of the problems are that the solution can leak into any gap between the active disk material and the insulating sheath. Also, noise from poor electrical contacts can lead to a problem. To avoid this problem the shaft of the RDE is

usually directly linked to the motor drive, and the contact is made with a high quality carbon brush contact (Ag/C material).

3 Objectives

As stated above, acute degradation of catalyst supports in PEMFCs is hindering the commercialization of these fuel cells. The objective of this study is to evaluate two types of oxidation-resistant catalyst supports for PEMFCs. The objectives for these investigations involve dispersing Pt on commercial tungsten carbide and indium tin oxide (ITO) and then determining the electrochemical and thermal stabilities of these materials. The Pt dispersion methods used for commercial materials were also used to disperse Pt on widely used carbon (Vulcan XC-72R, Cabot) in order to compare the activity of materials prepared by similar methods.

4 Experimental Procedure

Pt was supported on both WC and ITO, and the electrochemical stability of the supported catalyst was determined using oxidation cycles and cyclic voltammetry. The conventional method of Pt dispersion (referred to as method I for Pt addition) by hydroxylation of chlorplatinic acid with a base such as sodium hydrogen carbonate followed by reduction using formaldehyde was not successful to disperse Pt on WC. Pt addition by method I involved using sodium hydrogen carbonate, which reacted with WC and formed flakes of unknown material. Therefore, an alternative method needed to be designed. Pt addition using Pt (II) pentan-2,4-dionate precursor (referred to as method II for Pt addition) was developed in-house, leading to a successful Pt dispersion onto WC.

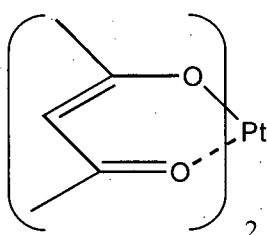
4.1 Pt addition using chlorplatinic acid (method I)

3.44g NaHCO_3 was dissolved in 200ml H_2O in a 500ml round bottom flask. To this was added 0.60g of the catalyst support. The mixture was refluxed for several hours to ensure complete wetting of the support. Using an addition funnel, 1g H_2PtCl_6 dissolved in 60ml H_2O was added drop-wise over several minutes. The mixture was again allowed to reflux for two hours. 780 μl formaldehyde (methanal HCHO) solution (37%) in 7.8ml H_2O was added by addition funnel over

approximately one minute. The mixture was allowed to react and reflux overnight before filtering, washing with water, drying, and grinding.

4.2 Pt addition using Pt (II) pentan-2,4-dionate (method II)

Pt (II) pentan-2,4-dionate (Alfa Aesar, ~48 wt% Pt) was used as the Pt precursor and then later reduced under hydrogen atmospheres. Pt (II) pentan-2,4-dionate was found to be insoluble in water, so acetonitrile was used.



Pt (II) pentan-2,4-dionate

To obtain 40 wt% Pt on WC, 0.50 g of Pt (II) pentan-2,4-dionate was dissolved into 110 mL acetonitrile. To this was added 0.36 g of Alfa Aesar WC. The solvent was allowed to evaporate and the resulting solid was heat treated in a tube furnace at 600°C for 5 hours under 20 vol% Ar/balanceH₂.

4.3 Pt addition to equal powder volumes of support (for WC studies only)

This procedure involves dispersing similar amounts of Pt onto supports that have a significant density difference; e.g., carbon compared to WC, which have densities of 1.8 g/cm³ and 15.6 g/cm³, respectively. Usually 40 wt% Pt is dispersed on carbon, but since the density difference between WC and C is large, direct comparison between 40 wt% Pt on WC and 40 wt% Pt on C does not provide sufficient information to directly compare activity levels and even degradation rates. Therefore, an alternative method was used in which 40 wt% Pt was dispersed on C and a similar volume fraction of Pt was dispersed on the WC support material, using tapped powder densities for comparison.

Tap density is the density of a powder when the volume receptacle is tapped or vibrated under specified conditions while being loaded. Tap density was used to measure similar powder volumes of the support materials. The tap density method involved packing 2 ml of a support powder in a glass cylinder. The cylinder was tapped on a counter top 200 times until 2 ml of well packed support material was achieved. Both carbon and tungsten carbide were tapped to a

volume of 2 mL. A solution of Pt (II) pentan-2,4-dionate (Alfa Aesar, ~48 wt% Pt) dissolved in 100 ml acetonitrile was prepared. For carbon, 40 wt% Pt was added, and a similar amount of Pt as that for carbon was added to WC. The Pt (II) solution was added to the 2 ml packed support material, and the solution was then heated to dry. The resulting solid was heat treated in a tube furnace at 600°C for 5 hours under 20 vol% Ar/balance H₂. The heat treatment allowed Pt (II) reduction to Pt metal.

4.4 Pt addition to carbon and tungsten carbide by solid density method (for WC studies only)

In section 4.3 carbon was tapped to a volume of 2 ml with a mass of 0.1140g. Using the solid densities of carbon and WC, 1.8 g/cm³ and 15.6 g/cm³, respectively, the amount of WC having the same solid volume was calculated to be 0.99 g. To 0.99 g of WC the same amount of Pt was added as in section 4.3 (40wt% Pt relative to carbon). Both the Pt addition and reduction were carried out as explained in section 4.3.

4.5 Thermogravimetric analysis (TGA)

Thermogravimetric analysis (TGA) was used to determine the stability of the conventional Pt/C, Pt/WC and Pt/ITO to oxidation in air (40 ml/min) as the temperature was ramped from 50°C to 1000°C at 2°C/min. The samples were held at 50°C for five minutes to allow more time for water to be removed gently. The same procedure was also used to test catalysts containing 40 wt% Pt on Vulcan XC-72R and commercially available Hispec 4000 (40 wt% Pt on Vulcan XC-72R; Johnson Matthey). The data were analysed by either plotting the derivative of the mass (dm/dT) as a function of sample temperature, or by plotting the normalized weight as a function of sample temperature.

4.6 Rotating disc electrode (RDE) and electrochemical test set-up

To test the electrochemical stability of the catalyst supports, 20mg of each supported catalyst was dispersed in 2ml of glacial ethanoic acid using ultrasound. Using a micropipette, 5µl of the suspension was dispensed onto the flat surface of a polished glassy carbon (GC) rotating disc electrode (RDE). The solvent was removed gently with a hot air blower, leaving supported

catalyst (50 μ g) on the disc. The commercial 5 vol% alcoholic Nafion™ (DuPont), with EW of 1100 was diluted by addition of 0.5 ml of 5 vol% alcoholic Nafion™ in 5 ml propanol. Using a micropipette, 5 μ l of diluted alcoholic Nafion™ was dispensed onto the disc. The solvent was allowed to slowly evaporate in still air in a glass enclosure so that a coherent Nafion™ film was cast over the catalyst and the disc. The RDE was then immersed in deoxygenated 0.5M H₂SO₄ at 30°C and rotated at 33.33Hz (2000rpm). The electrochemical cell comprised a glass working compartment with a water jacket connected to a circulating water bath and two side compartments: one containing a Pt gauze counter electrode connected by a glass frit, and the other containing the reversible hydrogen electrode (RHE) connected by a Luggin capillary.

Based on preliminary voltage cycling experimental results, the oxidation potential chosen for the electrochemical cycling tests was +1.8V vs. RHE. Above +1.8V, considerable gas was evolved, which separated the catalyst/ Nafion™ deposit from the disc. At lower potentials, the oxidation was not detectable in a suitable experimental timeframe. The oxidation cycling procedure was as follows. Using an EG&G 263 (PAR, Princeton, NJ) potentiostat with Corrware software (Scribner Associates), potential steps (oxidation cycles) between 0.6 V and + 1.8V were applied. The electrode was held at 0.6V for 60 seconds and at 1.8 V for 20 seconds. A Cyclic Voltammogram (CV) was recorded between 0.0V and 1.4V at 100mV/s before the oxidation cycles began and then again after every 10 oxidation cycles, until a total of 100 oxidation cycles had been applied. Three separate tests were completed for each sample to observe repeatability.

4.7 X-Ray Diffraction (XRD)

X-Ray Diffraction (XRD) was used to determine the presence of crystalline Pt on the supports and the average crystallite sizes. Crystallite sizes of the Pt and of the supports were calculated using the Scherrer equation⁴⁶:

$$t = 0.9 (\lambda/b) \cos \theta_b \quad \text{Equation 7}$$

where t = crystallite size in Å, λ is the wavelength, (1.5406 Å in this case for Cu K α radiation), b is the full-width at half maximum (FWHM) of a peak in the XRD spectrum, and θ_b is the diffraction angle for that peak.

4.8 Scanning electron microscopy (SEM)/Transmission electron microscopy (TEM) and Energy Dispersive X-Rays (EDX)

A 200kV Hitachi H-800 TEM, with the Quartz XOne EDX system and a S-4700 FESEM (Field Emission Scanning Electron Microscope) were used to characterize the supported and unsupported materials. Elemental maps from EDX were used to characterize the dispersion of Pt on a support.

5 Determining potential and time for electrochemical stability tests

Since acute degradation of catalyst support is observed during start-up/shutdown cycles for a PEMFC stack, there was a need to determine the conditions for ex-situ accelerated tests so that the stability of various catalyst supports could be tested. The ex-situ tests involved preparing RDE samples as explained in the experimental procedure section. For the experiments involving the determination of the potential and time to be used for electrochemical stability testing, commercial catalyst Hispec 4000 (40 wt% Pt supported on Vulcan XC-72R, Johnson Matthey) was used.

Oxidation cycles were applied with different potentials and times as shown in Table 1. For example, the RDE was held at +0.6V for 60s and then the potential was stepped up to +1.8V, where it was held for 20s, and then the potential was stepped down to +0.6V. A total of 100 oxidation cycles were applied. Cyclic voltammograms (CVs) were recorded before any oxidation cycles and then after every 10 oxidation cycles. The CVs were recorded between 0.0V and 1.4V at 100mV/s. Figure 5 shows an example of the results of oxidation cycles from +0.6 to +1.8V for Hispec 4000. These data were used to calculate the normalized activity (Figure 6), which was calculated by recording the last current point from the data set at 1.8V just before the current became negative under 0.6 V conditions. These points are marked with arrows as points 1, 2, 3, etc. in Figure 5. The current at point 1 was taken as the initial current for the normalized activity plots. The current decreased as the catalyst support oxidized; therefore, the currents subsequent to point 1 were normalized to the initial current value, and the curves in Figure 6 were plotted as the normalized activity vs. the cumulative number of oxidation cycles.

Comparing Hispec 4000 being held at 1.8V for 60s, 40s and 20s shows that the 1.8 V (60s) condition is too destructive, as almost all of the support is oxidized after only 4 oxidation cycles. A condition that would allow a drop in activity that can be detected over a "reasonable" range of

experimental conditions would be preferred so that the stability of various supports can be compared. When the conditions at 1.8V (60s) and 1.8 (40s) were used, the activity dropped rapidly; therefore, if the electrode is held at 1.8V, a holding time of 20s is preferred. When the electrode was held at 1.5 V for 60 or 20 seconds, the oxidation of the support was much slower, requiring longer experimental times to determine the electrochemical stability. Therefore, the 1.8V (20s) condition was preferred over the conditions using 1.8 V (60s or 40s) and 1.5V (60s or 20s).

Sample	Lower potential (V)	Hold time at lower potential (s)	Higher potential (V)	Hold time at higher potential (s)
1	0.6	60	1.8	60
2	0.6	60	1.8	40
3	0.6	60	1.8	20
4	0.6	60	1.5	60
5	0.6	60	1.5	20

Table 1: Parameters for determining conditions for electrochemical stability

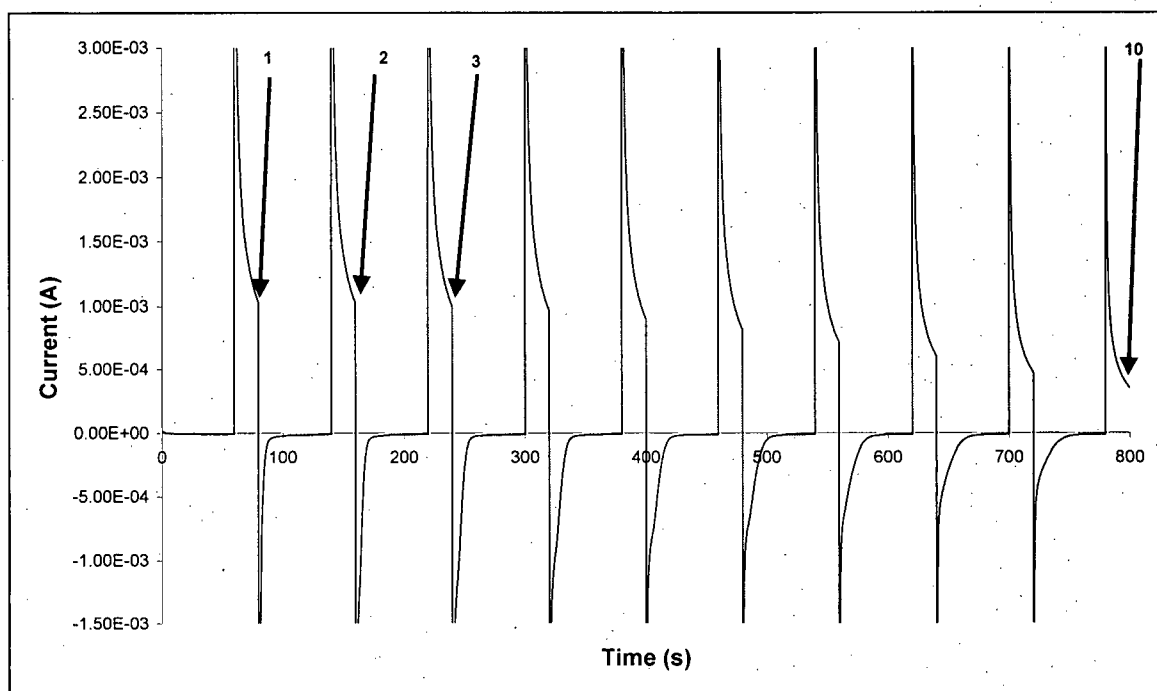


Figure 5: Current vs. time plot obtained from oxidation cycles for Hispec 4000 cycled between +0.6 V (held for 60s) and +1.8V (held for 20s); 0.5 M H_2SO_4 , 30°C, 100 mV/s, 2000 RPM.

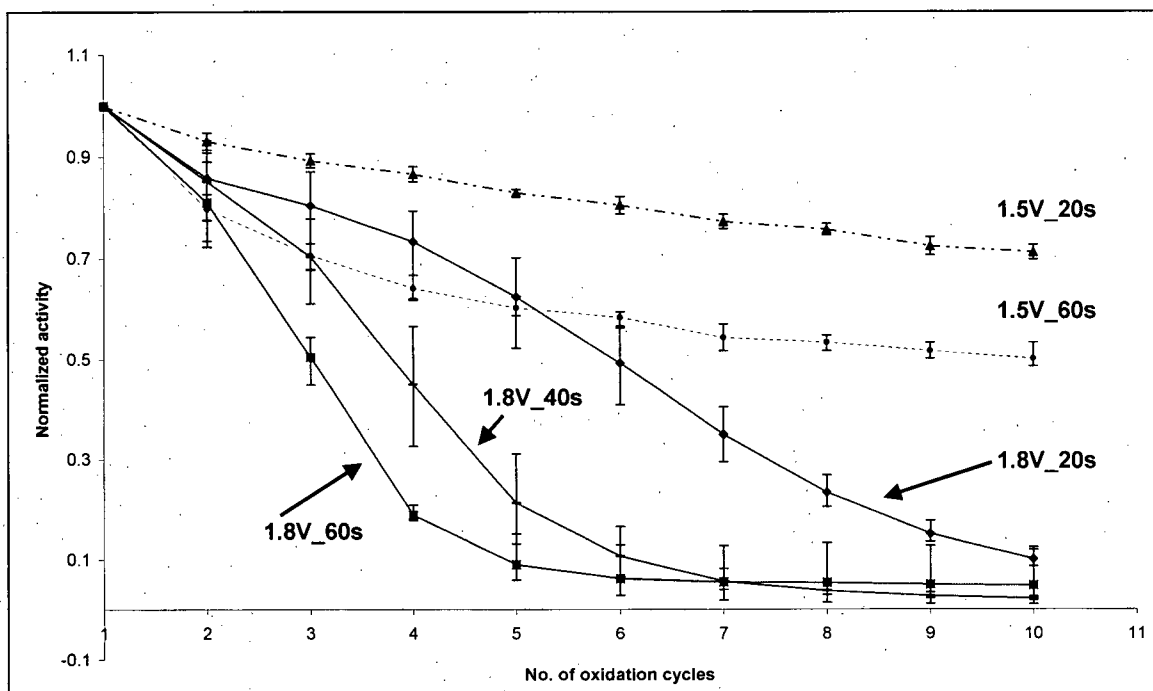


Figure 6: Normalized activity at different potentials and times as a result of repeated cycling for Hispec 4000. Average of three samples with limits of error for each condition are plotted.

6 Results and discussion for tungsten carbide studies

Oxidation stability of commercial tungsten carbide (Alfa Aesar) was evaluated in order to determine the viability of this material to be used as an oxidation-resistant catalyst support for PEMFCs.

6.1 Alfa Aesar WC with Pt deposition using chloroplatinic acid

In order to characterize Pt/WC, 40 wt% Pt was dispersed on WC. An XRD pattern of Pt dispersed on Vulcan XC-72R is shown in Figure 7. The average crystallite size for Pt was calculated using the Scherrer equation. The average tungsten carbide crystallite size was calculated to be 11.3 nm from the peaks at 2θ : 39.8° , 46.1° , and 67.6° . Pt was deposited using method I as explained in the experimental section. After Pt deposition on WC using method I, clear flakes were observed in the sample, which did not dissolve in water after washing the sample several times. XRD did not show any peaks other than the Pt and WC peaks. Therefore, the flakes were likely amorphous. To determine whether these flakes appeared due to WC

reacting with the NaHCO_3 , a blank reaction where WC was refluxed in NaHCO_3 was conducted, and these flakes were once again observed. The XRD of WC refluxed in the solution of NaHCO_3 shows the presence of WC with a broad peak at 2-theta of $\sim 23^\circ$, signifying the presence of an amorphous phase⁴⁷ (Figure 9). Ma et al³² evaluated electro-oxidation behavior of tungsten carbide electrodes in different electrolytes. They also found poor stability of WC in alkaline solution, since the WC is directly oxidized to WO_3 . The presence of unidentified amorphous flakes along with WC peaks suggests that some crystalline WC is present, but some of it transforms into amorphous flakes when exposed to a basic environment. Therefore, an alternative method, which does not use alkali, needed to be used when depositing Pt on WC.

The CV data show a complete loss of Pt surface area after only 10 oxidation cycles (Figure 10). The loss in surface area was determined from the loss of area of the Pt oxide reduction peak at 0.6 V. The CV pattern is slightly resistive due to problems with the RDE during the experiment. The normalized activity vs. the number of oxidation cycles plot (Figure 11) shows that WC as a support is not stable, since the percent loss in activity is similar for both Pt on Vulcan XC-72R and Pt on Alfa Aesar WC. The poor stability might result from the mixture of WC and amorphous flakes. Therefore, an alternative method for Pt deposition was developed, and the results from the Pt deposition method II are reported in section 0.

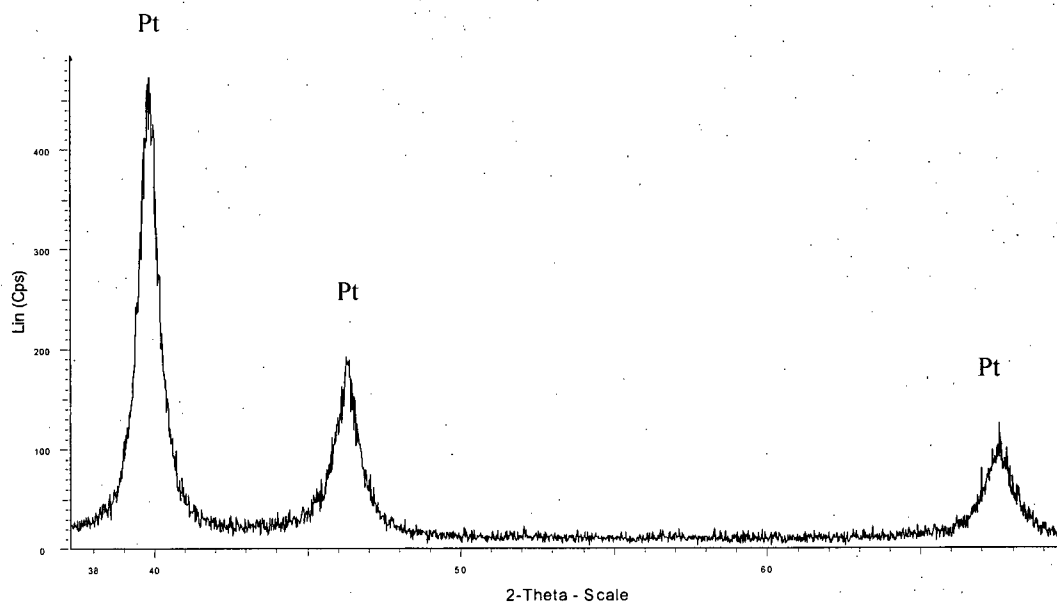


Figure 7: XRD spectrum of Pt dispersed on Vulcan XC-72R.

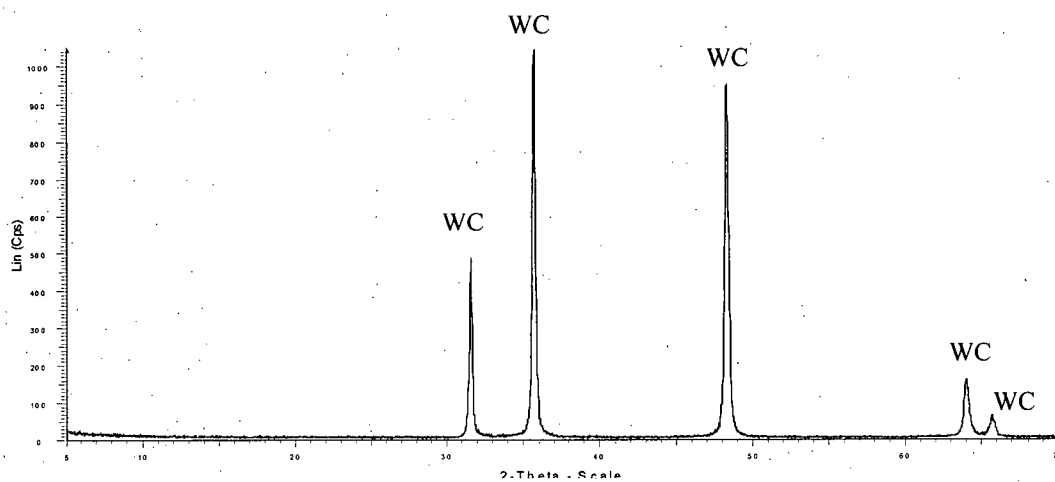


Figure 8: XRD spectrum of Alfa Aesar WC sample

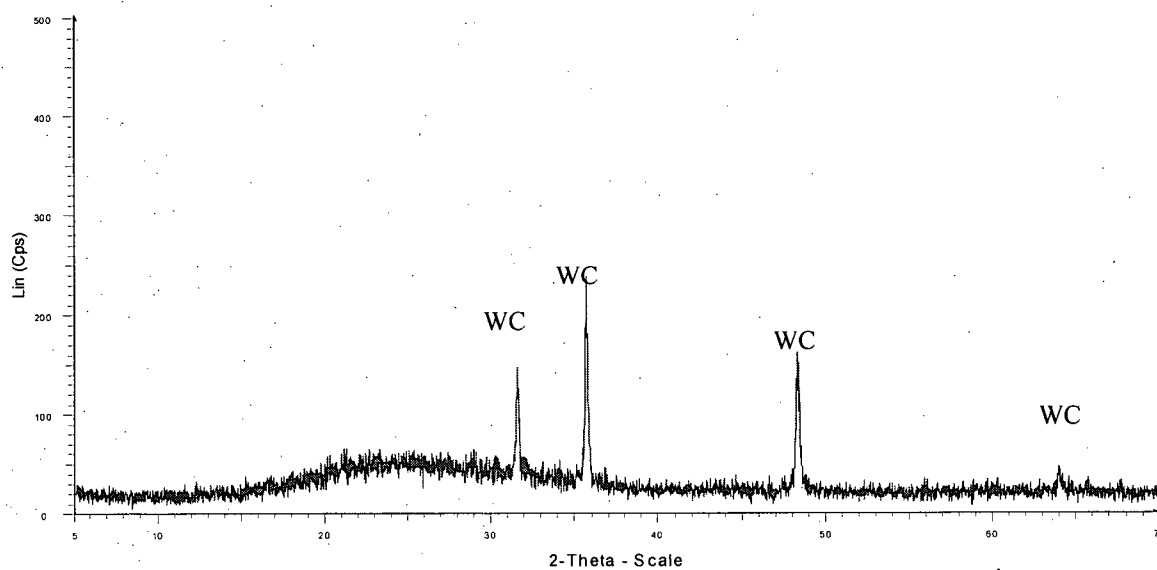


Figure 9: WC with flakes of unknown material

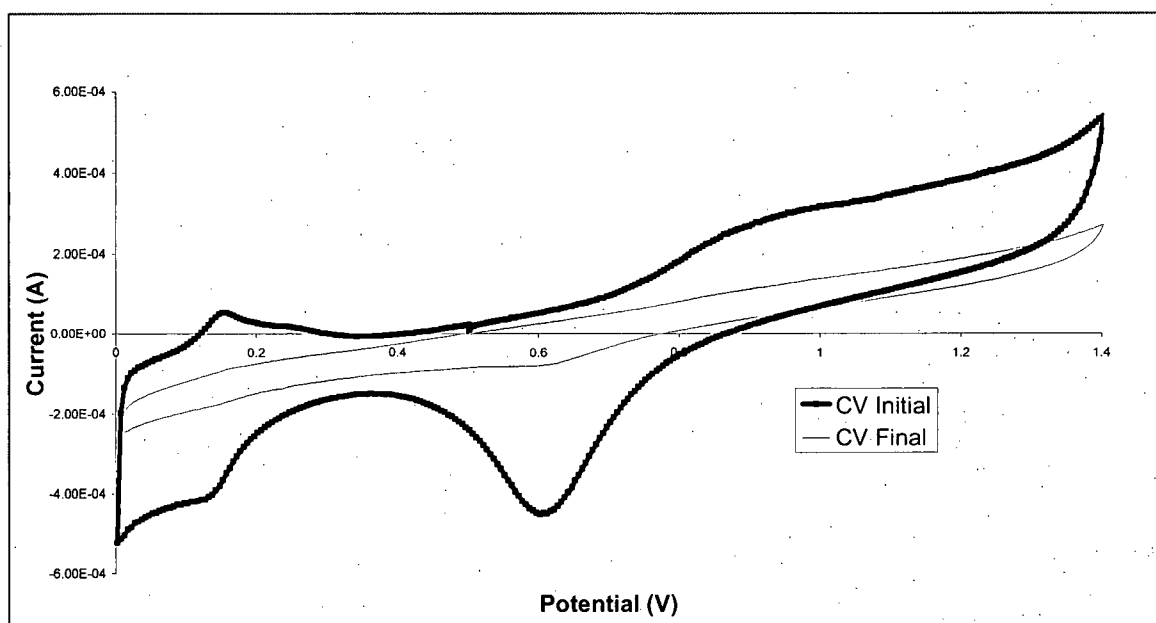


Figure 10: Cyclic voltammogram of Alfa Aesar WC supporting Pt, both before and after 10 oxidation cycles; 0.5 M H₂SO₄, 30°C, 100 mV/s, 2000 RPM.

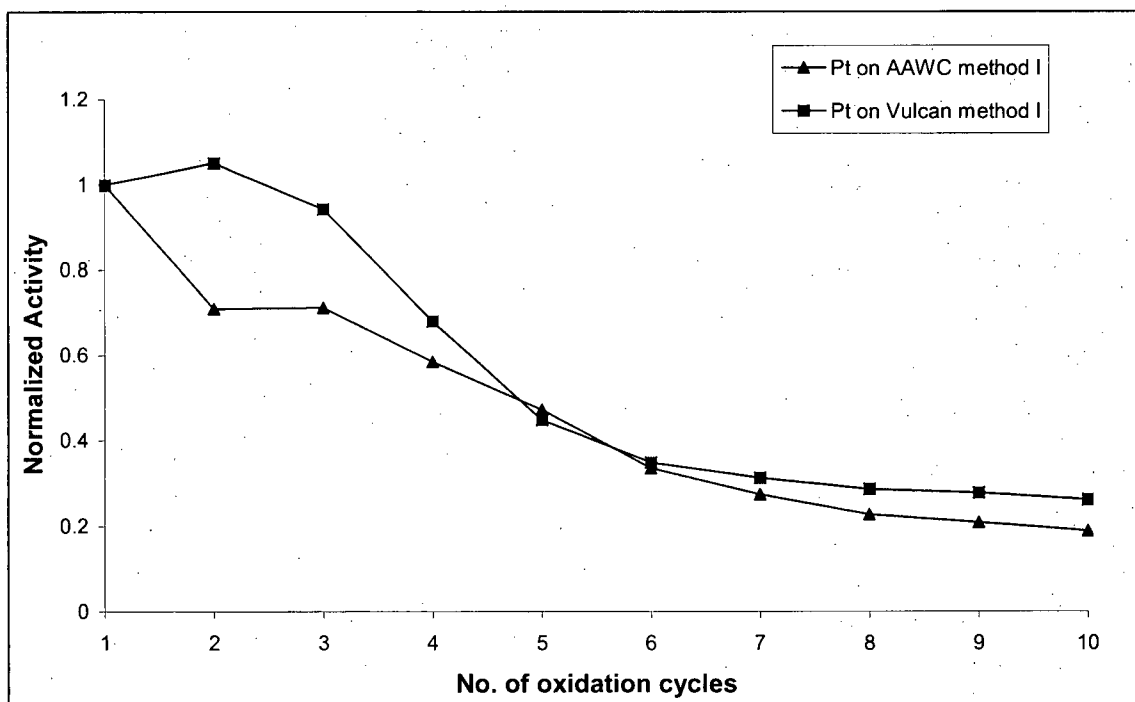


Figure 11: Change in anodic activity at 1.8 V as a result of repeated cycling for 40 wt% Pt/AAWC and 40 wt% Pt/Vulcan XC-72R.

6.2 Alfa Aesar WC with Pt deposition using Pt (II) pentan-2,4-dionate

In these studies 40 wt% Pt was dispersed on WC. The XRD spectrum of Pt (II) reduced to Pt onto Alfa Aesar WC is shown in Figure 12. The average crystallite size for WC calculated from the peaks at 2θ 31.5°, 35.6°, and 48.3° was 36 nm. The average crystallite size for Pt calculated from peaks at 2θ 39.8° and 46.1° was 30 nm. There were no flakes observed resulting from this synthesis method, and the XRD shows the presence of Pt and WC peaks only, with no evidence of an amorphous phase present. The average crystallite size for Pt supported on Vulcan XC-72R (Figure 13), calculated from peaks at 2θ 40° and 46° was 33.6 nm. Pt deposition on WC and Vulcan XC-72R was successful, but the Pt crystallite size needs to be reduced to 7-10 nm.

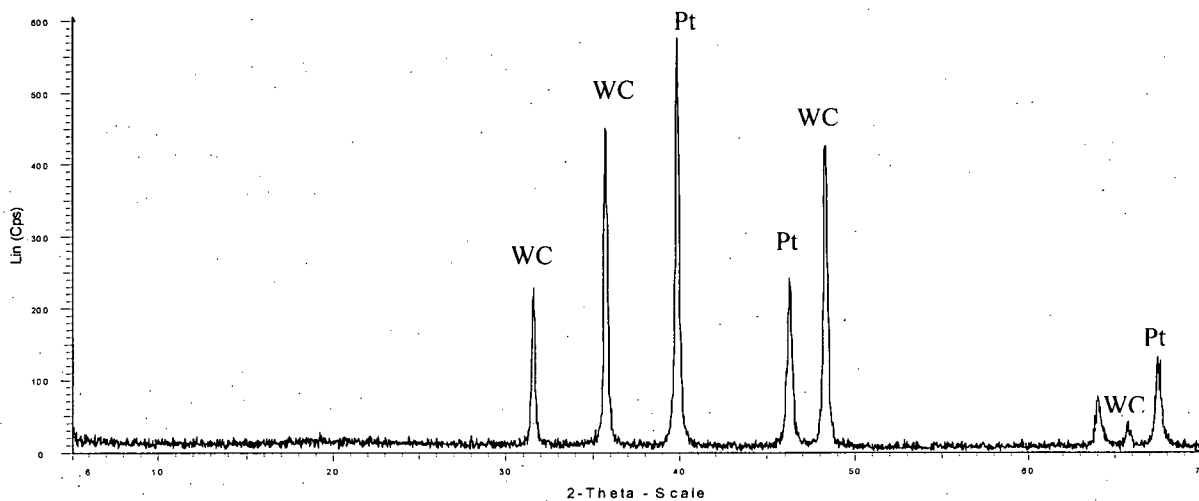


Figure 12: XRD pattern for Alfa Aesar WC with Pt deposition by Pt (II) reduction to Pt.

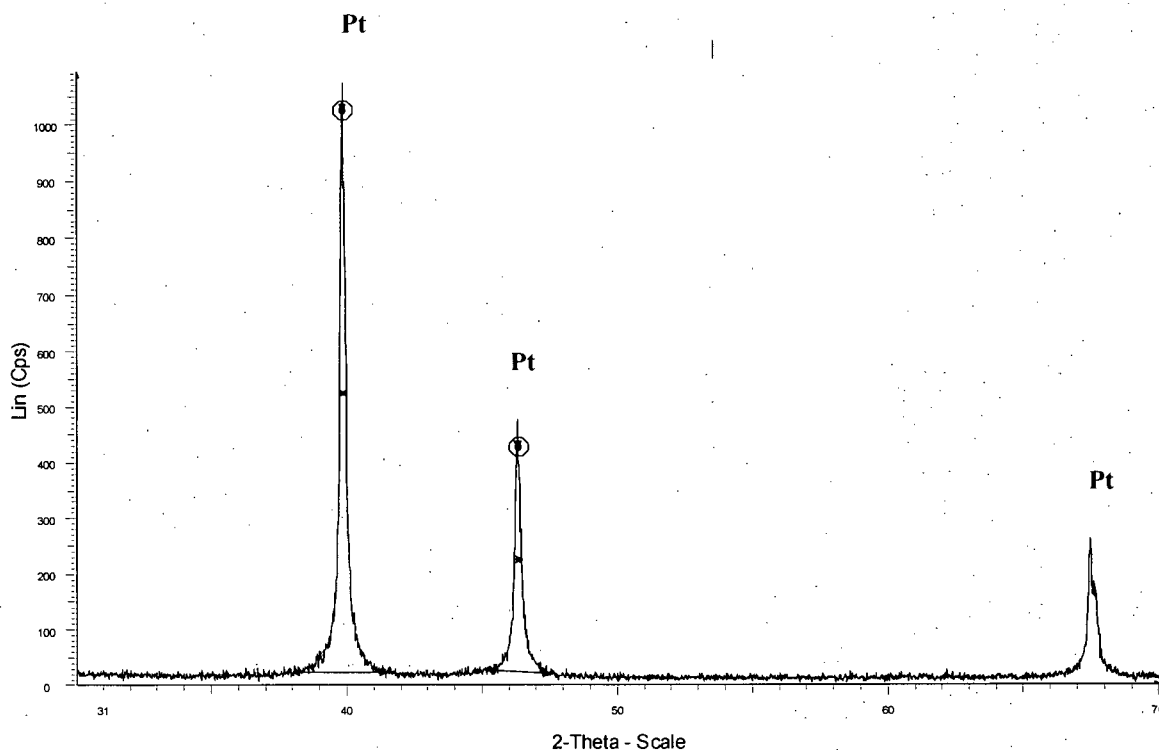


Figure 13: XRD pattern for 40wt % Pt on Vulcan XC-72R with Pt deposition by Pt (II) reduction to Pt.

TGA data were used to observe the materials' stability to chemical oxidation. The thermal stability data for Alfa Aesar WC, 40 wt% Pt on Alfa Aesar WC, and 40 wt% Pt on Vulcan XC-72R are shown in Figure 14. Pt supported on Vulcan XC-72R loses ~55% of the material, which corresponds to the loss of carbon. Both Alfa Aesar WC and Pt supported on WC gained weight above ~450°C. The gain in weight may be attributed to tungsten oxide formation. Tungsten oxide is a yellow powder and it was observed that both Alfa Aesar WC and Pt supported on WC had turned from dark gray powders to yellow powders after the TGA run was complete. Since PEMFCs are low temperature operating fuel cells the tungsten carbide oxidation may not be an issue. However, with the low pH and high potential conditions in PEMFCs, tungsten carbide may undergo oxidation. Detailed electrochemical tests would help in understanding whether tungsten carbide oxidation is an issue for PEMFC operation.

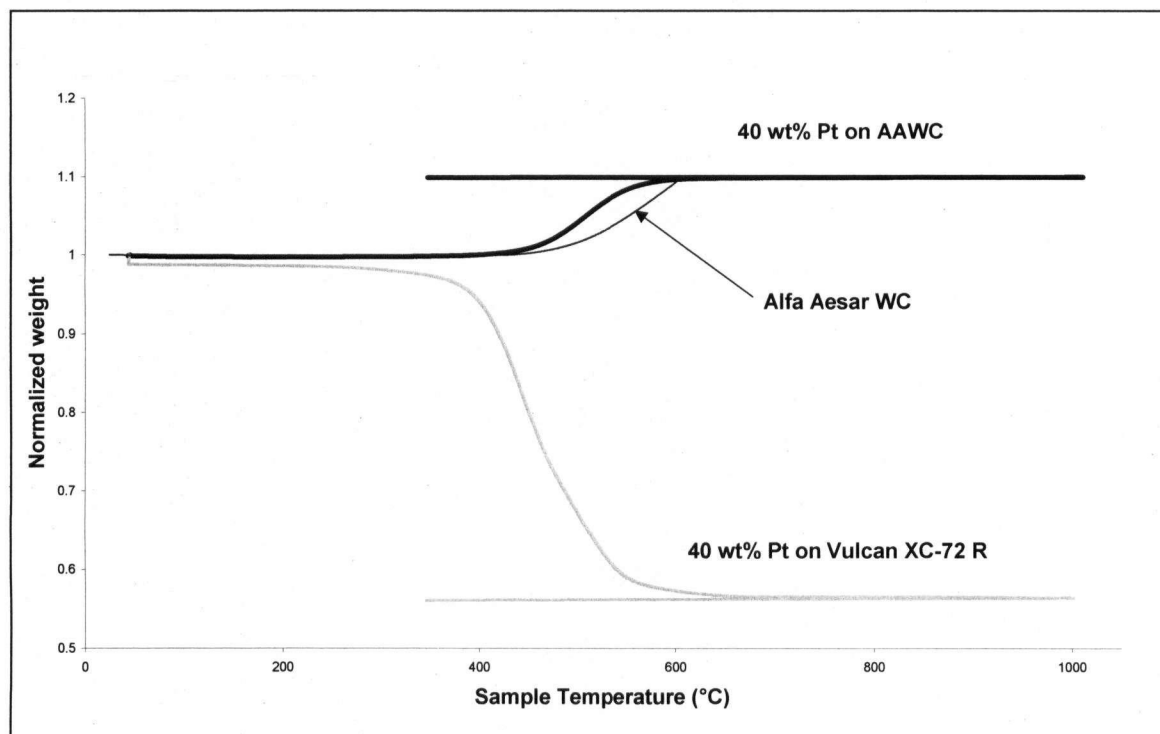
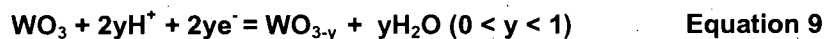
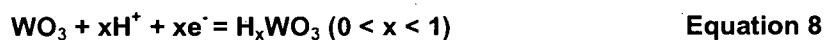


Figure 14: TGA data for Alfa Aesar WC, 40 wt% Pt on Alfa Aesar WC, and 40 wt% Pt on Vulcan XC-72R under air at 40ml/min, temperature ramped from 50°C to 1000°C at 2°C/ min.

The electrochemical stability was determined for Alfa Aesar WC, 40 wt% Pt on Alfa Aesar WC, and 40 wt% Pt on Vulcan XC-72R (Figure 15). The electrochemical stability determined by accelerated testing on RDE shows that WC is more stable than Pt supported on Vulcan XC-72R when cycled between +0.6V and +1.8V. The CV for pure Alfa Aesar WC (Figure 16) may form tungsten bronze in the hydrogen adsorption/desorption region. The CV after 100 cycles develops reversible peaks at 0.65 V in the anodic region and at 0.55 V in the cathodic region. The ~100 mV difference between the peaks indicates the presence of reversible solution species rather than adsorption of any species⁴⁸. The reversible peaks might be from quinone/hydroquinone or other carbon-oxygen species³.

The CV for Pt supported on WC (Figure 17) shows a sharp anodic peak above 1.2V, which might result from tungsten oxide on the surface of the catalyst. A sharp anodic peak was not observed as more CVs were acquired. The oxidation of the WC by anodic polarization has been reported by Lee et al³¹. They report that a sharp anodic peak above 0.8V for CV of pure WC has also been observed. The oxidation of WC is considered to follow equation 5.

In the current study the sharp anodic peak was not observed after the initial CV scan. This might result from surface oxidation of W during the first scan and no further oxidation during the subsequent CV scans. The structure of the support might have changed from Pt supported on WC to Pt supported on a WO₃ shell encapsulating a WC core. Also, on the positive scan a broad peak between 0.3 and 0.45 V with no apparent counter-part on the negative scan is observed. Similar results have been reported by other researchers^{49, 50}. Tungsten oxide could form two stable hydrogen tungsten bronzes, H_{0.18}WO₃ and H_{0.35}WO₃, and sub-stoichiometric oxides, WO_{3-y} by reaction with hydrogen⁴⁹:



Also, hydrogen spill-over from Pt has been reported⁴⁹:



The increase in hydrogen ads/des peak area along with a broad anodic peak between 0.3 and 0.45 V probably occurs due to tungsten bronze formation. These results suggest that WC might be oxidizing under the current electrochemical conditions used to test the stability of this support material. Tungsten carbide may not be stable under PEMFC conditions and may oxidize to WO₃ with operation. However, the Pt reduction peak at ~0.75V does not decrease in area even after 100 oxidation cycles for Pt/WC (Figure 17). Even if WC is oxidized to WO₃ the oxidized tungsten is sufficiently conductive to be used as a support. The extent of oxidation under operation and the impact on fuel cell performance need to be carefully determined before ruling out the option of using WC as a catalyst support in PEMFCs.

The Pt reduction peak is completely lost after 100 oxidation cycles for Pt supported on Vulcan XC-72R (Figure 18). It is extremely difficult to compare the activities for Vulcan XC-72R and WC by supporting Pt by weight% since the densities of these supports are significantly different (with densities of 1.8 g/cm³ for C and 15.6 g/cm³ for WC). These experiments were done to observe the thermal and electrochemical characteristics of WC; however, an alternative method should be used to compare the stability of Pt/Vulcan XC-72R and Pt/WC more directly according to surface area. Another comparison between the activities of Pt/Vulcan XC-72R and Pt/WC can be made

by supporting exactly the same amount of Pt on supports that have same volume. Results for Pt supported on both Vulcan XC-72R and WC with similar volumes are reported in section 6.3.

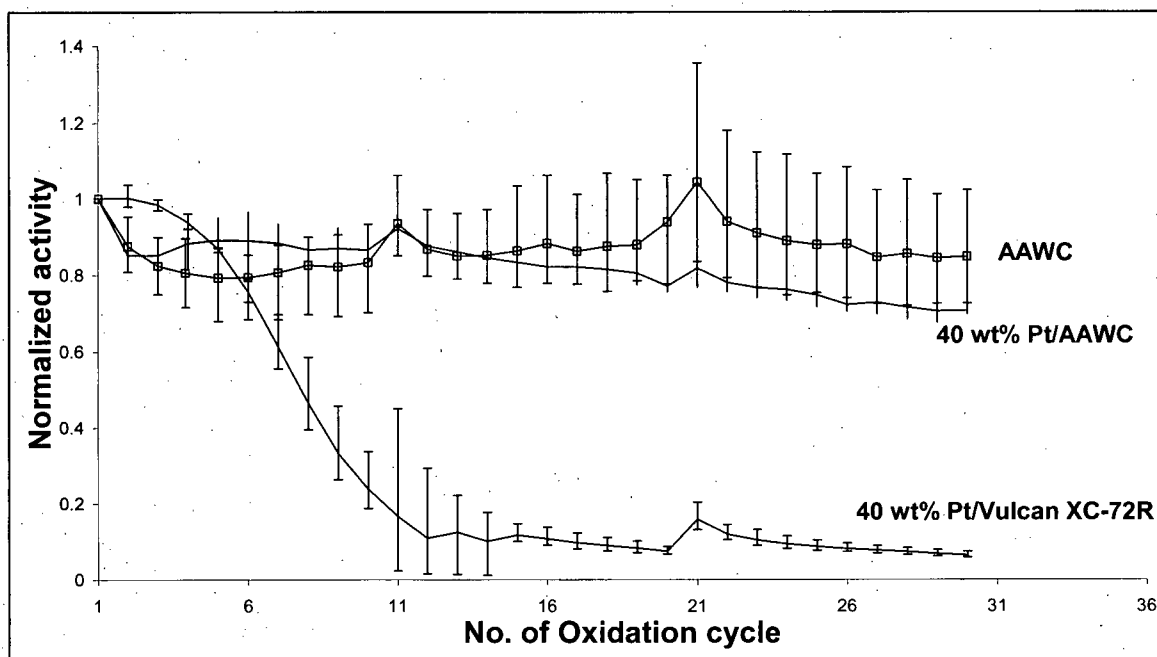


Figure 15: Change in anodic activity at 1.8 V as a result of repeated cycling for Alfa Aesar WC, 40 wt% Pt on Vulcan XC-72R and 40 wt% Pt on Alfa Aesar WC. Average of three samples with limits of error for each material are plotted.

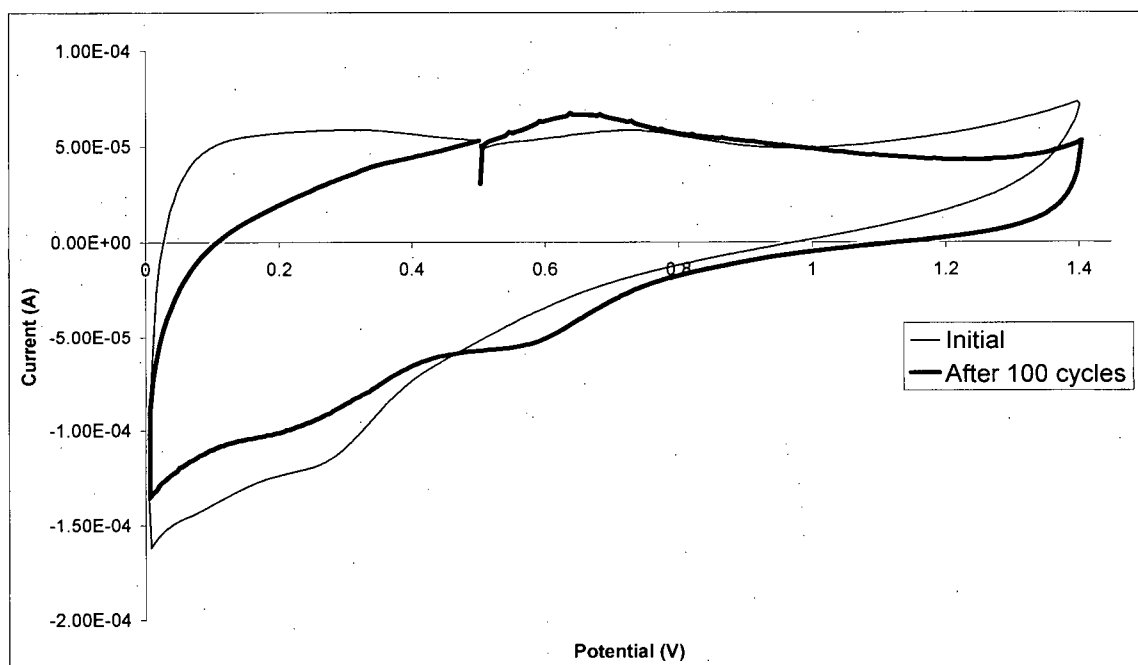


Figure 16: Cyclic voltammograms for Alfa Aesar WC both before and after 100 oxidation cycles; 0.5 M H₂SO₄, 30°C, 100 mV/s, 2000 RPM.

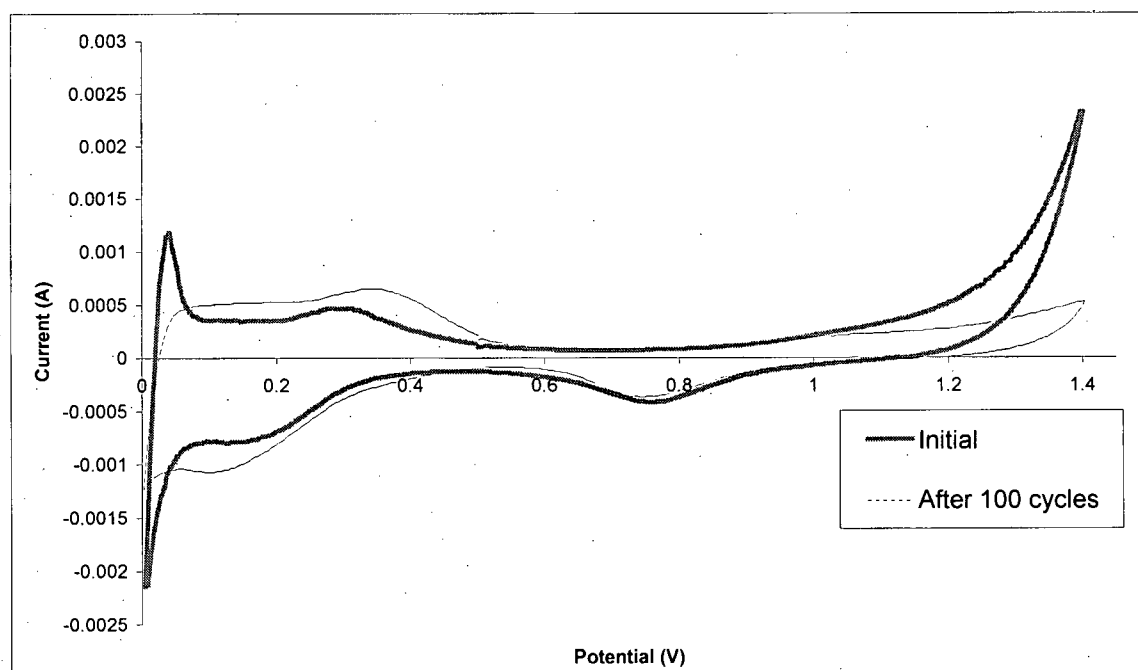


Figure 17: Cyclic voltammograms for 40 wt% Pt on WC both before and after 100 oxidation cycles; 0.5 M H₂SO₄, 30°C, 100 mV/s, 2000 RPM.

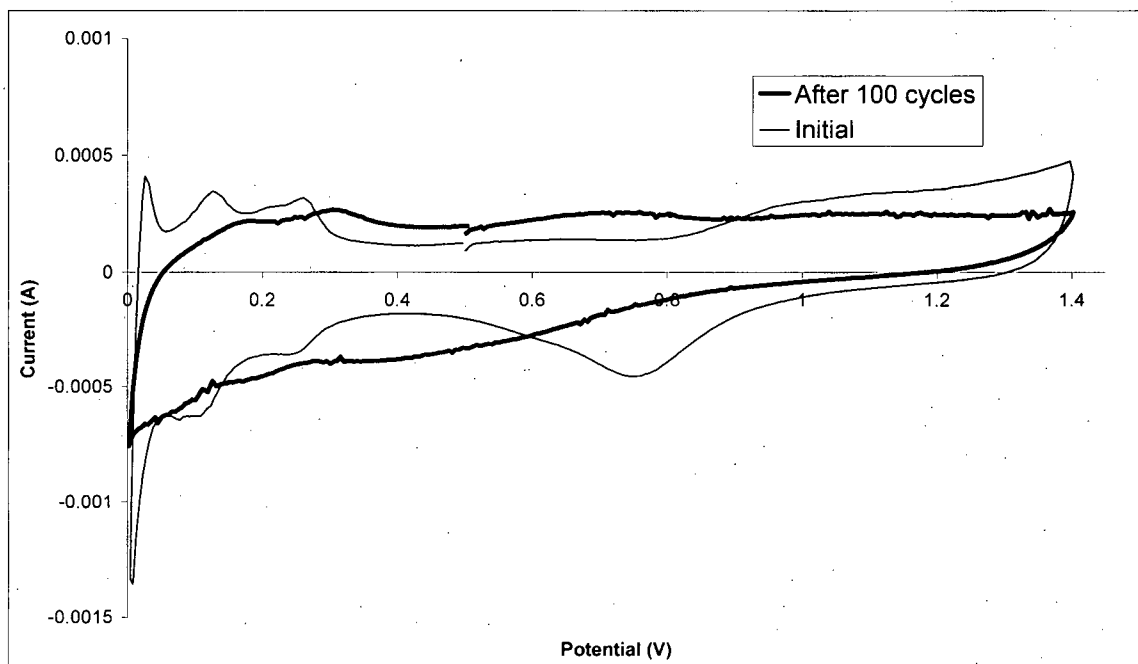


Figure 18: Cyclic voltammograms for 40 wt% Pt on Vulcan XC-72R, both before and after 100 oxidation cycles; 0.5 M H₂SO₄, 30°C, 100 mV/s, 2000 RPM.

SEM and TEM images

SEM images of Alfa Aesar WC show the presence of dense spheres packed together with some irregularly-shaped particles (Figure 19). It is difficult to distinguish between Pt and WC particles in the high-resolution SEM images of Pt on WC (Figure 20).

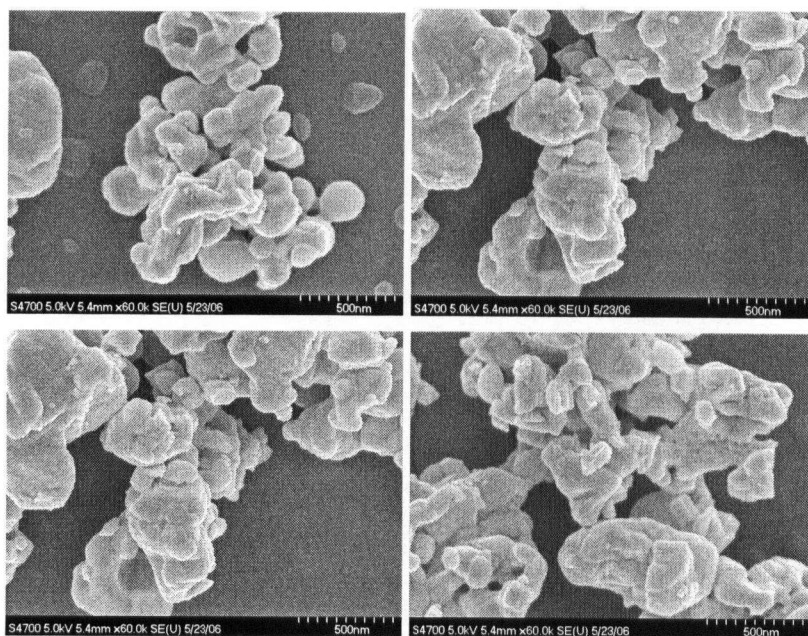


Figure 19: SEM images of Alfa Aesar WC

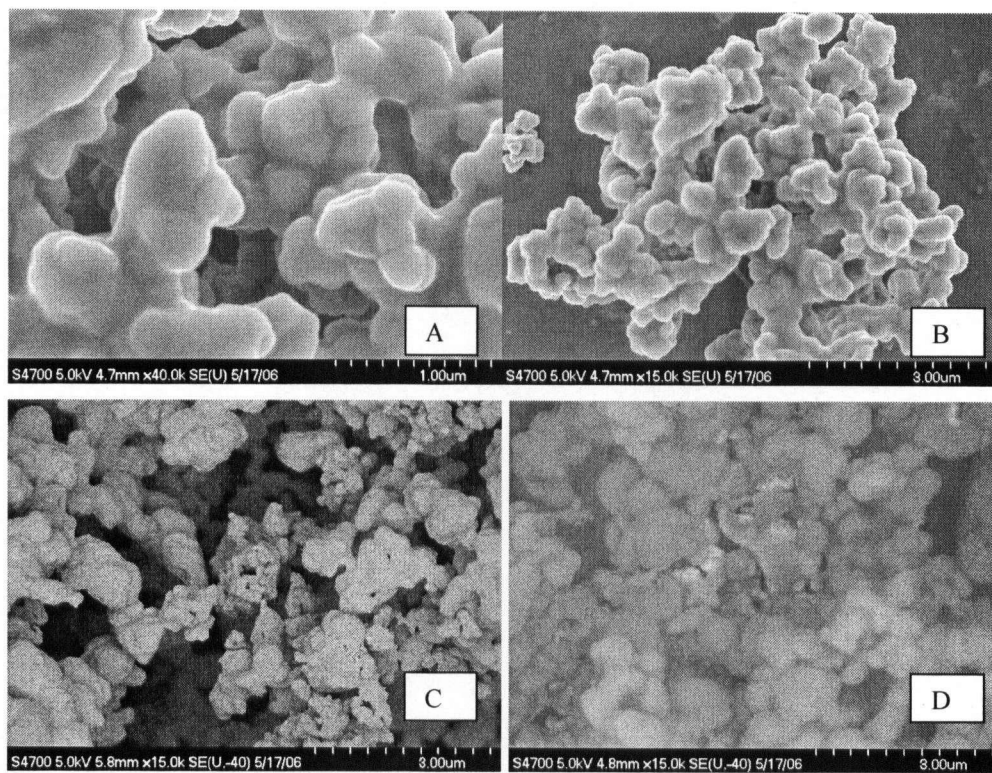


Figure 20: SEM images of 40 wt% Pt on Alfa Aesar WC, (A), (B) secondary electron mode; (C), (D) mixed secondary and backscattered electron mode.

The SEM images of Pt on Vulcan XC-72R deposited by method I (Figure 21) and method II (Figure 22) show fine Pt particles dispersed on carbon. Pt particle size ranging from 10-20 nm was observed for Pt/C prepared by method I, which is close to the average crystallite size of 11.6 nm calculated from the XRD results. Pt particle sizes ranging from 10 to 60 nm are observed for Pt/C deposited by method II. Average crystallite size for this material was calculated to be 36 nm from the XRD results. The Pt particle size needs to be optimized for method II. The optimization work for Pt deposition is recommended for future studies.

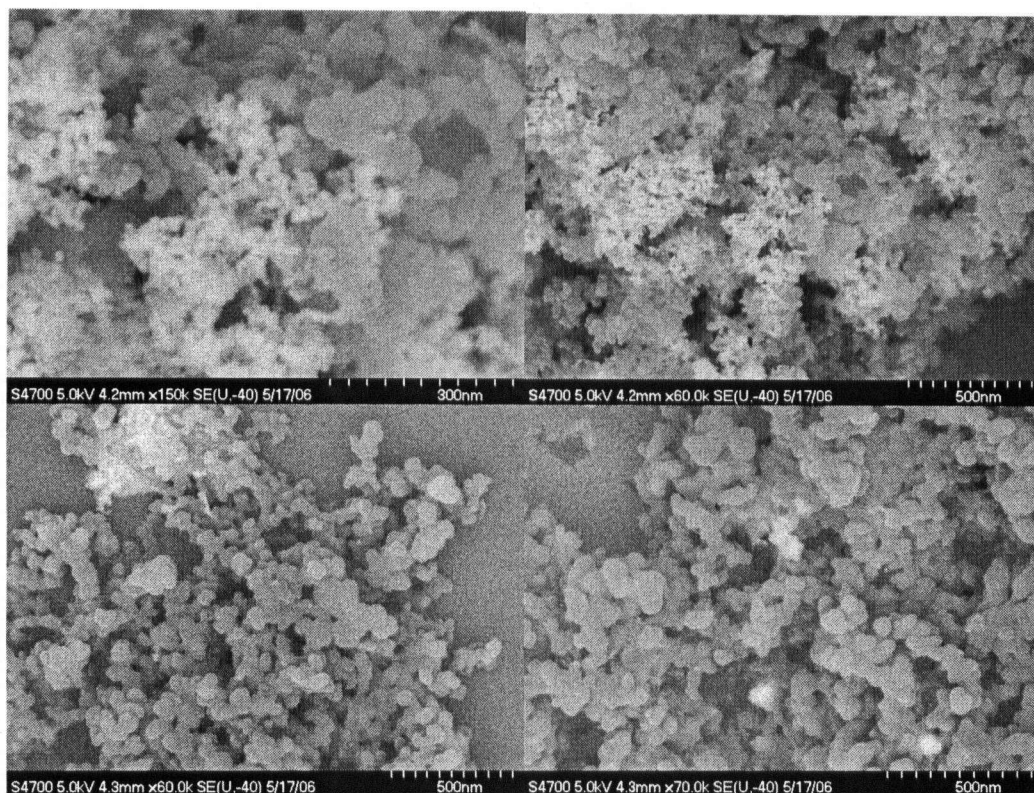


Figure 21: SEM images of 40 wt% Pt on Vulcan XC-72R deposited using chlorplatinic acid; images taken using mixed secondary and backscattered electron mode.

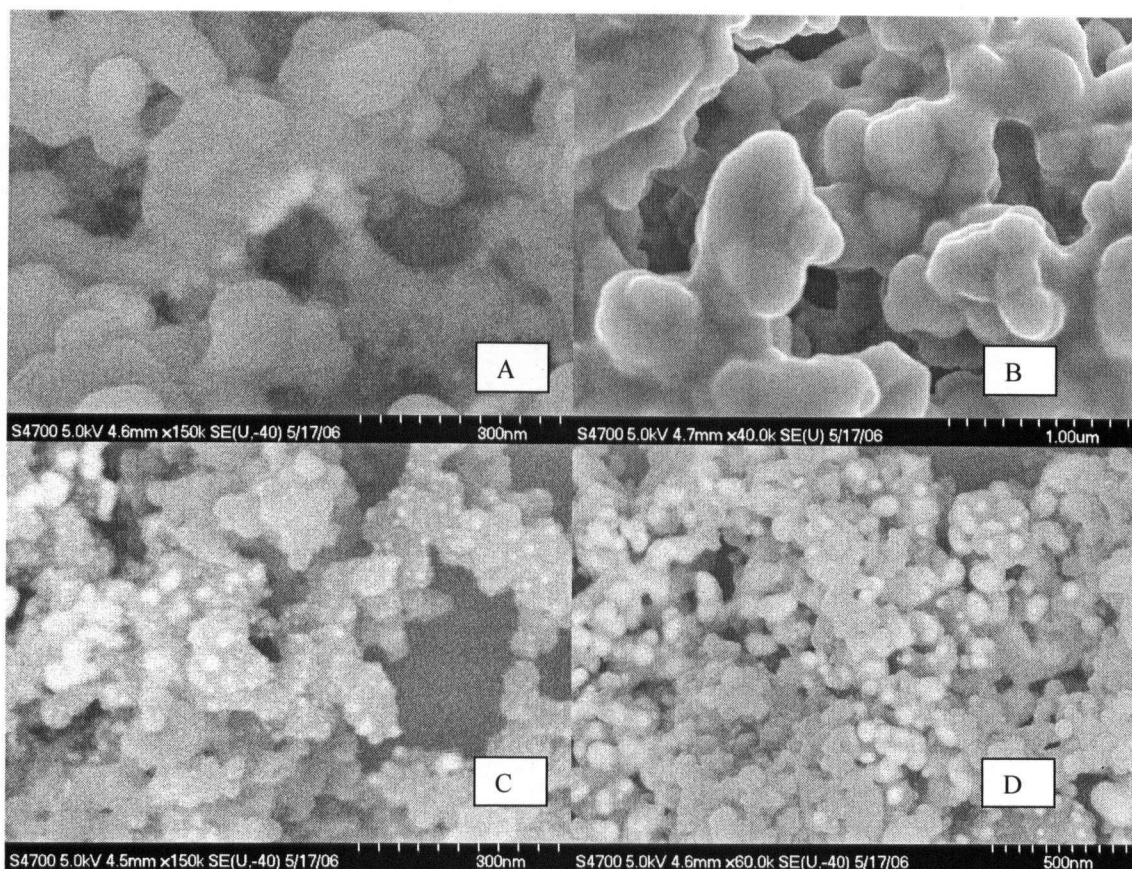
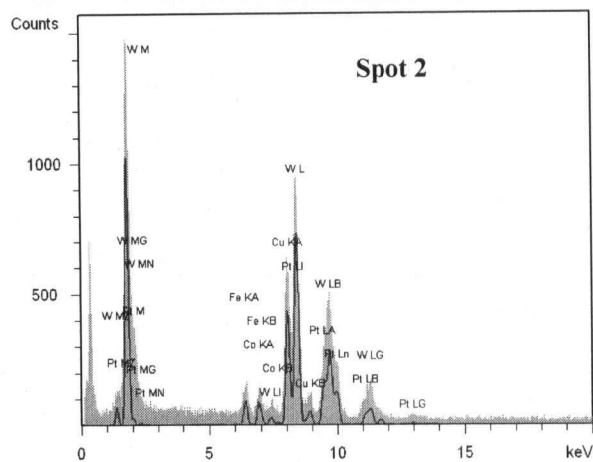
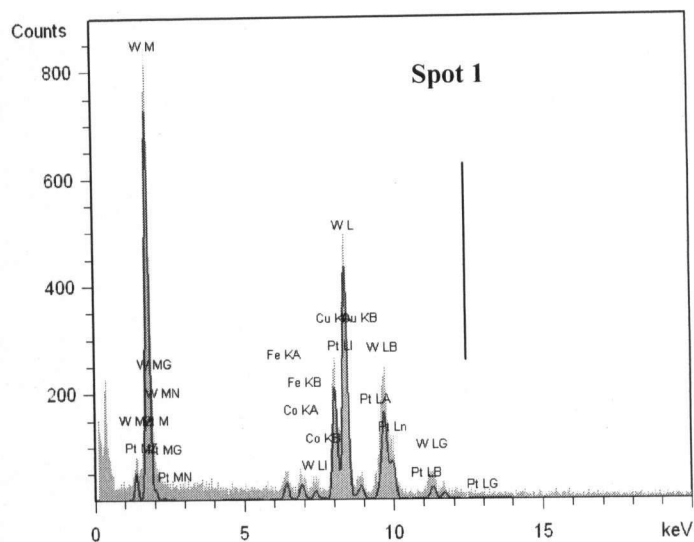
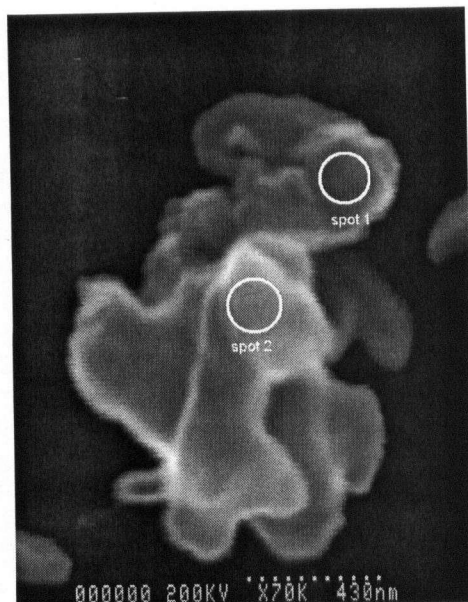


Figure 22: SEM images of 40 wt% Pt on Vulcan XC-72R deposited using Pt (II) pentan-2,4-dionate; (A-C) mixed secondary and backscattered electron mode, (D) secondary electron mode.

TEM of Pt dispersed on Alfa Aesar WC using Pt (II)-pentan-2,4-dionate

A TEM image of Pt dispersed on Alfa Aesar WC is shown in Figure 23. The elemental spectrum along with the concentrations for spot 1 and spot 2 on the TEM image of Pt dispersed on Alfa Aesar WC show that the dark area (spot 1) has a Pt:W ratio of 0:100, and spot 2 has a Pt:W ratio of 22:78 by weight. It is difficult to distinguish between Pt and WC in TEM images, but the elemental maps can be used to obtain the relative ratios of each element. The presence of iron, cobalt, and copper result from the sample holder. The TEM images, along with elemental map of Pt/Vulcan XC-72R (Figure 24), show the presence of Pt clusters dispersed on carbon. The dispersion needs to be optimized so that fine Pt particles are evenly dispersed on the support material.



	Spot 1	Spot 2
Iron	4.38 wt%	5.75 wt%
Cobalt	3.42 wt%	4.75 wt%
Copper	38.78 wt%	35.81 wt%
Tungsten	53.39 wt%	41.99 wt%
Platinum	0.02 wt%	11.71 wt%

Figure 23: TEM images and EDX of Pt dispersed on Alfa Aesar WC using Pt (II) pentan-2,4-dionate. Elemental spectrum and weight concentration for spots 1 and 2 on the TEM image of Pt dispersed on Alfa Aesar WC.

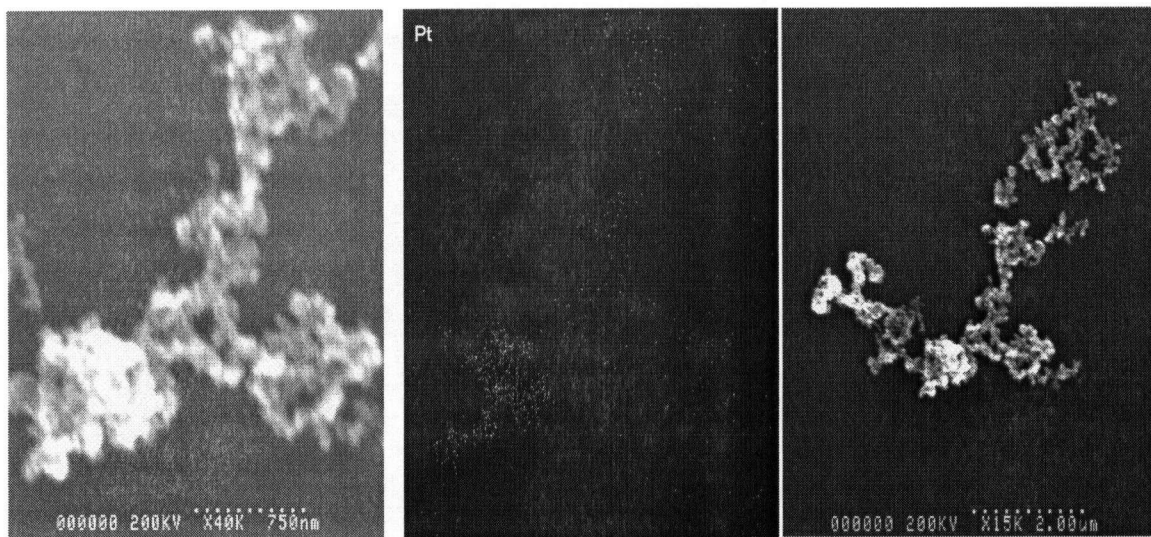


Figure 24: TEM image and Pt map for Pt dispersed on Vulcan XC-72R using Pt (II) pentan-2,4-dionate.

6.3 Comparing activities of Pt deposited using Pt (II) pentan-2,4-dionate on similar volumes of both Alfa Aesar WC and Vulcan XC-72R

It is difficult to directly compare the activities for Vulcan XC-72R and WC supporting comparable weight percent of Pt, since the densities of these supports are significantly different. Therefore, similar volumes of the supports with the same amount of Pt on each were also tested in order to further compare the two supports. Since carbon can be made by many methods leading to different morphologies each time, the tap density is usually used to characterize the density of these materials. Tap density involves packing material to a certain volume by tapping it. Both tungsten carbide and Vulcan XC-72R were tapped 200 times until exactly 2 ml of the material was obtained. To each of the supports was added the same amount of Pt, which was 40 wt% relative to 2ml of packed carbon. The method for Pt deposition on similar volumes of Vulcan XC-72R and WC is reported in section 4.3.

The CV for Pt/Vulcan XC-72R (Figure 25) shows the initial Pt characteristics, and a complete loss of the platinum oxide reduction peak that is observed after 100 cycles. The XRD pattern for Pt/Vulcan XC-72R shows the presence of Pt (Figure 26), which was not observed for the XRD pattern for Pt/WC (Figure 28).

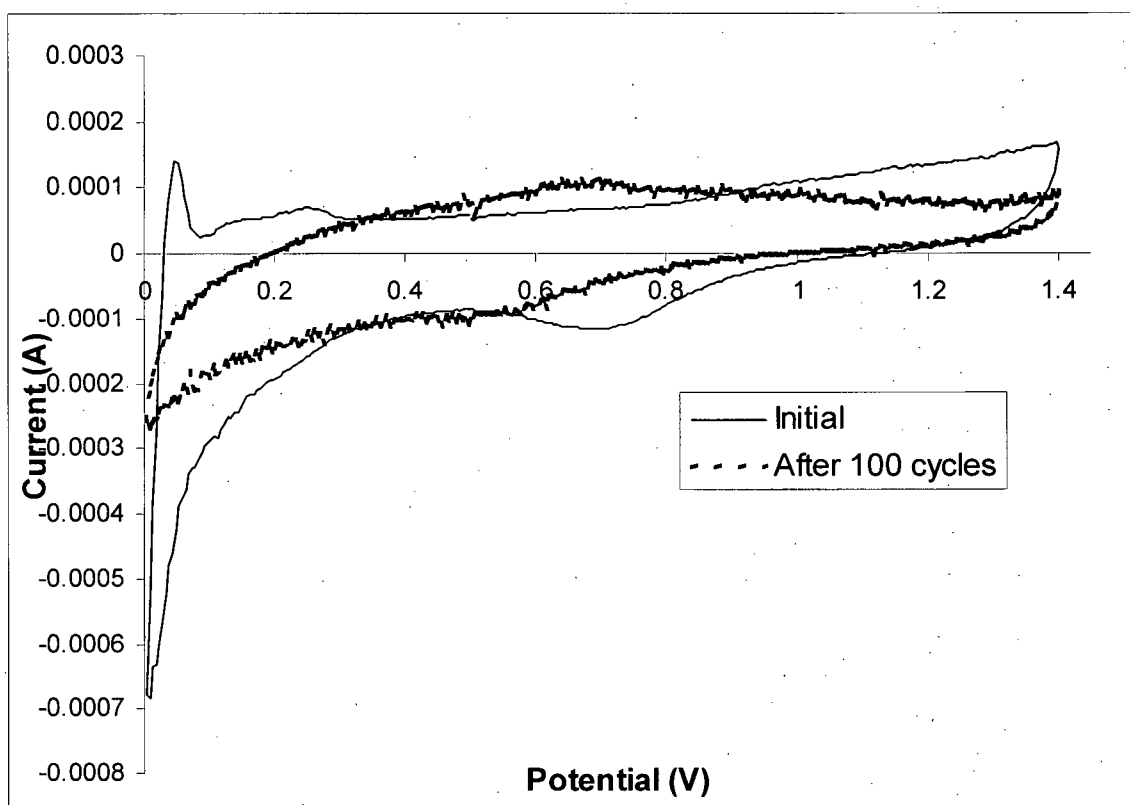


Figure 25: Cyclic voltammograms for Pt dispersed on Vulcan XC-72R; 0.5 M H₂SO₄, 30°C, 100 mV/s, 2000 RPM.

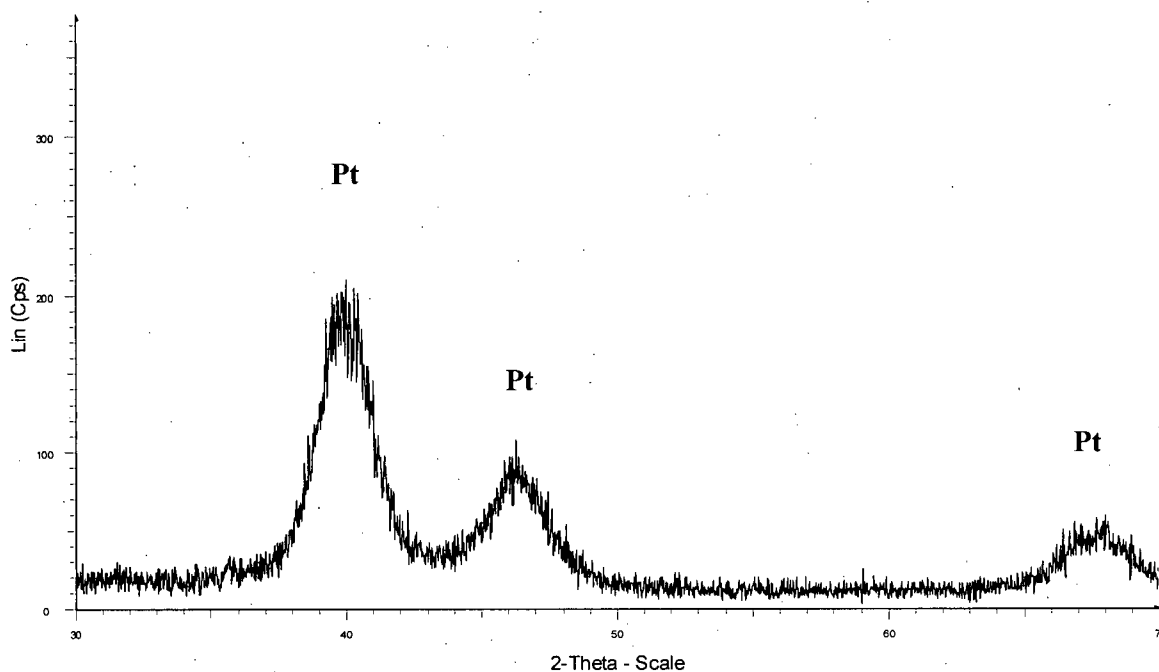


Figure 26: XRD pattern for Vulcan XC-72R with Pt deposition by Pt (II) reduction to Pt.

The CV for Pt/WC (Figure 27) does not exhibit any Pt characteristics such as hydrogen adsorption/desorption or Pt oxidation/reduction. Even though a similar amount of Pt was deposited on both Vulcan XC-72R and WC, no Pt characteristics were observed in the CV or in the XRD pattern (Figure 28). Similar packing techniques were used in packing both the Vulcan XC-72R and WC powders to a volume of 2 ml. However, WC being very dense with small particle size (~ 36 nm), will pack very closely and have a very high surface area per unit volume. Even with similar powder volume (tap density), Vulcan XC-72R has agglomerates with sizes up to the μm range, and therefore has a very different surface area compared to Alfa Aesar WC. Therefore, the Pt content by surface area would be very low on WC compared to Vulcan XC-72R when the tap density volume method is used for Pt deposition. The calculated Pt weight percents relative to AAWC and carbon are shown in Table 2. The Pt wt% for AAWC was calculated to be only 0.91%, which is well below the detection limit of the XRD. An alternative method involved comparing the stability of the two supports with similar solid volume ratios of Pt to support material. The results of this comparison are presented in section 6.4.


	Amount of Pt (II) precursor (g)	Pt metal (g)	Mass of material (g)	Pt content (wt%)
AAWC	0.16	0.08	8.23	0.91
C	0.16	0.08	0.11	39.95

Table 2: Amount of AAWC and C tapped in a 2ml volume and the calculated wt% of Pt added to each support material

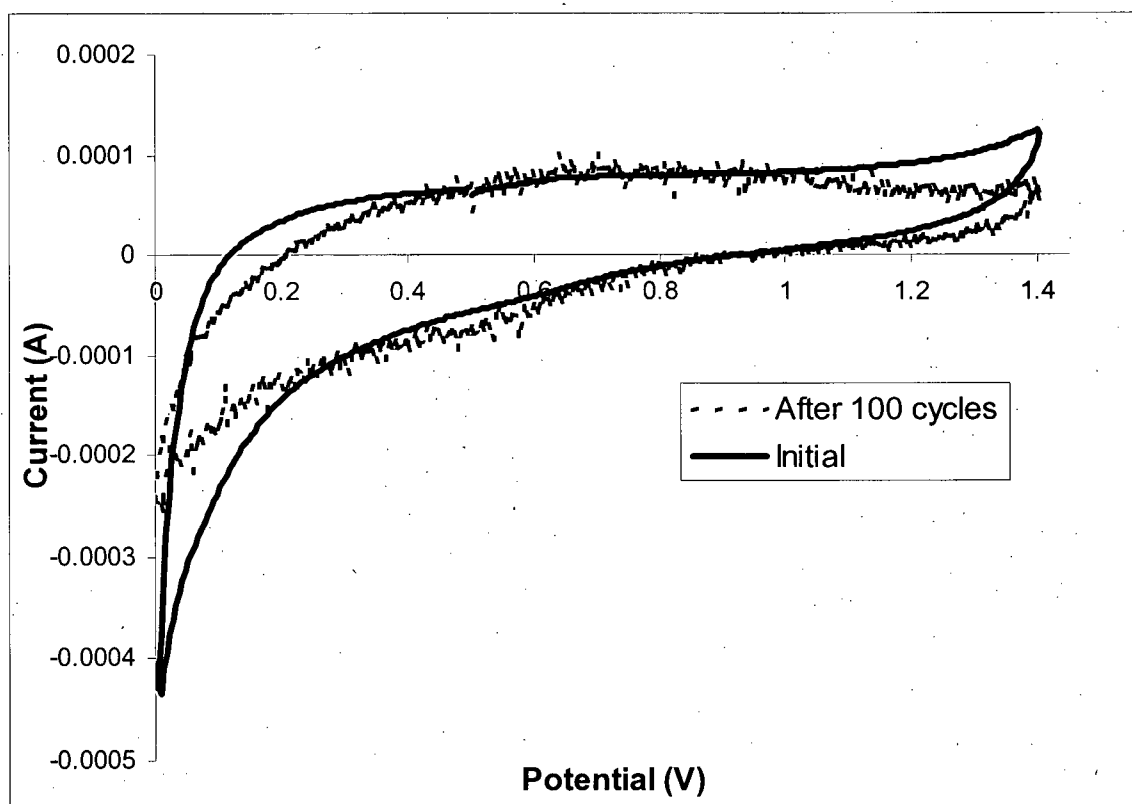


Figure 27: Cyclic voltammograms for Pt dispersed on Alfa Aesar WC, initially and after 100 oxidation cycles; 0.5 M H_2SO_4 , 30°C, 100 mV/s, 2000 RPM.

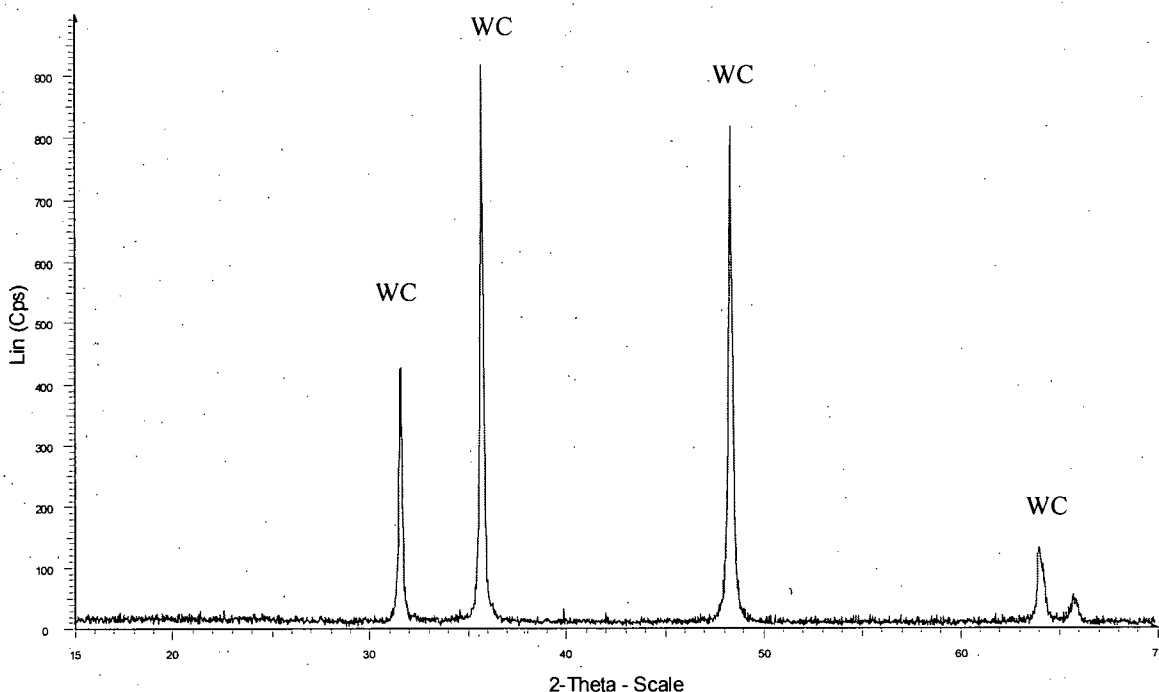


Figure 28: XRD pattern for Alfa Aesar WC with Pt deposition from Pt (II) reduction to Pt.

6.4 Pt addition in equal solid volume ratios to carbon and tungsten carbide

Using the same weight ratio of Pt to C (40 wt%) used in section 6.3, the amount of WC required to obtain equal solid volume ratios of Pt to both C and WC was calculated. The CV for Pt/WC (Figure 29) does not exhibit any Pt characteristics such as hydrogen adsorption/desorption or Pt oxidation/reduction. Even though a similar volume ratio of Pt was deposited on both Vulcan XC-72R and WC, no Pt characteristics were observed in the CV. However, there are low intensity Pt peaks observed in the XRD pattern (Figure 30). The calculated Pt weight percent relative to AAWC and carbon are shown in Table 3. Equal solid volume ratios resulted in 6 wt% Pt on AAWC, which was well within the XRD detection limit. However, the effect of Pt was not observed in the cyclic voltammogram.

Table 3 compares the Pt:support ratios for tests involving Pt dispersion using the same weight ratio (40wt% Pt, section 0), tapped powder volume ratio (section 6.3) and solid volume ratio (section 6.4). For the same weight ratio method, where 40wt% Pt was dispersed on AAWC, the

Pt:WC solid volume ratio was ~ 0.49 , which was much higher compared to the Pt: C solid volume of ~ 0.5 . Despite the high amount of Pt volume dispersion on AAWC both the cyclic voltammetry and oxidation cycle data showed that the AAWC support material was much stable when compared to carbon. However, none of the Pt dispersion methods used in this study can directly compare the electrochemical stability of AAWC and carbon. There is a need to normalize Pt content per unit surface area of the support in order to better compare the activities of conventional carbon supports and WC. Pt with similar surface area can be supported on both carbon and WC with similar surface areas. Both Brunauer-Emmett-Teller (BET) and mercury porosimetry can be used to determine the total surface area available in both C and WC supports. A more detailed study is required to develop a surface area based method and is recommended for future work. Carbon is known to have internal microporosity that can be measured by BET (N_2 adsorption), but the internal porosity will not be available for Pt deposition. Therefore, the actual surface area of Pt that can be supported on carbon will be lower than that which can be measured by BET. Mercury porosimetry can be used to determine the pore volume of pores with microporosity; however, high pressures are required for mercury to be filled in to the small pores, and this could lead to ruptured carbon particles. Therefore, even normalizing Pt content per unit surface area of the support cannot be done directly. However, the electrochemical stability data based on similar amounts of Pt supported on similar surface area supports could be more comparable than the comparisons made in this study.

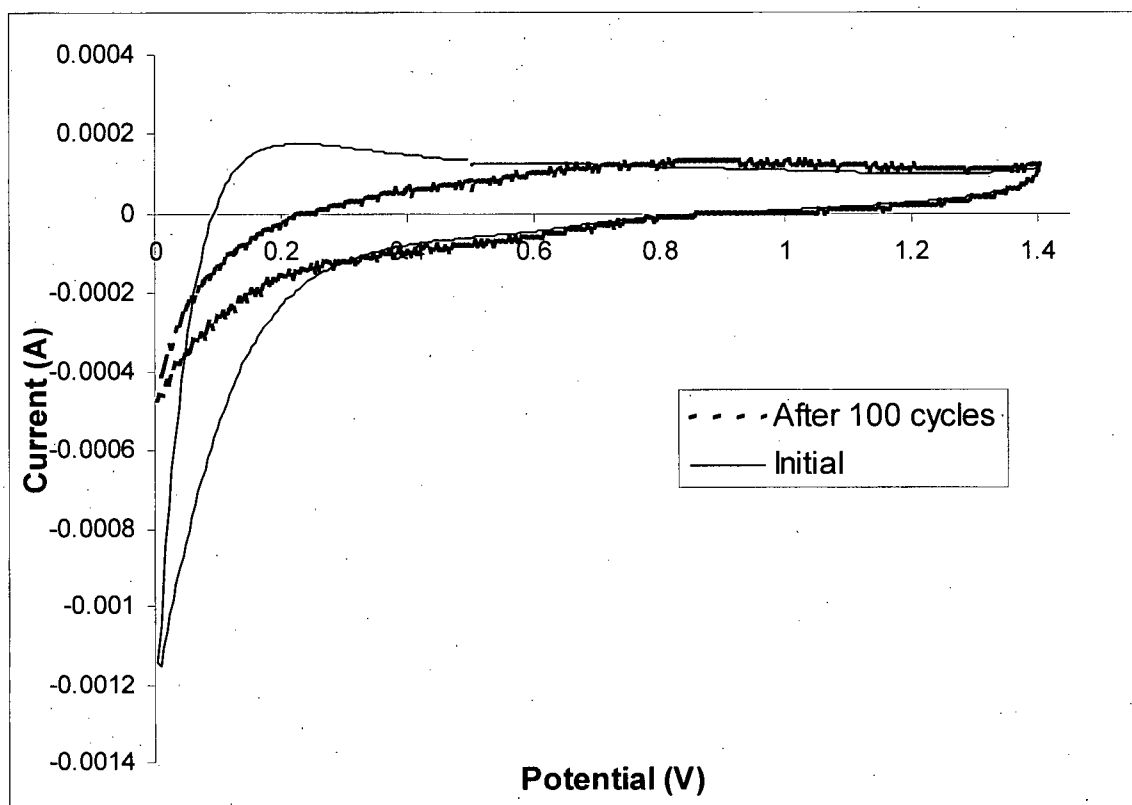


Figure 29: Cyclic voltammograms for Pt dispersed on Alfa Aesar WC, initially and after 100 oxidation cycles; 0.5 M H₂SO₄, 30°C, 100 mV/s, 2000 RPM.

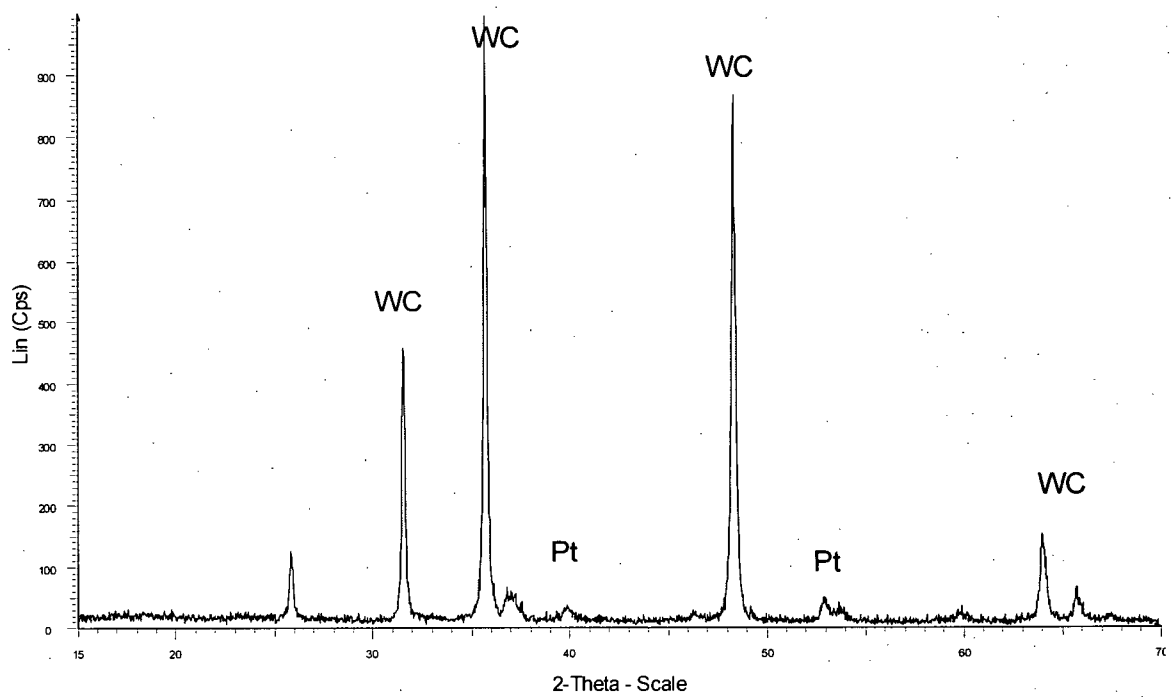


Figure 30: XRD pattern for Alfa Aesar WC with Pt deposition from Pt (II) reduction to Pt.

		Amount of Pt (II) precursor (g)	Pt (g)	WC (g)	Pt content (wt%)	WC volume (cm ³)	Pt volume (cm ³)	Pt vol: solid WC vol
wc	40 wt% Pt	0.500	0.240	0.360	40.000	0.023	0.011	0.485
	Tap powder density	0.156	0.075	8.266	0.898	0.530	0.003	0.007
	Solid density	0.156	0.075	0.994	7.003	0.064	0.003	0.055
		Amount of Pt (II) precursor (g)	Pt (g)	C (g)	Pt content (wt%)	C volume (cm ³)	Pt volume (cm ³)	Pt vol: solid C vol
c	40 wt% Pt	0.500	0.240	0.360	40.000	0.200	0.011	0.056
	Tap powder density	0.156	0.075	0.114	39.644	0.063	0.003	0.055
	Solid density	0.156	0.075	0.114	39.644	0.063	0.003	0.055
Solid density used for calculations (g/cm ³): C = 1.8; Pt = 21.45; WC = 12.6								

Table 3: Comparison of Pt wt%, and Pt to WC volume ratio for each method used to disperse Pt on AAWC

7 Results and discussion for indium tin oxide (ITO) studies

Both thermal and electrochemical stability of commercially available ITO (Nanophase) and Pt supported on ITO were evaluated. Pt was deposited using two methods (I and II) as explained in the experimental procedure section.

7.1 ITO with Pt deposition using chlorplatinic acid

TGA Results

Figure 31 shows TGA data for Hispec 4000, Vulcan XC-72R, and Pt deposited in-house on Vulcan XC-72R. The peak at temperatures below 50°C is due to the loss of moisture. Hispec 4000, which is more active than the catalyst made in-house (40 wt% Pt on Vulcan XC-72R), starts to thermally oxidize at ~300°C, while the in-house Pt/Vulcan XC-72R starts to oxidize at ~325°C. Vulcan XC-72R without Pt does not start to oxidize until ~650°C. The thermal oxidation results of Pt supported on Vulcan XC-72R agree with the findings by Roen et al⁶ that Pt catalyzes

the oxidation of carbon. Figure 32 shows the normalized weight loss for several catalyst support materials as a function of temperature. After heating the materials to 1000°C under air, Vulcan XC-72R lost 100% of its weight, Hispec 4000 lost 57 wt%, ~40 wt% Pt on Vulcan XC-72R lost 55 wt%, ITO lost 1 wt%, and Pt/ITO lost 0.7 wt%. The losses for Hispec 4000 and 40 wt% Pt on Vulcan XC-72R correspond to a complete loss of carbon, and the remaining weight corresponds to the Pt metal left in the TGA crucible. This result clearly indicates that the ITO support is thermally stable, in contrast to the other support materials studied.

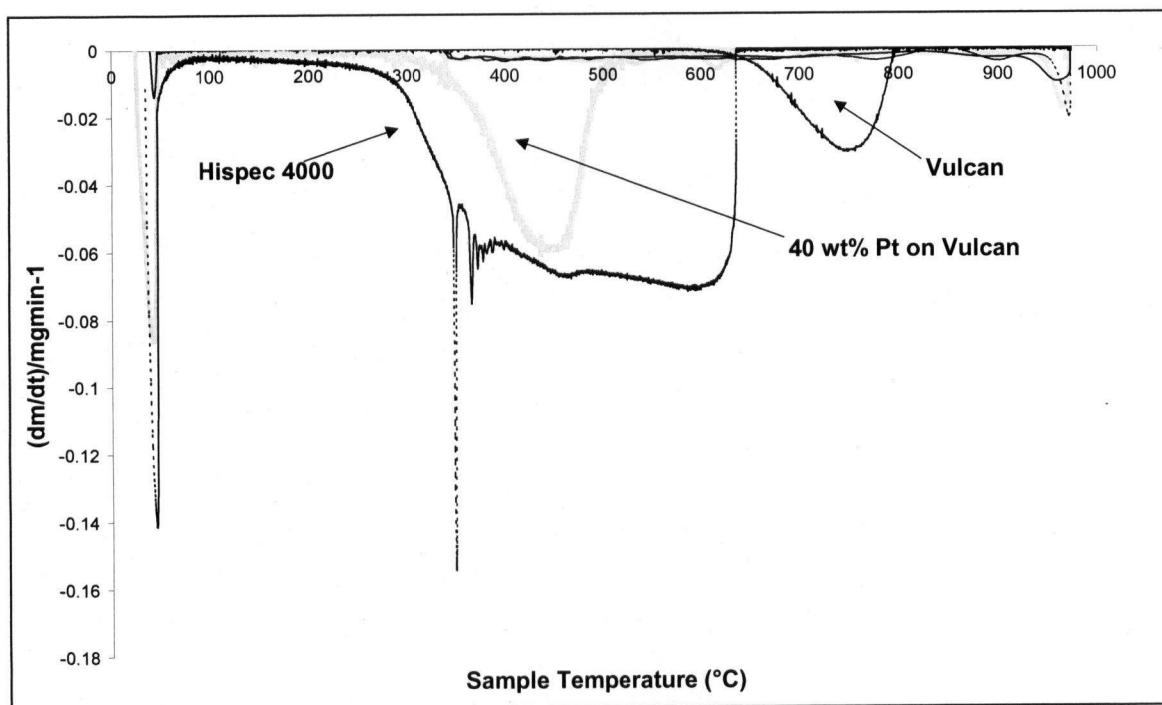


Figure 31: TGA data for Hispec 4000 and Vulcan XC-72R; under air at 40ml/min, temperature ramped from 50°C to 1000°C at 2°C/min.

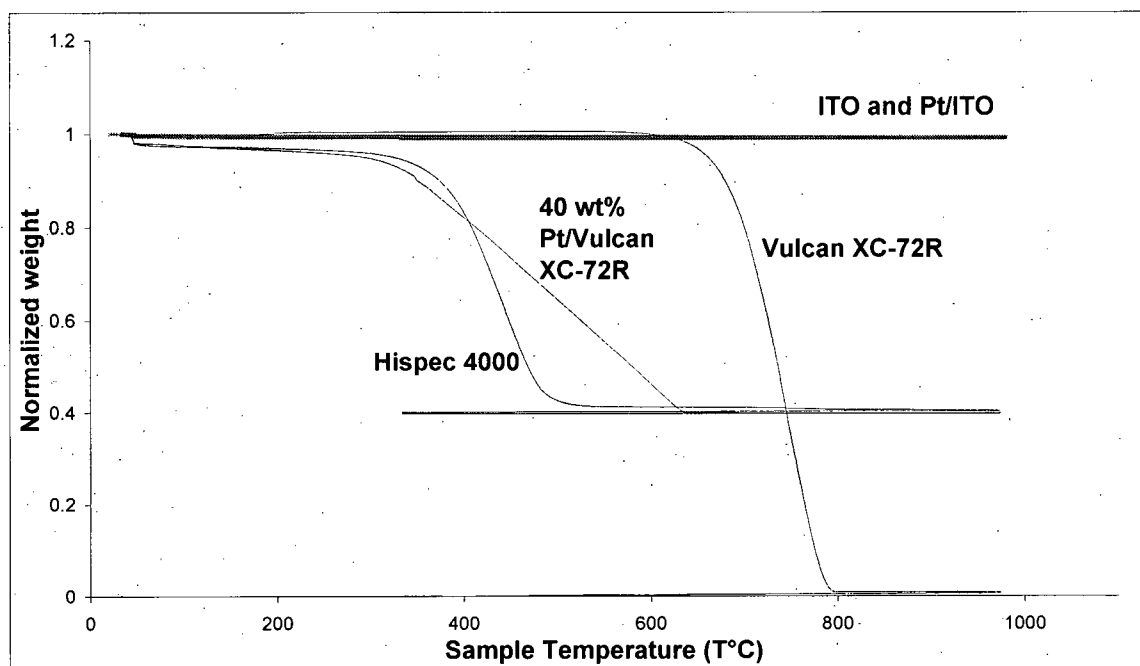


Figure 32: TGA data for Hispec 4000, Vulcan XC-72R, Pt on Vulcan XC-72R, Pt on ITO, and ITO; under air at 40ml/min, temperature ramped from 50°C to 1000°C at 2°C/min.

X-Ray Diffraction Results

Figure 33 shows the XRD pattern for 40 wt% Pt supported on commercially available ITO powder (Nanophase). Using the Scherrer equation, the crystallite size for Pt was calculated to be 13 nm, and that of ITO was 38 nm.

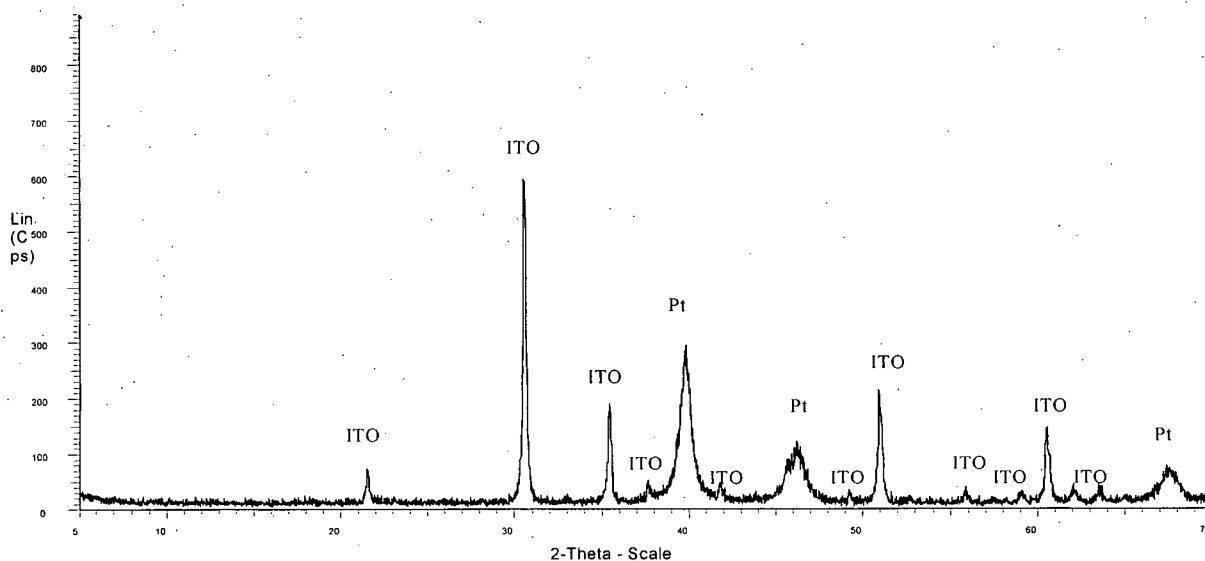


Figure 33: XRD pattern for 40 wt% Pt on ITO deposited using method I

Electrochemical Testing: Rotating Disc Electrode (RDE)

The results of oxidation cycles from 0.6 to 1.8V were used to calculate the normalized activity for ITO, Hispec 4000 and Pt/ITO, as shown in Figure 34. The normalized activity was calculated by recording the last current point from the data set at 1.8V just before the current became negative under 0.6 V conditions. Comparing Hispec 4000, Pt on ITO, and Pt on Vulcan XC-72R being held at 1.8V for 20 s per cycle, the stability follows the order of: Pt/ITO \gg Hispec 4000 \approx 40wt% Pt on Vulcan XC-72R. Pt on Vulcan XC-72R and Hispec 4000 lost most of their activity after 10 cycles. Pt on Vulcan XC-72R had similar thermal stability and activity loss under oxidation cycles to those of Hispec 4000, indicating that the method used in-house to disperse Pt yields catalyst with similar stability as commercially available Hispec 4000. Pt on ITO after 10 cycles only lost \sim 25% of its activity, indicating that ITO is a much more stable support than Vulcan XC-72R. The ITO particle size is lower than that of Vulcan XC-72R; however, by using sol-gel methods, the surface area of ITO can be enhanced. It would be useful to study the activity of ITO with optimized surface area, with catalyst dispersed by similar methods as used in the current study. This work will be left for a future study. The slight increase in activity at oxidation cycles 11 and 21 for ITO are observed because after 10 cycles, a CV test was performed, which increased the activity just before the start of the next set of oxidation cycles.

The CV for pure ITO in Figure 35 shows the stability of this material. The normalized activity plot shows that the activity increased to over 1 possibly due to surface roughening from oxidation-reduction cycles. Since In can have multiple oxidation states, the surface oxidation can increase the area, leading to higher activity than at the starting point. Figure 35 and Figure 36 show the cyclic voltammograms of Pt on ITO and Hispec 4000, respectively, both before and after 100 oxidation cycles. Pt on ITO showed significantly better electrochemical stability, as determined by a lower loss of electrochemically active surface area. This surface area was determined from the area under the hydrogen adsorption curves. Hydrogen adsorption peaks were present for the Pt on ITO even after 100 cycles from 0.6 to 1.8 V. On the other hand, most of active surface area of the Hispec 4000 was lost after 100 cycles. The Pt oxide reduction peak for Hispec 4000 was also observed to shift to lower potentials (0.75 V to 0.55V), whereas the same peak for Pt supported on ITO did not shift, even after 100 cycles. The 40 wt% Pt on Vulcan XC-72R lost almost all of its active area after only 50 cycles (Figure 38). The total currents in the cyclic voltammetry tests for ITO supporting Pt were much lower than those for Hispec 4000 because the active surface area of the Pt particles on the ITO is much lower than that in Hispec 4000. Changing the microstructure of the catalyst/support combination in future tests can modify this total activity.

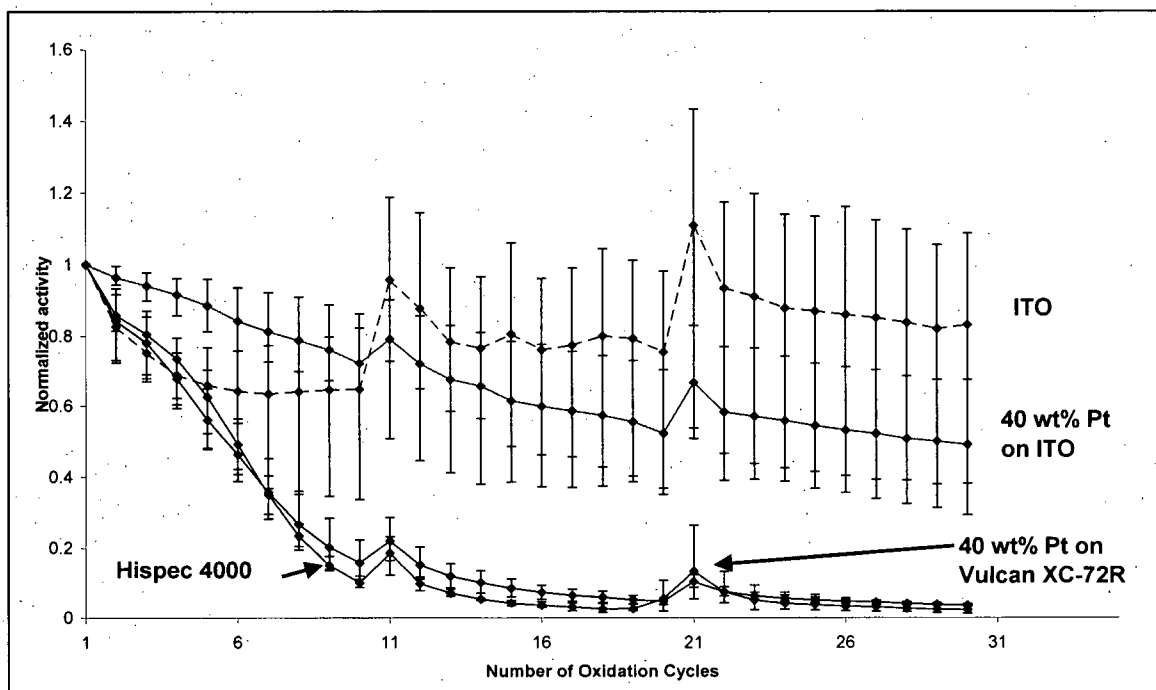


Figure 34: Normalized activity at different potentials as a result of repeated cycling for different 40 wt% Pt catalysts. Average of three samples with limits of error for each material are plotted.

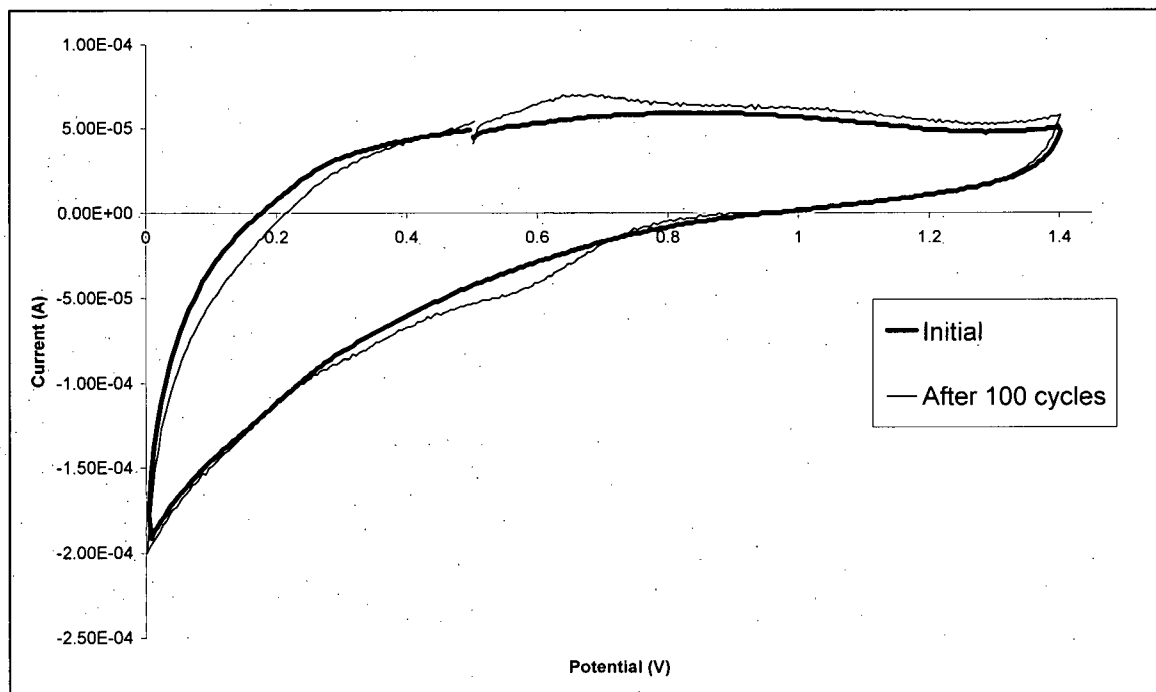


Figure 35: Cyclic voltammograms for ITO both before and after oxidation cycles at 1.8V. 100 oxidation cycles were run; 0.5 M H_2SO_4 , 30°C, 100 mV/s, 2000 RPM.

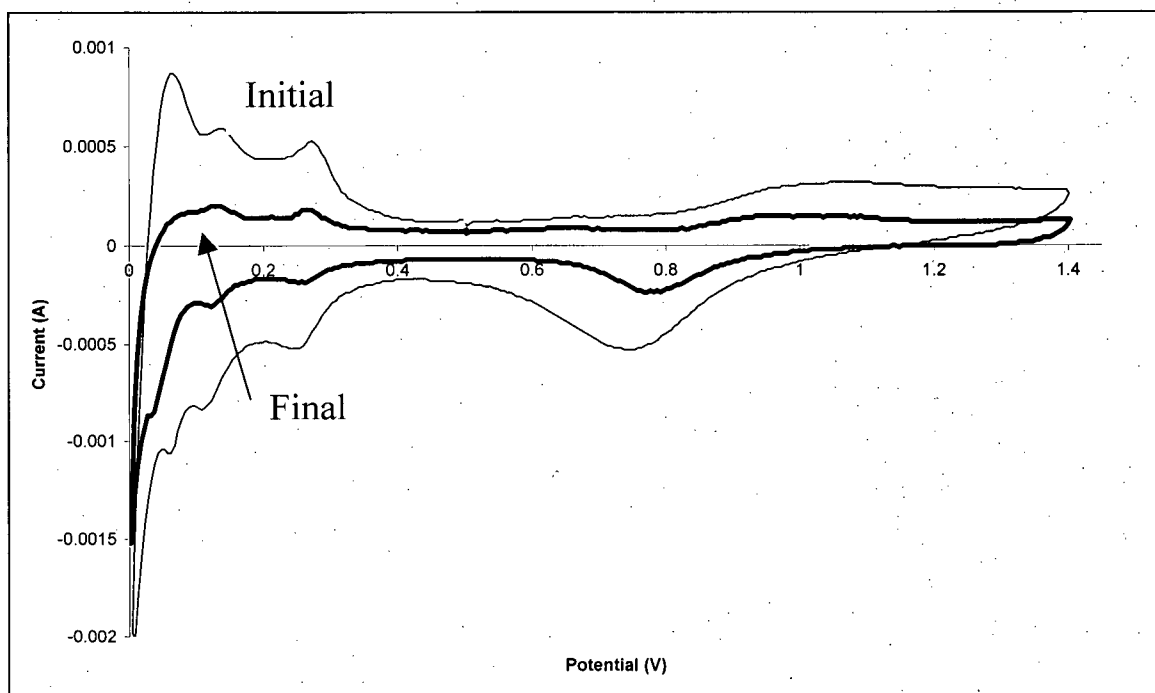


Figure 36: Cyclic voltammograms for 40 wt% Pt on ITO both before and after oxidation cycles at 1.8V. 100 oxidation cycles were run. Electrochemical stability with no change in the CV curves is observed from cycle 30 onwards; 0.5 M H₂SO₄, 30°C, 100 mV/s, 2000 RPM.

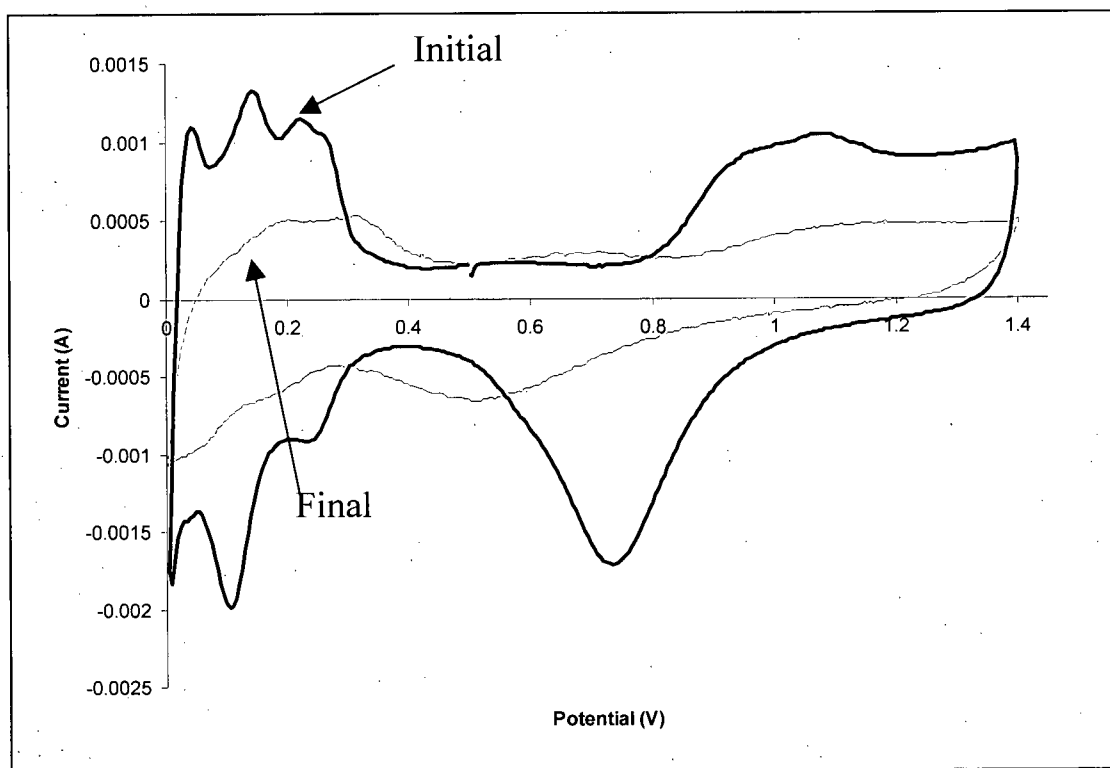


Figure 37: Cyclic voltammograms for Hispec 4000, both before and after 100 oxidation cycles; 0.5 M H₂SO₄, 30°C, 100 mV/s, 2000 RPM.

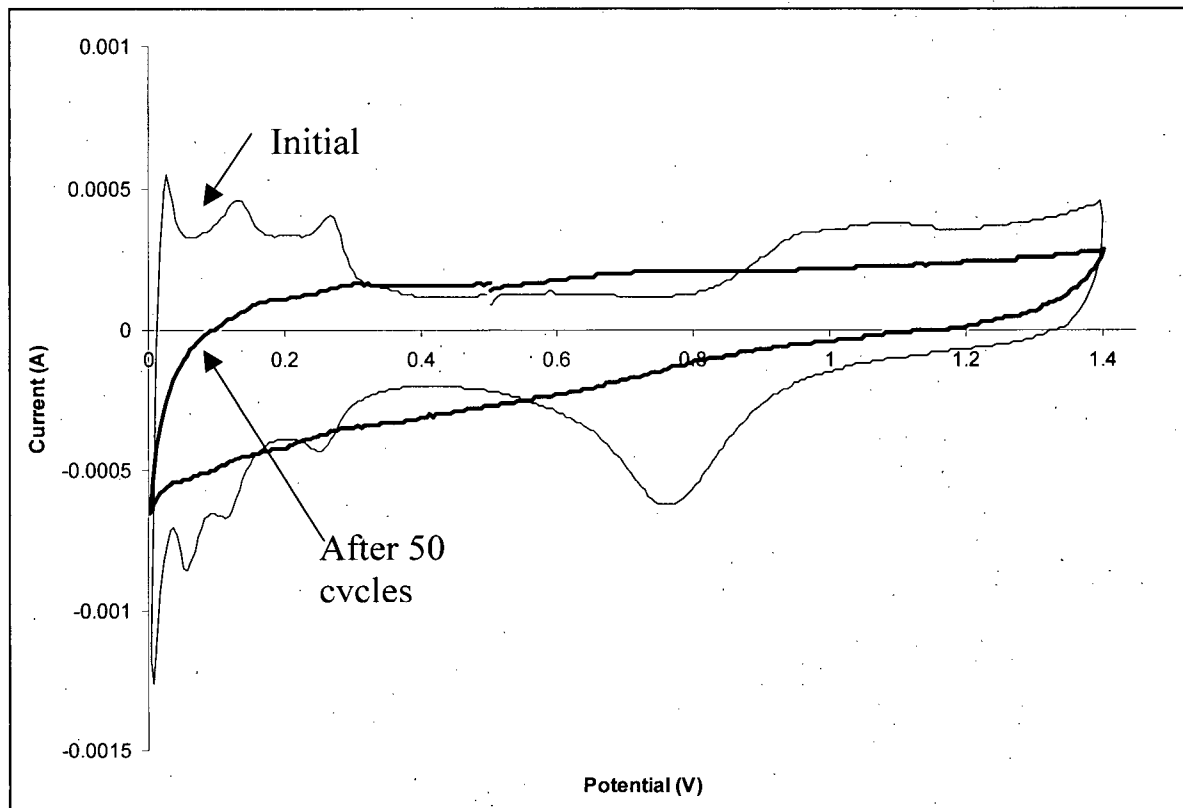


Figure 38: Cyclic voltammograms for 40 wt% Pt on VulcanXC-72R, both before and after 50 oxidation cycles; 0.5 M H₂SO₄, 30°C, 100 mV/s, 2000 RPM.

TEM and SEM images

Figure 39 and Figure 40 show SEM images for Nanophase ITO and 40 wt% Pt on Nanophase ITO, respectively. A mixture of spherical and octahedral structure of ITO crystallites is visible for the Nanophase ITO sample. Small Pt particles are observed for the 40 wt% Pt on Nanophase ITO sample in the SEM images. Figure 41 shows three TEM images of 40 wt% Pt on ITO. The EDX data indicate that Pt clusters are dispersed on small ITO particles. Further microstructural optimization of the ITO can lead to further increases in overall electrochemical activity.

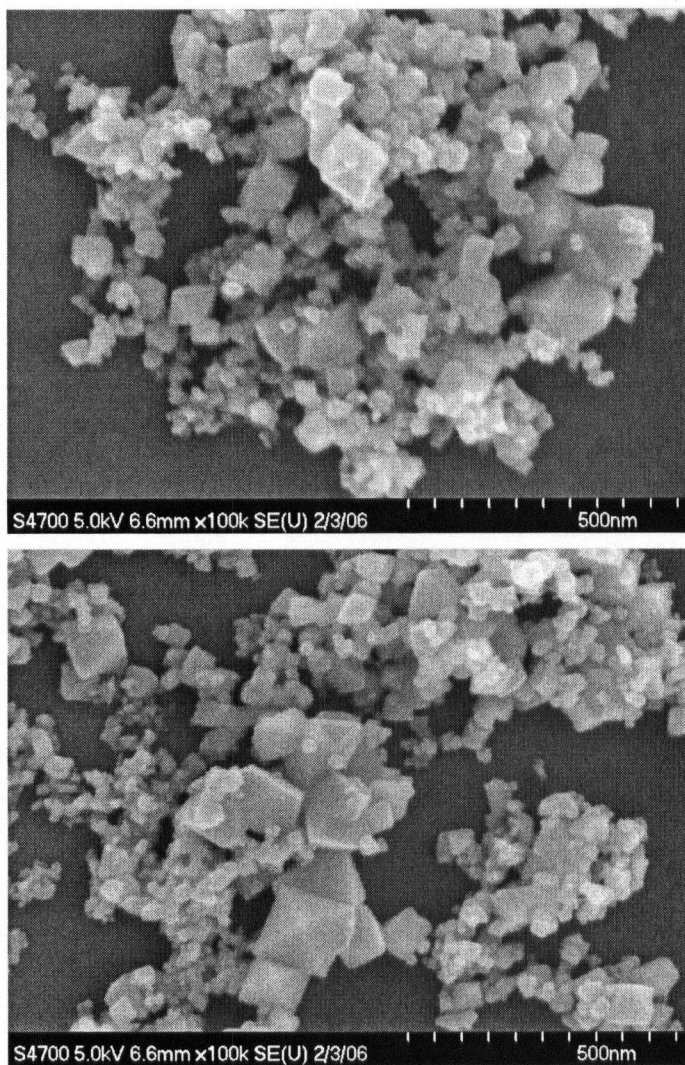


Figure 39: SEM images of ITO

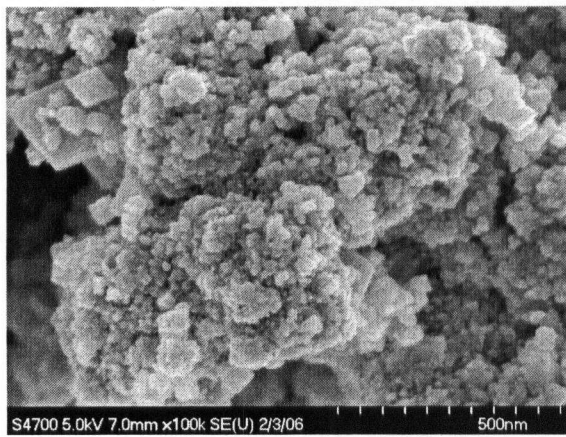
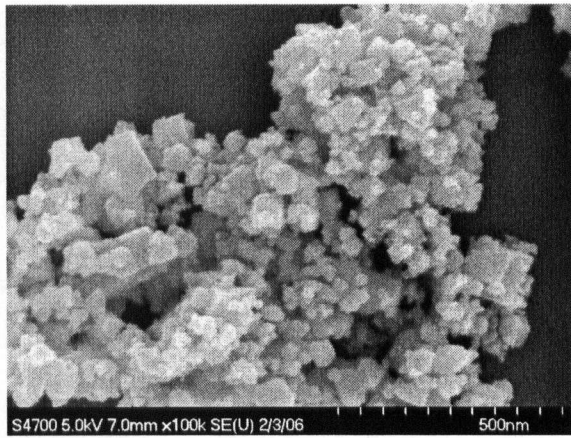
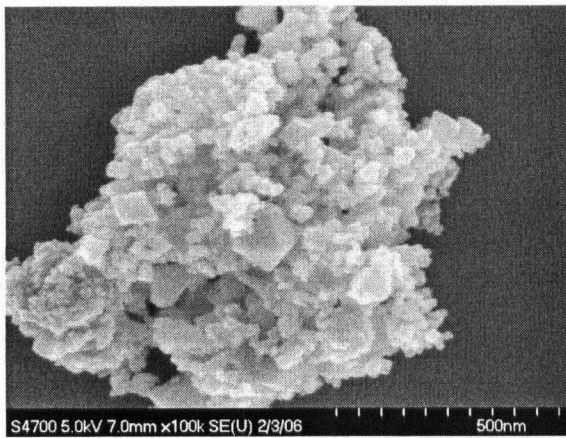


Figure 40: SEM images of 40 wt% Pt on ITO

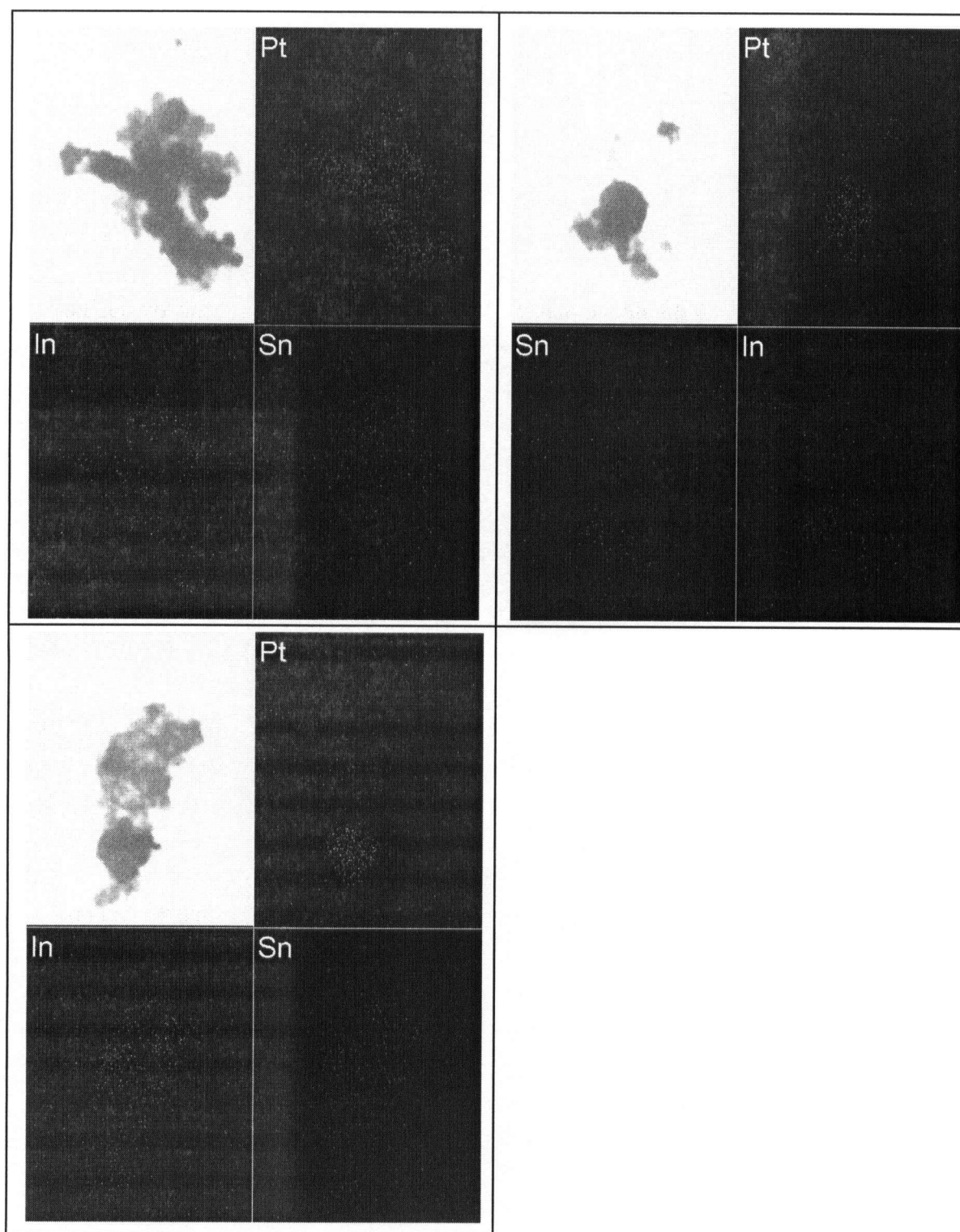


Figure 41: TEM/EDX of 40 wt% Pt on ITO

7.2 ITO with Pt deposition using Pt (II) pentan-2,4-dionate

XRD data

The XRD pattern for ITO with Pt from deposition method II is shown in Figure 42. The Pt deposition method II involved dispersing Pt (II) salt onto ITO and later reducing it to Pt metal in a tube furnace. The reducing atmosphere caused Pt to alloy with In, forming In_2Pt .

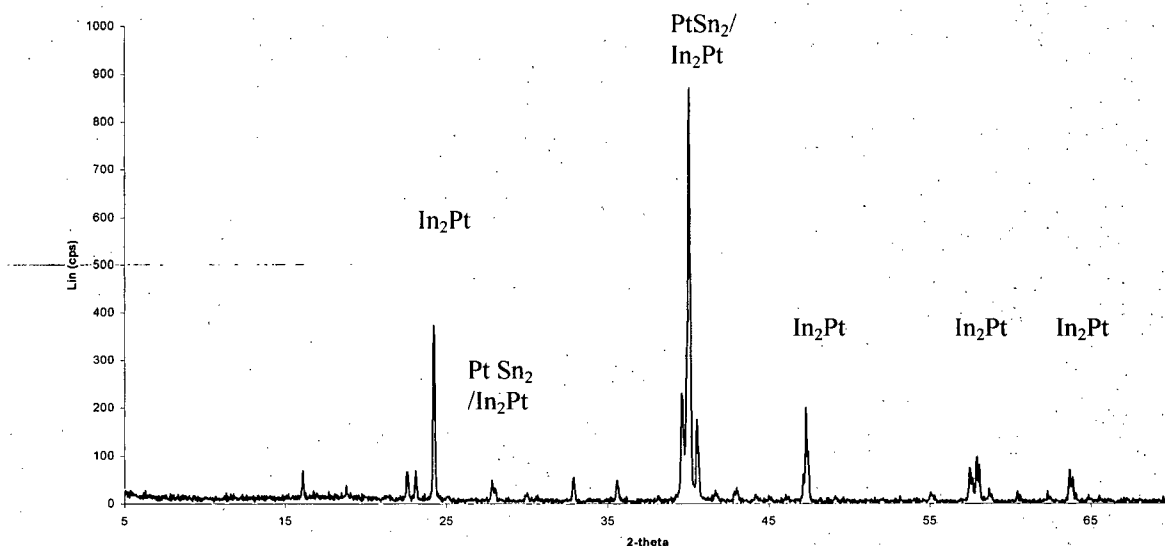


Figure 42: XRD pattern for Pt deposited on ITO by reduction of Pt (II) pentan-2,4-dionate.

Electrochemical testing: Rotating Disc Electrode (RDE)

The CV after cycle 2 and 4 for Pt on ITO is shown in Figure 43. The inset shows the initial CV with no Pt characteristics. The absence of Pt CV characteristics initially might be from the formation of In-Pt alloy on the surface. As more CV scans were taken, the CVs exhibited Pt characteristics such as hydrogen adsorption/desorption and Pt oxidation/reduction peaks. The oxidation cycles (Figure 44) show that Pt deposited by method II on ITO has a lower activity than Pt on ITO deposited by method I. The Pt deposition method II is not preferred for ITO since the In and Pt form an alloy, and the electrochemical stability of this material is poorer than that of the sample prepared by method I.

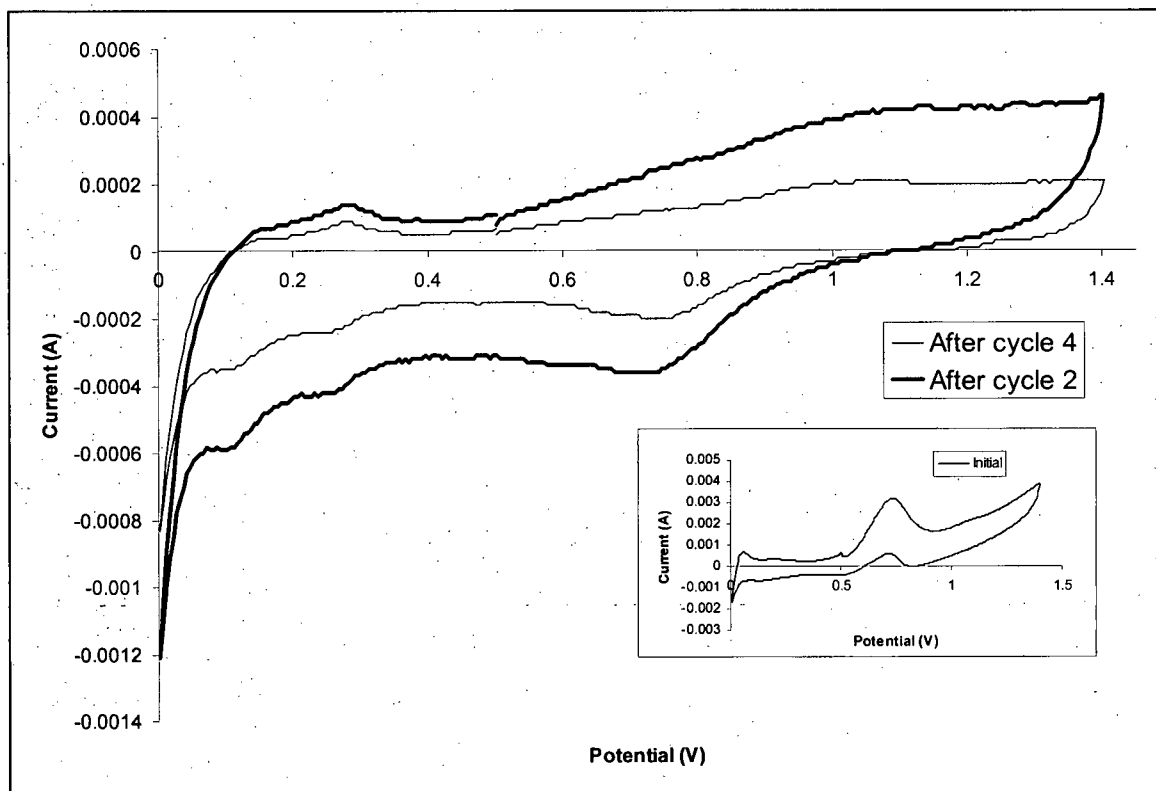


Figure 43: Cyclic voltammograms of Pt deposited on ITO by reduction of Pt (II) pentan-2,4-dionate after oxidation cycles 2 and 4. The inset shows the CV at initial point.

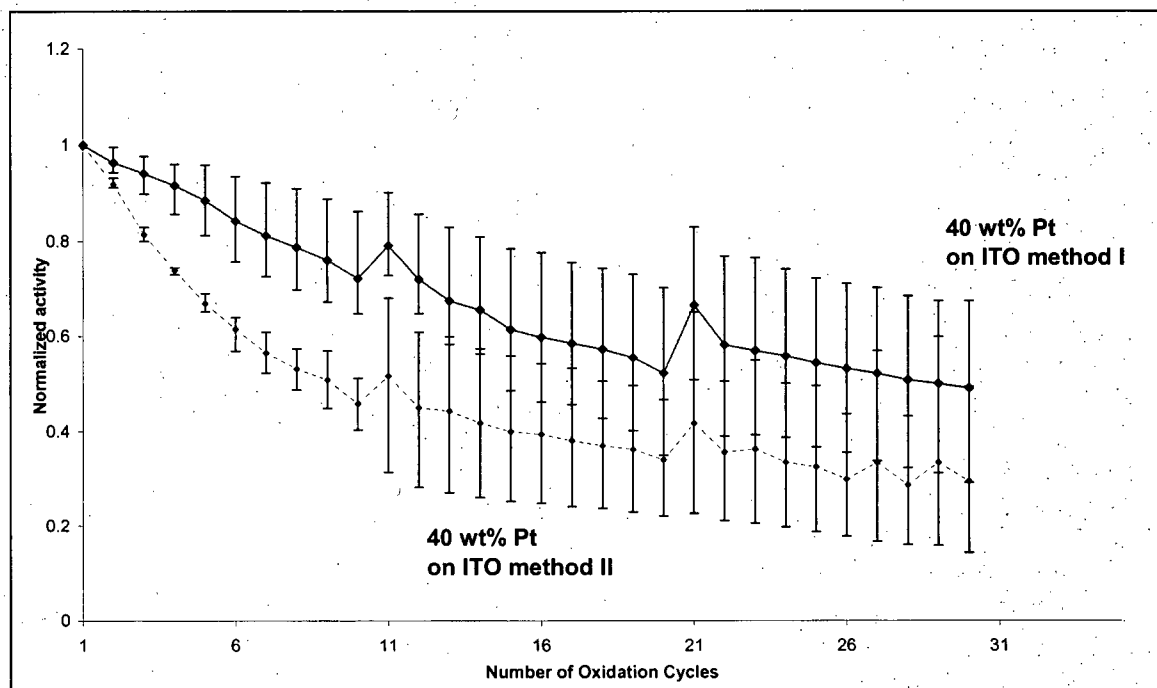


Figure 44: Normalized activity at different potentials as a result of repeated cycling for Pt deposited using chlorplatinic acid (method I) and Pt (II) pentan-2,4-dionate (method II) on ITO. Average of 3 separate samples with limits of error for each material are plotted.

8 Conclusions

8.1 Tungsten carbide

Pt deposition involving alkaline materials cannot be used for Pt dispersion on WC. An alternative method was created involving dispersion of Pt (II) salt, which was later reduced to produce Pt dispersed on WC, as confirmed by XRD.

Direct comparison of the electrochemical stability between carbon and WC is difficult due to the large differences in density. Different tests with varying amounts of reactants were studied, the tests involved comparisons with the same weight ratio of Pt on WC and C, tapped powder volume ratio, and finally the solid volume ratio. The 40wt% Pt on WC and C was not a successful test compare the electrochemical stability of WC and C due to the large density differences between WC and carbon. The tap density method was used to tap similar volumes of the support material.

For carbon that was tapped to a certain volume 40wt% Pt was added and similar amount of Pt as for carbon was added to WC. Finally, the solid volume ratio test involved dispersing similar amount of Pt on carbon and WC, where the volumes of the supports used were calculated based on the solid density of the support materials. The Pt volume to WC volume ratio data is summarized in Table 3. The Pt to WC volume ratio for the 40wt% Pt/WC was 0.49, which was significantly higher than compared to Pt:C volume ratio of 0.06. Based on higher content of Pt in case of 40 wt% Pt the electrochemical stability of this support was significantly better than carbon. But, since the surface area of WC was a lot lower than carbon and the significant density difference, direct comparison between carbon and WC cannot be made. With the tap density volume ratio test the Pt wt% relative to WC was only 1% and was not detected both in XRD and in the CVs. Some Pt was detected in the XRD for the Pt/WC using the solid density volume ratio test but no Pt characteristics were observed in the CV. Alternative methods need to be determined in order to directly compare the electrochemical stability of WC and carbon and the suggestions are explained in future work section 9.1.

8.2 Indium tin oxide

Results for Pt deposition by method II indicate that this method results in the formation of In_2Pt alloy, and the Pt/ITO has a lower electrochemical stability compared with the Pt/ITO prepared by method I.

Comparing Hispec 4000, Pt on ITO, and Pt on Vulcan XC-72R being held at 1.8V for 20s per cycle, the stability follows the order of: Pt/ITO >> Hispec 4000 \approx 40wt% Pt on Vulcan XC-72R. Pt on Vulcan XC-72R and Hispec 4000 lost most of their activity after 10 oxidation cycles. Pt on ITO after 10 oxidation cycles only lost \sim 25% of its activity, indicating that ITO is a much more stable support than Vulcan XC-72R.

The total currents in the cyclic voltammetry tests for ITO supporting Pt were much lower than those for Hispec 4000 because the active surface area of the Pt particles on the ITO is much lower than that in Hispec 4000. Changing the microstructure of the catalyst/support combination in future tests can modify this total activity. Overall, ITO has potential as an oxidation-resistant candidate material for catalyst supports in PEMFCs.

9 Future Work

9.1 Tungsten carbide

There is a need to normalize Pt content per unit surface area of the support in order to more directly compare the activities of conventional carbon support and WC. Both Brunauer-Emmett-Teller (BET) and mercury porosimetry can be used to determine the total surface area available in both supports.

High surface area tungsten carbide needs to be synthesized in order to enhance the catalyst layer activity. Encapsulating high surface area carbon with tungsten carbide may lead to an oxidation resistant high surface area WC coated carbon support.

If carbon oxidizes, it is lost as carbon dioxide gas, causing Pt to fall off the support and leading to low Pt surface area and significant performance degradation. However, if tungsten carbide oxidizes to tungsten oxide, it remains conductive, and little loss in Pt surface area is expected. Potential use of tungsten oxide as a catalyst support for PEMFCs needs to be investigated. Synthesis routes such as sol-gel methods that can provide high surface area tungsten oxide also need to be investigated. Finally, the electrochemical stability of tungsten oxide needs to be studied.

9.2 Indium tin oxide

The ITO particle size is lower than that of Vulcan XC-72R; however, by using sol-gel methods, the surface area of ITO can be enhanced. It will be useful to study the activity of ITO with optimized surface area, with catalyst dispersed by similar methods as used in the current study.

Further studies are required to optimize the particle size distribution and dispersion of the catalyst on the support material. Performance in a working fuel cell cathode of Pt supported on ITO also needs to be characterized.

10 References

- (1) Stevens, D. A.; Dahn, J. R. Carbon 2005, 43, 179-188.
- (2) Mathias, M.; Makharia, R.; Gasteiger, H.; Conley, J.; Fuller, T.; Gittleman, C.; Kocha, S.; Miller, D.; Mittesteadt, C.; Xie, T.; Yan, S.; Yu, P. Interface 2005, 14, 24-35.
- (3) Kangasniemi, K.; Condit, D.; Jarvi, T. Journal of the electrochemical society 2004, 151, E125-E132.
- (4) Interface Fall 2005, 21-44. 2005.
Ref Type: Magazine Article
- (5) Kinoshita, K. Carbon; Electrochemical and Physicochemical Properties; Wiley, New York: 1988; pp 316-334.
- (6) Roen, L. M.; Paik, C. H.; Jarvi, T. D. Electrochemical and solid-state letters 2004, 7, A19-A22.
- (7) Knights, S.; Taylor, J.; Wilkinson, D.; Campbell, S. [WO0115254]. 2001.
Ref Type: Patent
- (8) Ye, S.; Beattie, P.; Campbell, S.; Wilkinson, D.; Theobald, B.; Thompson, D. [US2004013935 (A1)]. 2005.
Ref Type: Patent
- (9) Ballard unpublished results. 2006.
Ref Type: Generic
- (10) Reiser, C.; Bregoli, L.; Patterson, T.; Yi, J.; Yang, J.; Perry, M.; Jarvi, T. Electrochemical and solid-state letters 2005, 8, A273-A276.
- (11) Gruver, G. A. Journal of the electrochemical society 1978, 125, 1719-1720.
- (12) Kinoshita, K.; Bett, J. Carbon 1973, 11, 237-247.
- (13) Kinoshita, K.; Bett, J. Effects of graphitization on the corrosion of carbon blacks. Advances in instrumentation, Proceedings, 43-55. 1974.
Ref Type: Conference Proceeding
- (14) Heckman, F.; Harling, D. Rubber Chem. Technol. 1966, 39, 1-13.
- (15) Schmid, K.; Roth, J. Journal of Nuclear Materials 2002, 302, 96-103.
- (16) Willsau, J.; Heitbaum, J. Journal of Electroanalytical Chemistry 1984, 6, 93-101.
- (17) Stevens, D. A.; Hicks, M. T.; Haugen, G. M.; Dahn, J. R. Journal of the electrochemical society 2005, 152, A2309-A2315.
- (18) Kinoshita, K.; Bett, J. Carbon 1974, 12.

- (19) McDonald, J. P.; Stonehart, P. Production of stable, high surface area carbons electrocatalyst support through doping with Boron. Conference on Carbon, 16th, 150-151. 1983. 1983.
Ref Type: Conference Proceeding
- (20) Young, J.; Lee, J.; Jubisa, L.; Radovic, R. Carbon 2003, 1987-1997.
- (21) Samant, P.; Rangel, C.; Romero, M.; Fernandes, J.; Figueiredo, J. Journal of power sources 2005, 151, 79-84.
- (22) Yang, R.; Qiu, X.; Zhang, H.; Li, J.; Zhu, W.; Wang, Z.; Huang, X.; Chen, L. Carbon 2005, 43, 11-16.
- (23) Serp, P.; Corrales, M.; Kalck, P. Applied Catalysis, A: General 2003, 253, 337-358.
- (24) Wang, J.; Swain, G. M. Journal of Electrochemical Society 2003, 150, E24-E32.
- (25) Qi, Z.; Lefebvre, M. C.; Pickup, P. G. Journal of Electroanalytical Chemistry 1998, 459, 9-14.
- (26) Marie, J.; Berthon-Fabry, S.; Achard, P.; Chatenet, M.; Pradourat, A.; Chainet, E. Journal of non-crystalline solids 2004, 350, 88-96.
- (27) Rajesh, B.; Thampi, K. R.; Bonard, J.M.; Mathieu, H. J.; Xanthopoulos, N.; Vishwanathan, B. Journal of Power Sources 2005, 141, 35-38.
- (28) Jalan, V.; Frost, D. G. Fuel Cell Electrocatalyst Support Comprising an Ultra-fine chainy-structured Titanium Carbide. [4,795,684], 1989.
Ref Type: Patent
- (29) Pierson, H. O. Handbook of Refractory Carbides and Nitrides; Noyes Publications: 1996; pp 1-115.
- (30) Meng, H.; Shen, P. K. Chemical Communication 2005, 2005, 4408-4410.
- (31) Lee, K.; Ishihara, K.; Mitsushima, S.; Kamiya, N.; Ota, K. Electrochimica Acta 2004, 49, 3479-3485.
- (32) Ma, C.; Gan, Y.; Chu, Y.; Huang, H.; Chen, D.; Zhou, B. Transactions of nonferrous metals society of China 2004, 14, 11-14.
- (33) Ma, C.; Zhang, W.; Chen, D.; Zhou, B. Transactions of nonferrous metals society of China 2002, 12, 1015-1019.
- (34) Christian, J. B.; Mendenhall, R. G. Tungsten-containing fuel cell catalyst and method of making same. Osram Sylvania Inc. [US6,656,870 B2], 1-9. 2003.
Ref Type: Patent
- (35) Christian, J. B.; Dang, T. A.; Mendenhall, R. G. Supported tungsten carbide material. Osram Sylvania Inc. [US6,551,569 B1], 1-9. 3 A.D.
Ref Type: Patent

- (36) Boudart, M.; Oyama, S. T.; Volpe, L. Board of Trustees of Leland Stanford Jr. University. [4,515,763]. 4 A.D.
Ref Type: Patent
- (37) Claridge, J. B.; Yor, A. P. E.; Brungs, A. J.; Alvarez, C. M.; Sloan, J.; Tsang, S. C.; Green, M. L. H. Journal of catalysis 1998, 180, 85-100.
- (38) Thompson, L. T.; Wixom, M.; Tarnowski, D.; Pu, C. [US 6,297,185 B1]. 2001.
Ref Type: Patent
- (39) Reddy, B. M.; Khan, A. Catalysis Reviews 2005, 47, 257-296.
- (40) Chen, G.; Bare, S. R.; Mallouk, T. E. Journal of Electrochemical Society 2002, 149, A-1092-A-1099.
- (41) Liu, J.; Radlein, E.; Frischat, G. H. Phys. Chem. Glasses 1999, 277-281.
- (42) Matveeva, E. Journal of the electrochemical society 2005, 152, H138-H145.
- (43) Mason, T. O.; Gonzalez, G. B.; Kammler, D. R.; Masourian-Hadavi, N.; Ingram, B. J. Thin Solid Films 2002, 411, 106-114.
- (44) Sceel, M. Fuel cell Electrode comprising conductive zeolite support material. [6,117,581]. 2000.
Ref Type: Patent
- (45) Higuchi, E.; Uchida, H.; Fujinami, T.; Watanbe, M. Solid State Ionics 2004, 171, 45-49.
- (46) Cullity, B. D. Elements of X-Ray Diffraction; 1967; pp 96-103.
- (47) Cullity, B. D. Elements of X-Ray Diffraction; Addison Wesley Publishing Company, Inc: 1978; pp 1-30.
- (48) Greef, R.; Peat, R.; Peter, L. M.; Robinson, J.; Pletcher, D. Instrumental Methods in Electrochemistry; Ellis Horwood limited: 1985.
- (49) Shim, J.; Lee, C. R.; Lee, H. K.; Lee, J. S.; Cairns, E. J. Journal of power sources 2001, 102, 172-177.
- (50) Kulesza, P. J.; Faulkner, L. R. Journal of the electrochemical society 1989, 136, 707-713.